AFRL-RQ-WP-TR-2022-0032V1

Evaluation of Prognostic & Probabilistic Individual Aircraft Tracking (P^2IAT): Volume 1 - Results

Eric J. Tuegel
Air Force Research Laboratory
Aerospace Systems Directorate

MARCH 2022
Final Report

AIR FORCE RESEARCH LABORATORY
AEROSPACE SYSTEMS DIRECTORATE
WRIGHT-PATTERSON AIR FORCE BASE, OH 45433-7542
AIR FORCE MATERIEL COMMAND
UNITED STATES AIR FORCE

NOTICE PAGE

Using Government drawings, specifications, or other data included in this document for any purpose other than Government procurement does not in any way obligate the U.S. Government. The fact that the Government formulated or supplied the drawings, specifications, or other data does not license the holder or any other person or corporation; or convey any rights or permission to manufacture, use, or sell any patented invention that may relate to them.

This paper was cleared for public release by AFRL Public Affairs, AFRL/PA and is available to the general public, including foreign nationals.

Copies may be obtained from the Defense Technical Information Center (DTIC) (https://discover.dtic.mil).

AFRL-RQ-WP-TR-2022-0032V1 has been reviewed and is approved for publication in accordance with assigned distribution statement.

This paper is published in the interest of scientific and technical information exchange and its publication does not constitute the Government's approval or disapproval of its ideas or findings.

REPORT DOCUMENTATION PAGE

PLEASE DO NOT RETURN YOUR FORM TO THE ABOVE ORGANIZATION.

1. REPORT DATE	2. REPORT TYPE	3. DATES COVERED	
		START DATE	END DATE
31-03-2022	Final	11-02-2022	31-03-2022

4. TITLE AND SUBTITLE

Evaluation of Prognostic & Probabilistic Individual Aircraft Tracking (P^2IAT): Volume 1 - Results

5a. CONTRACT NUMBER	5b. GRANT NUMBER	5c. PROGRAM ELEMENT NUMBER
In-House		62201F
5d. PROJECT NUMBER	**5e. TASK NUMBER**	**5f. WORK UNIT NUMBER**
		Q2K0

6. AUTHOR(S)

Tuegel, Eric J.

7. PERFORMING ORGANIZATION NAME(S) AND ADDRESS(ES)

Air Force Research Laboratory
Aerospace Systems Directorate
Wright-Patterson Air Force Base, OH 45433-7542

8. PERFORMING ORGANIZATION REPORT NUMBER

9. SPONSORING/MONITORING AGENCY NAME(S) AND ADDRESS(ES)	10. SPONSOR/MONITOR'S ACRONYM(S)	11. SPONSOR/MONITOR'S REPORT NUMBER(S)
Air Force Research Laboratory Aerospace Systems Directorate Wright-Patterson Air Force Base, OH 45433-7542 Air Force Materiel Command	AFRL/RQVS	AFRL-RQ-WP-TR-2022-0032V1

12. DISTRIBUTION/AVAILABILITY STATEMENT

DISTRIBUTION STATEMENT A. Approved for public release. Distribution is unlimited. PA# AFRL-2022-2155; Clearance Date: 06 May 2022.

13. SUPPLEMENTARY NOTES

PA Clearance Number: AFRL-2022-2155; Clearance Date: 06 May 2022

14. ABSTRACT

A probabilistic fatigue damage tracking method for airframe structure with an inspection criterion of Single Flight Probability of Failure (SFPOF) exceeding 10^{-7} was compared to the conventional method for fatigue tracking. Two retired fighter aircraft wings were experimentally loaded with different load histories. Fatigue at 14 locations in the outer portion of each wing were tracked with both methods. It was thought that probabilistic tracking would results in fewer inspections because it was believed that SFPOF at inspections with conventional tracking was significantly less than 10^{-7}. Probabilistic fatigue tracking resulted in the same or greater number of inspections as conventional tracking. SFPOF at the time of inspection with conventional tracking was frequently greater than 10^{-7}. Thus, the greater number of inspections with probabilistic fatigue tracking.

15. SUBJECT TERMS

Airframe Digital Twin, individual aircraft fatigue tracking, condition-based maintenance, full-scale durability experiment, probability of fracture, single flight probability of failure

16. SECURITY CLASSIFICATION OF:			17. LIMITATION OF ABSTRACT	18. NUMBER OF PAGES
a. REPORT	b. ABSTRACT	C. THIS PAGE		
Unclassified	Unclassified	Unclassified	SAR	80

19a. NAME OF RESPONSIBLE PERSON	19b. PHONE NUMBER *(Include area code)*
Eric J Tuegel	(937) 656-8826

TABLE OF CONTENTS

LIST OF FIGURES

LIST OF TABLES

Table **Page**

1 SUMMARY

A Probabilistic and Prognostic Individual Aircraft Tracking software (P^2IAT) for tracking fatigue damage in airframe structure, which used Single Flight Probability of Failure (SFPOF) as the inspection criterion, was compared to Conventional Individual Aircraft Tracking (CIAT). The criterion for scheduling structural inspections for fatigue cracks in P^2IAT is SFPOF exceeding 10^{-7}. This is in contrast to the conventional criterion of half the fatigue life from a prescribed crack size.

P^2IAT tracking process was implemented in a computer software package structured as a Dynamic Bayesian Network (DBN). The DBN explicitly mapped the relationships between all the random variables in the analyses. The mapping changes as needed with each new time increment during the tracking process. Furthermore, the fatigue tracking analysis can be updated using information about the state of fatigue cracking obtained from nondestructive inspection (NDI) results input to P^2IAT.

The P^2IAT software is adaptable to various aircraft and structural configurations. However, the software uses its own fatigue crack growth algorithm. P^2IAT cannot use any of the proven fatigue crack growth codes that are available. Another major drawback is that the P^2IAT software was written in Python 2.7, which is no longer supported. An effort to translate the P^2IAT software into Python 3 was unsuccessful. A substantial rewriting of the software is necessary to bring it up to the latest standards if there is to be further development of P^2IAT.

Fourteen locations on the outer portion of a fighter aircraft wing were chosen for demonstrating P^2IAT. Two retired wings were experimentally loaded with different flight histories, i.e., load histories that were created specifically for the experiment. P^2IAT and the conventional method tracked the loading to determine when structural inspections were necessary. The results from both P^2IAT and CIAT were compared to see if P^2IAT reduced the number of structural inspections. The experiment was conducted in anticipation that P^2IAT would significantly reduce the number of inspections. It needed to be demonstrated that the inspections were still frequent enough to find fatigue cracks before they caused failure.

The frequency of inspections with P^2IAT was the same or greater than with CIAT. Since there are few safety, or structural integrity, issues with CIAT, protecting structural integrity with P^2IAT was a moot point. Calculation of SFPOF with the Probability of Fracture software, PROF, for CIAT inspections showed that in most cases SFPOF exceeded 10^{-7} prior to inspections. So, P^2IAT should have more inspections than CIAT since P^2IAT is trying to keep SFPOF below 10^{-7}.

P^2IAT did not demonstrate an advantage over CIAT. A reason for this may be all of the uncertainties included in the P^2IAT analyses. It was thought that updating the analyses from inspection results and known loading would significantly reduce the overall uncertainty through the DBN. Such a reduction in uncertainty did not seem to occur.

2 INTRODUCTION

The objective of the Airframe Digital Twin program was to reduce the frequency of structural inspections for fatigue cracking by developing and demonstrating a probabilistic approach to fatigue tracking of critical locations in an airframe. Inspections for fatigue cracking are necessary in order to avoid catastrophic fracture of structure and potential loss of the aircraft. Therefore, any new approach to fatigue tracking must demonstrate that it maintains structural integrity and ensures safety. The probabilistic fatigue tracking approach was codified in a software package called Prognostic and Probabilistic Individual Aircraft Tracking (P^2IAT). P^2IAT was demonstrated by tracking fatigue damage at a number of locations on a representative aircraft structure subjected to prescribed loading. The number of inspections called for with P^2IAT was compared to the number of inspections called out by conventional fatigue tracking.

The development of P^2IAT is detailed in references [1], [2], and [3]. Section 3 begins description of the full-scale experiment that was tracked with P^2IAT. This is followed by a brief overview of how P^2IAT performs fatigue damage tracking. Then, the methods used in performing fatigue tracking with conventional Individual Aircraft Tracking (CIAT) and calculating SFPOF in CIAT are discussed. Section 3 concludes with an explanation of how the results of P^2IAT and CIAT were compared. Section 4 compares the results of fatigue tracking by the two methods, especially the probability of failure throughout the loading history. Section 5 gives the conclusions about the performance of P^2IAT. Finally, Section 6 provides some recommendations regarding alternative implementations of the probability of failure-based fatigue tracking approach if the USAF is interested in further exploration of this approach to fatigue tracking.

3 METHODS, ASSUMPTIONS AND PROCEDURES

The demonstration of P^{2}IAT consisted of several elements:

- Full-scale ground experiment of two aircraft wings to simulate service;
- Tracking the two wings with P^{2}IAT;
- Tracking the two wings with CIAT; and
- Comparison of the P^{2}IAT and the CIAT results.

The methods, assumptions, and procedures used in the experiment and the two aircraft fatigue tracking approaches are discussed in the following sections. The comparison of P^{2}IAT and CIAT results is presented in Section 4.

3.1 Full-Scale Ground Experiment

In anticipation of the success of P^{2}IAT, a full-scale ground durability experiment to simulate service usage was planned and executed. Demonstration of P^{2}IAT tracking fatigue damage in real structure under representative loading is necessary prior to transition of the technology to field application. Considering that it takes years to plan, construct the load fixture, and then execute a full-scale durability experiment, there would be a huge gap between development of P^{2}IAT and physical demonstration if we had waited until a computational demonstration was successful to start planning a physical experiment.

The plans for the full-scale durability experiment can be found in [2] and [4]. A summary of the experimental details that influence the comparison between P^{2}IAT and CIAT are presented here.

The left wing (LW) and right wing (RW) from a retired fighter aircraft were used in the ground experiment. Both wings were on the same aircraft for its entire service life of 5,137.9 actual flight hours (8,931.1 equivalent flight hours). The LW is shown in the load frame in Figure 1. A diagram of the internal structure of the LW showing the wing coordinate system is show in Figure 2.

Figure 1. LW in the Load Frame

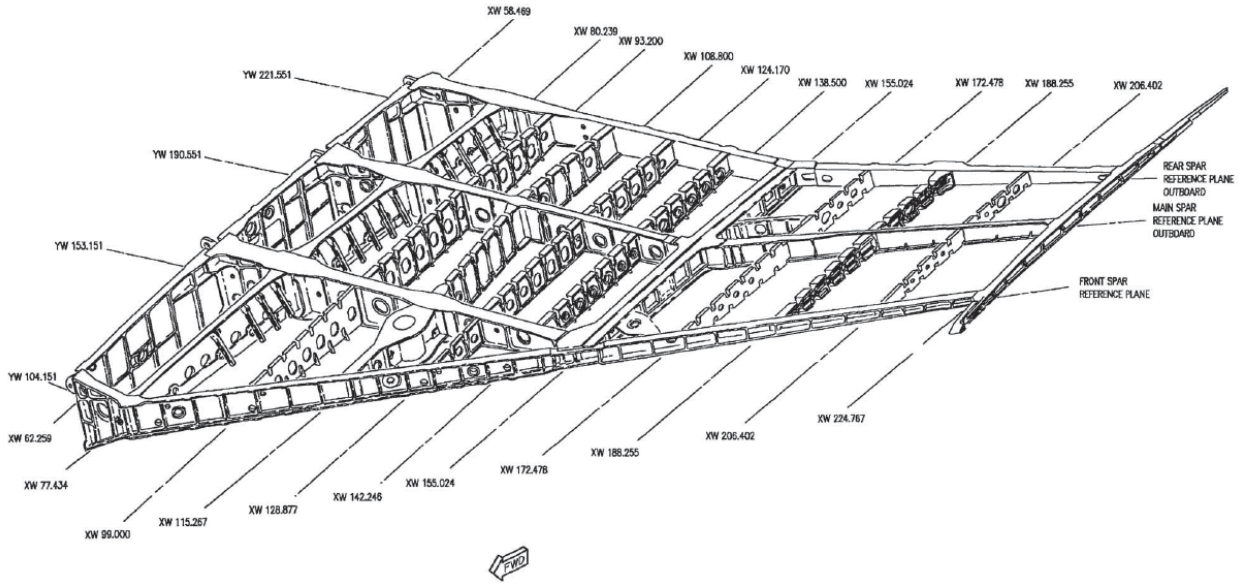

Figure 2. Internal Structure and Coordinate System for LW

The wings were shipped from the 309th Aerospace Maintenance and Regeneration Group (AMARG) at Davis-Monthan Air Force Base to Mercer Engineering Research Center (MERC) in Warner-Robins, GA to be prepared for the experiment. MERC removed wiring, piping and the fuel cell from the wings. The wings were inspected and any cracks or elongated fastener holes were repaired. MERC also made sure that all of the latest structural modifications were installed. Internal strain gages and Jentek eddy current sensors were installed while the wings were at MERC with the upper skins removed.

Fourteen locations were selected in the outer wing, outboard of XW155, for fatigue tracking. The fourteen tracking locations, or control points (CP), are listed in Table 1 and shown on a diagram of the outer wing in Figure 3. Loads were only applied to the outer wing according to the configuration in Figure 4. The inner wing served as transition structure between the outer wing test article and the test fixture. The wing lugs were the attachment points. The ailerons on the inner wings were left off; however, the flaps were used and loaded during the experiment.

Table 1. Description of Control Points

Control Point	Description
CP01	Lower wing skin at XW206.4, first fastener hole forward of the main spar, hole common to XW206 rib
CP02	Trailing Edge lower wing skin at Trailing Edge closure beam, thickness step at approximately XW157
CP03	Trailing Edge lower wing skin, 3rd fastener hole outboard of XW155 rib along the Trailing Edge closure beam
CP04	Lower Trailing Edge skin at Rear Spar
CP05	Lower Forward wing skin, edge thickness step at XW158
CP06	Lower Forward wing skin at XW188, 1st fastener hole inboard of XW188 and forward of the 2nd stringer from the Leading Edge
CP07	Lower Forward wing skin at Front Spar
CP08	Lower Aft wing skin, fastener hole common with Rear Spar at approximately XW162
CP09	Lower Aft wing skin at Main Spar, XW 163.6, 5th fastener hole from XW155
CP10	Front Spar, lower cap, fastener hole at XW166
CP11	Front Spar web, tooling hole at XW200
CP12	Front Spar, lower cap, fastener hole at XW169
CP13	Rear Spar, lower cap, fastener hole at XW167
CP14	Rear Spar, lower cap, fastener hole at XW191

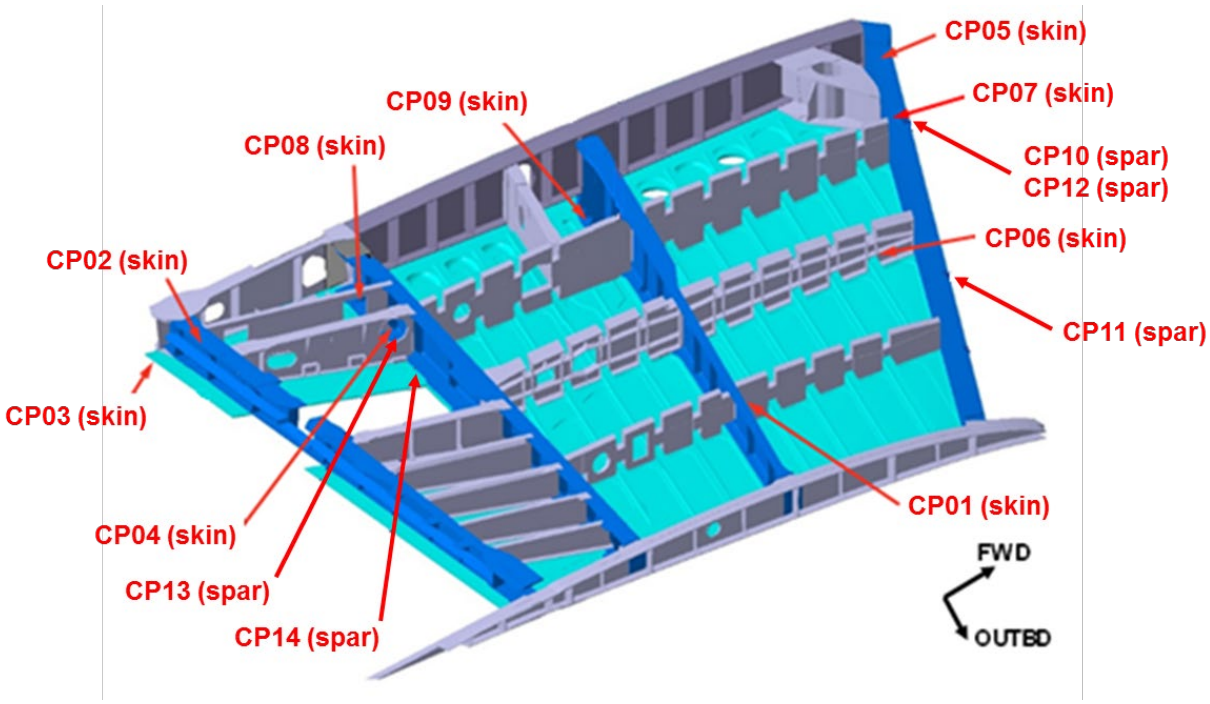

Figure 3. Control Point Locations in the Outer Wing

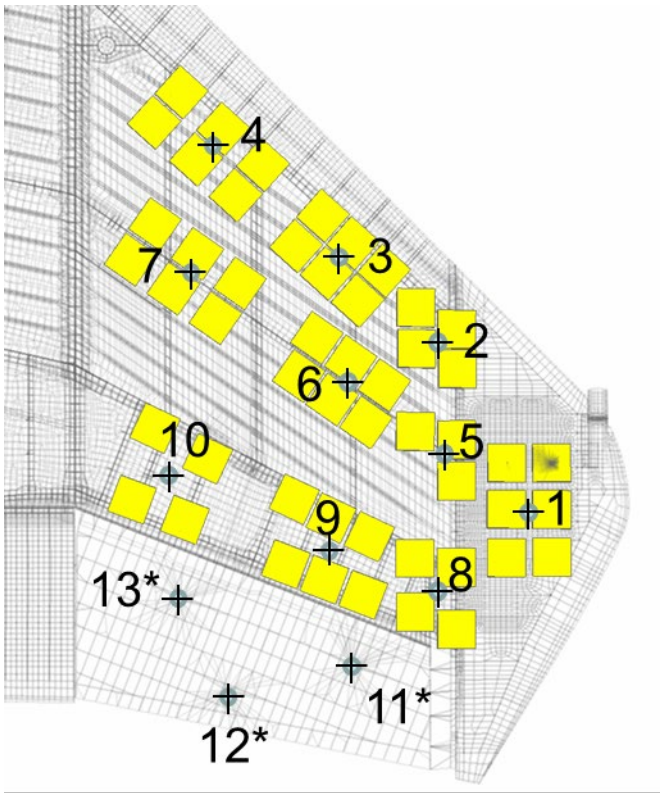

Figure 4. Schematic of Load Actuator and Load Pad Arrangement

A 1,000 flight hour (FH) baseline flight spectrum was created for the experiment. The baseline spectrum consisted of 1000 flights plus a marker band "flight" intended to create marker bands on fatigue crack faces. The flights in the baseline spectrum were divided into five mission types based primarily on the duration. The marker band flight was its own sixth mission type. Each point in the baseline spectrum consisted of:

- Flight number and mission type;
- Eleven parameters that would be recorded by a flight data recorder (FDR): flight time, altitude, gross weight, Mach number, Nx_{cg}, Ny_{cg}, Nz_{cg}, pitch acceleration, pitch rate, roll acceleration, and roll rate;
- Wing bending moment (WBM) and torque (WT) at Wing Station 3 (24.3 inches outboard of XW155 along the 40% chord);
- Stress at each CP (from appropriate elements in the finite element model);
- Loads to be applied by each of the load actuators; and
- Reaction loads at each of the wing lugs.

Different non-repeating 16,000 flight hour spectra were created for each wing. The spectrum for the LW was more benign than the baseline spectrum; the spectrum for the RW was more aggressive. This was done by creating a fatigue crack growth curve to failure for each individual flight in the baseline spectrum, plus the baseline spectrum, for each CP using the software AFGROW [5]. The 1,001 distinct flights in the baseline spectrum plus the baseline spectrum gives 1,002 fatigue crack growth curves for each of the CPs. The crack size versus the number of flight passes was stored for each crack growth curve. Four MATLAB scripts used this crack growth database to create the spectra for the LW and RW using the steps outlined in Figure 5. The marker band flight was applied every 1,000 spectrum flight hours (SFH).

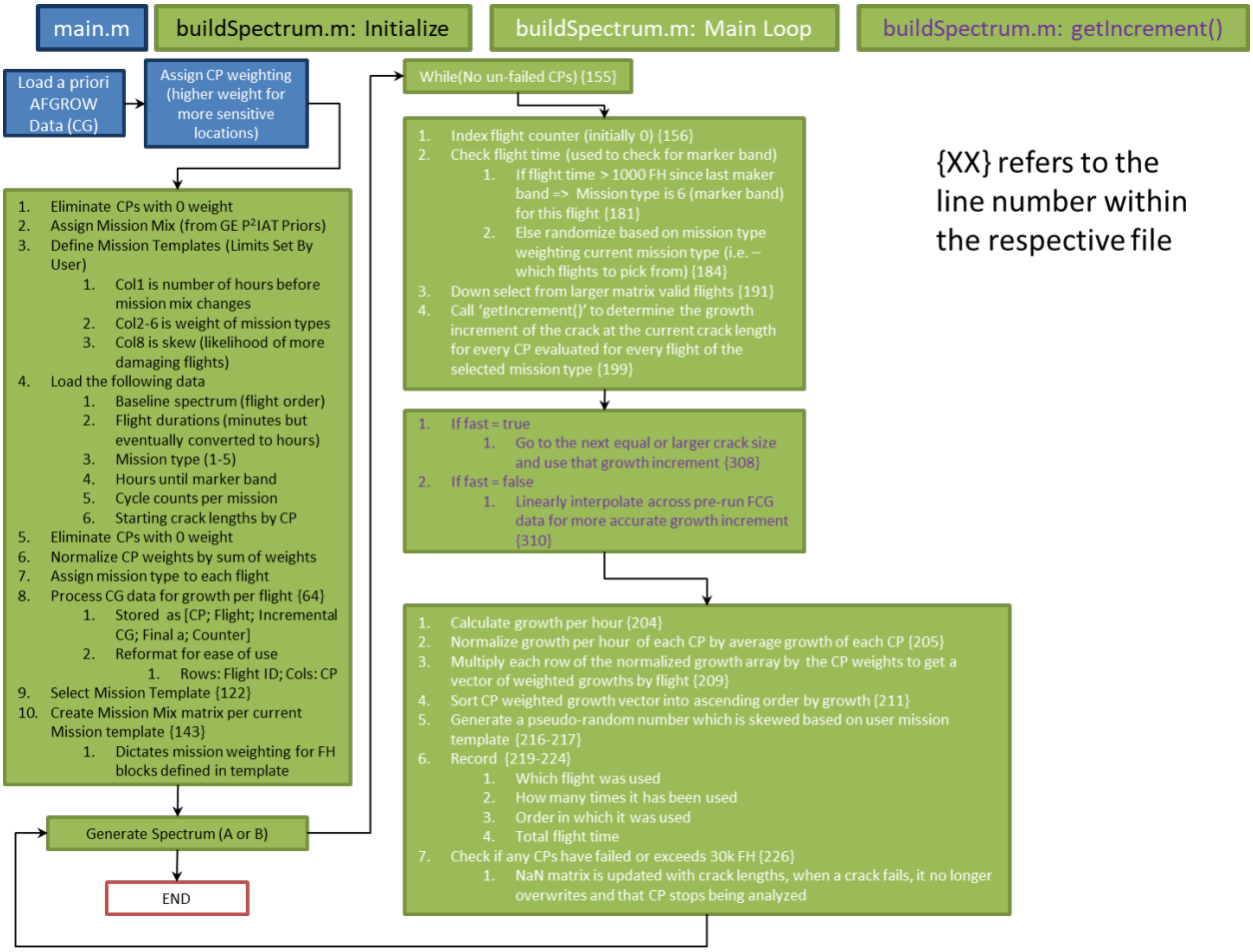

Figure 5. Flowchart for Creating Spectra for the Experiment

The spectra were broken up into approximately 200 SFH blocks that were typically applied in three days, leaving a day or two available each week to inspect all the CPs for cracks. Nondestructive inspections (NDI) were performed every week on all the CPs, however the inspection results were only supplied to P²IAT when an inspection was requested for that CP. An inspection needed to be planned at least two weeks (approximately 400 SFH) prior to when it was performed to simulate the lead-time that would be required for an inspection in service. Once inside that two week window, an inspection could not be changed.

Seven of the CPs (01, 03, 04, 06, 07, 08, and 09) were accessible from the exterior. These were inspected with eddy current ring probes. CPs 10, 11, 12, 13 and 14 were not accessible without disassembling the wings. Disassembling the wings for inspections would have added considerable time and expense to the experiment. These five locations were monitored each week with permanently mounted Jentek eddy current sensors. The Jentek system was not operational after September 30, 2019 (week 25 of loading on the RW and week 36 on the LW). No inspections occurred at these five CPs after that date.

A crack at CP02 was expected to start internally at the fillet for a thickness step. It would not be detectable externally until the crack became a through-thickness crack. Crack gages were

mounted internally along the fillet for early crack detection. These gages were backed up with external eddy current inspection with a pencil probe.

CP05 was completely hidden under the Leading Edge Skin. Without removing the Leading Edge, a crack would not be detectable until it grew out from under the Leading Edge Skin. Visual inspection of the Forward Lower Wing Skin at the border of the Leading Edge Skin was implemented for CP05.

No cracks were detected at any of the CPs in the LW during 52 weeks of loading. In the RW, a crack was found in the area of CP05 after 20 weeks of loading. The decision was made at the start of the experiment that any cracks found would not be repaired, so this crack was allowed to grow. Another crack was detected at CP07 after 31 weeks of loading. Eventually these two cracks grew together and caused failure of the RW as week 43 of loading started. A picture of the crack after failure of the RW is shown in Figure 6.

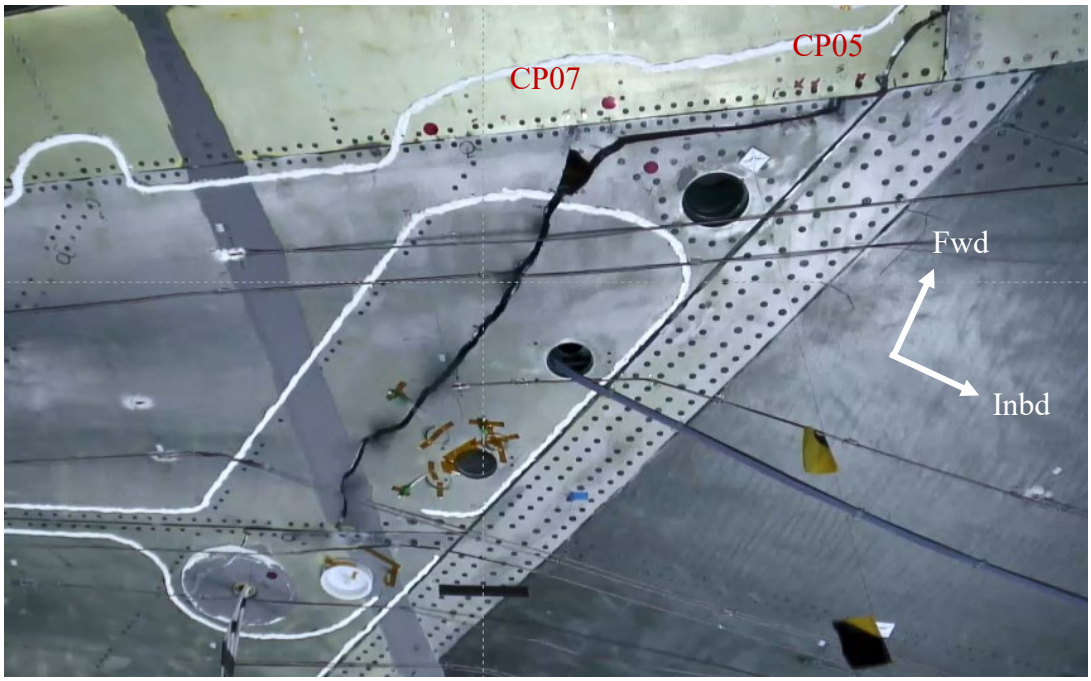

Figure 6. Failure of the RW

3.2 Probabilistic Fatigue Tracking

A complete description of the P^{2}IAT software can be found in references [1], [2], and [3]. This section will focus on how fatigue tracking was done in P^{2}IAT.

The main idea behind P^{2}IAT was to capture the uncertainty about the wing and the loading in the analysis. As more information about the wing and the loading was obtained during the experiment, this information was to be used to reduce the uncertainty in the analyses. The Dynamic Bayesian Network (DBN), upon which P^{2}IAT was built, was the structure to accomplish this. A DBN is a map of how all the parameters relate to each other and how the uncertainty from one parameter influences other parameters. The network is dynamic because

the map can change from one time step to the next if the relationship between parameters changes. The significant thing about a DBN is that if new information is obtained about a parameter that affects the uncertainty in that parameter, the change in uncertainty can flow forward and backward in the DBN to change the uncertainty in other parameters as well.

The main source of new information are the inspections at the CPs. Inspections that find no indications of a crack indicate that the probability of a large crack being present is small. The crack size distribution is updated using Bayes' Theorem [6]. This reduction in uncertainty could result in reduced uncertainty in other parameters as well. When an inspection finds an indication of a crack, the crack size distribution is updated to account for the higher probability of larger cracks. If the size of the crack can be measured, then there is a deterministic value, within measurement error, for the crack size.

P^2IAT was also supposed to learn the frequency at which each wing was experiencing the different mission types. The forecast of future flights would change then from an equal probability of any flight in the baseline spectrum to being biased towards those flights that occurred more frequently. However, during every analysis a warning came up stating that "previous samples for mission mix" could not be found and that the distribution was being used. It is not clear that the refinement of the future flight forecasts actually occurred.

Many of the input parameters for crack growth analysis for each CP were treated as random variables characterized by probability distributions. For CPs that were fastener holes, these parameters included:

- The diameter of the fastener hole;
- The in-plane location of the fastener hole (the distance from the intended location);
- The equivalent initial damage size (EIDS) at the CP (and the resulting crack size later);
- The wing bending moment (WBM) and torque (WT) (as a function of the flight parameters);
- The stress intensity as a function of the stress and crack size;
- The material crack growth rate (only Region 2, the Paris regime, was considered);
- The NDI probability of detection (POD); and
- How the wing will be loaded in the future.

Uncertainty in the thickness of the part was originally included, but in the final implementation, thickness was set equal to the nominal part thickness from the part drawing. The probabilistic models for each of these parameters are discussed in references [1], [2], and [3].

Prior to tracking the experiment, a Bayesian hybrid model (BHM) [7] was built that transforms the eleven flight parameters into the WBM and WT. Next, a BHM for the stress intensity factor (SIF) as a function of crack size at each CP was created using WBM, WT, and the geometry of the CP. Gaussian process models [8] were the primary function in all of the BHMs. A BHM adds an uncertainty term to the primary function. This is important to note because the uncertainty added in the WBM and WT BHMs goes into the SIF BHM where more uncertainty is added.

Tracking starts by making an initial inspection forecast with the baseline load spectrum and the EIDS distributions for each CP. P^2IAT calculates the SFPOF and the updated damage, or crack,

size distribution at the end of each week for the first four weeks. This is to see if any inspections are needed after Week #1 or #2 loadings.

After the first week of loading has been applied, the load spectrum for Week #1 and the EIDS distributions for each CP are used to calculate the SFPOF and the updated damage, or crack, size distribution at the end of Week #1 loading. Then P^{2}IAT proceeds to forecast how the SFPOF and crack size distribution will grow for loading 1,000 SFH beyond the end of Week #1 in order to plan for inspections. All inspections must be scheduled at least two weeks in advance to simulate the need for lead time to prepare for an inspections in real life. Once an inspection is two weeks or less away, it cannot be changed.

In P^{2}IAT, inspections are required whenever the SFPOF exceeds 10^{-7} based upon the requirements in Mil-Std-1530 [8]. SFPOF is the predicted failure rate during a flight [10]. SFPOF is calculated using a Particle Filter with Sequential Importance Resampling (SIR), which is a sophisticated Monte Carlo sampling method. Reasonable computation times were maintained by using 2,500 samples. Variability in results between the same analyses for a CP performed at different times indicated that this may be too few samples.

Unlike CIAT, P^{2}IAT uses the results from inspections to update the fatigue state of a CP using Bayesian statistics. Files containing the results of inspections performed at the end of each week are read in prior to analyzing usage from the subsequent reporting period. The structure of the filenames and the format of these files are hard coded into the software. These would likely need to be changed for any other application.

P^{2}IAT tracks fatigue damage as a function of the number of flights rather than the usual flight hours. This is because the flights for each sample can be of different lengths of time, so every sample has a different number of accumulated flight hours after the same number of flights. Samples can only be gathered on the basis of the number of flights as the software currently is written.

The resulting probability of failure, POF, versus number of flights curve is not smooth and monotonic because of sampling. Johnson's distribution was fit to the POF versus flight data to produce a smooth POF curve [3]. Johnson's distribution provided the best fit to the early tail behavior of the POF curve. The cumulative distribution function (CDF) of Johnson's distribution is

$$F(t) = \Phi\left[\gamma + sinh^{-1}\left(\frac{t-\xi}{\lambda}\right)\right] \tag{1}$$

where $\Phi(\cdot)$ is the standard normal CDF, t is the number of flights, and γ, ξ, and λ are parameters of the distribution.

SFPOF is found from

$$SFPOF(t) = \frac{\frac{dF(t)}{dt}}{1-F(t)} \tag{2}$$

3.2.1 P^{2}IAT Output

P^{2}IAT provides four different outputs after each analysis: (1) a control point summary file, (2) a maintenance summary file, (3) graphs of forecasted SFPOF for each CP, and (4) files containing the POF and SFPOF for each CP from the start of the loading to 1,000 flights beyond the end of the loading.

The CP summary file contains crack size percentiles of the user's choice at the start of the each week, end of the week, and at the next inspection for each CP. The file also provides the time for the next inspection if it is within 1,000 flights of the end of the week. Incremental and cumulative loading severities are reported for each CP. It was thought that this information would be useful in managing actual aircraft, but for this report, the information was not used.

The maintenance summary file contains lists of the CPs to be inspected after each of the next four weeks, expected to be 200, 400, 600, and 800 flights beyond the end of the current week. The inspections called for at 200 and 400 additional flights cannot be changed because of the lead-time requirement for all inspections. Results of inspections of the CPs in the full-scale experiment were input into P^{2}IAT when the maintenance summary specified an inspection was needed. The maintenance summary files also provided a record of when inspections occurred for comparison with the CIAT inspection schedule.

The pictures of SFPOF plots enable rapid visualization of how the risk is changing without needing to post-process any data. However, these plots only contained SFPOF values for the forecasted loading, not for the current week of loading. The SFPOF and POF values for the current week of loading, as well as the forecasted loading, are contained in the POF-SFPOF data files. The POF-SFPOF data files are the source of data for the comparison of SFPOF values between P^{2}IAT and CIAT that follows.

3.3 Conventional Fatigue Tracking

AFGROW was used to perform the fatigue crack growth analyses for CIAT. The standard single corner crack at a hole and single through crack at a hole stress intensity models were used for most of the CPs at fastener holes. CPs 07, 10, 12, and 14 had a crack growing from a hole towards another hole. The advanced modeling feature where a geometry with multiple holes could be constructed was used for these CPs. CPs 02 and 05 had cracks growing at fillets. AFGROW does not have standard model for this, nor can this type of model be created with the built-in advanced modeling. Therefore, comparisons between P^{2}IAT and CIAT focused on the CPs at holes.

Since P^{2}IAT does not include residual stresses or interference fit fasteners at this time, the typical methods of accounting for these (0.005 inch initial crack) were not used in CIAT even though most of the locations had interference fit fasteners. This keeps the results of the two approaches comparable. Either a durability (0.01 inch) or a damage tolerance (0.05 inch) initial crack was used depending upon whether the location was durability critical or a damage tolerance CP in the original mission design series that the wings came from.

Cycle-counted spectra for each CP were created using the local CP stresses developed with the baseline spectrum and the flight sequences created for the LW and the RW. A single pass was made through each weekly loading spectrum. The crack dimensions at the end of that pass became the initial crack dimensions at the start of the next week. After an inspection occurred, the crack dimension, c, at the start of the next week was set to the largest crack that could be missed, c_{NDI}, as discussed in the next paragraph.

An analysis to failure for each CP using the 1,000 hour baseline spectrum (with marker band loading) established the initial inspection and recurring inspection intervals. The initial inspection was at half the flight hours for a fatigue crack to grow from the initial crack size to failure. Recurring inspections were at half the life from c_{NDI}. For eddy current inspections at fastener holes, c_{NDI} was taken to be 0.075 inches based upon the 90th percentile crack in the 95th percentile lower bound POD curve for eddy current in P^{2}IAT (see Section 3.3.1.3). c_{NDI} for the Jentek sensors was taken as the thickness of the part based upon the POD curve in P^{2}IAT (see Section 3.3.1.3).

Inspections were planned when the equivalent flight hours (EFH) [11] calculated at the end of each week was within 200 SFH of the time for the next inspection.

3.3.1 SFPOF for Conventional IAT

It was decided to compare SFPOF values at inspections for CIAT and P^{2}IAT because it was believed that the SFPOF at an inspection from CIAT was orders of magnitude less than 10^{-7}. SFPOF calculations were made using the PRObability of Fracture (PROF) code [12] for the CIAT inspections. The inputs for the PROF analyses are discussed below.

Of the fourteen locations tracked on each wing, three locations on the Right Wing and two locations on the Left Wing did not require inspections with either tracking approach: CP01 and CP06 on both wings, and CP14 on the Right Wing. CP14 on the Left Wing required one inspection after Week 30 according to CIAT and none with P^{2}IAT. There is little that can be learned from these CPs, so they are not discussed further. As mentioned previously, CP02 and CP05 are fillet geometries and were not considered in comparing P^{2}IAT and CIAT. That leaves nine CPs on each wing for comparing the two methods.

CP10, CP11, CP12, and CP13 are internal locations – not accessible for NDI. Jentek eddy current sensors were mounted around the holes and interrogated at the end of every week. The sensor at CP11 on the Right Wing was not operable after Week 17. The sensors at CP10, CP11, and CP12 on the Left Wing were not operable after Week 34. The entire Jentek system was no longer operational after September 27, 2019, which corresponded to the end of Week 25 loading on the Right Wing and Week 36 loading on the Left Wing. Without inspection results to update P^{2}IAT, the SFPOF value increases with every flight and inspections will occur every week once the SFPOF threshold is crossed. This is not an accurate representation of how P^{2}IAT works. Therefore, tracking of these CPs was stopped once valid inspection data was unavailable.

The inputs required by PROF are discussed in the next sections.

3.3.1.1 EIDS and Fracture Toughness Distributions

The EIDS and fracture toughness distributions from P^2IAT were used in the PROF calculations. The EIDS distribution was a Lognormal distribution with a median crack size of 0.0041 inch and a standard deviation of 0.6902. The fracture toughness distribution was a Normal distribution with a mean of 32 ksi√in for CPs 03 and 04 (Al7075-T651 sheet), 30 ksi√in for CPs 07 and 08 (Al2124-T851 plate), or 33 ksi√in for CPs 10, 11, 12, and 13 (Al7075-T7352 forging) with a standard deviation of 1.947 for all.

3.3.1.2 Average Flight Duration and Maximum Stress during a Flight Distribution

The average length of a flight was 1.1 hours based upon the baseline spectrum. A Gumbel distribution with a scale parameter of 0.083 and a location parameter of 0.794 for the maximum stress during a flight was generated from the four highest values in the exceedances for the maximum stress in each flight of the normalized baseline spectrum. These parameters were multiplied by the reference stress (maximum spectrum stress) for the normalized load spectrum for each CP listed in Table 2 to obtain the Gumbel distribution for that CP.

Table 2. Spectrum Reference Stress for Each CP

CP	Spectrum Reference Stress (ksi)
03	15.2
04	28.3
07	26.4
08	25.0
09	15.3
10	20.5
11	16.8
12	16.4
13	16.6

3.3.1.3 POD Curves

The inspections at CPs 03, 04, 07, 08, and 09 were performed with an eddy current ring probe. P^2IAT used a probit function to describe the POD curve for the eddy current ring probe [3]. 95% confidence bounds were constructed for the POD curve as shown in Figure 7. PROF only allows a log-logistics or a lognormal curve for the POD. A log-logistics curve was fit to the confidence bounds of the P^2IAT POD curve concentrating on getting a better fit at the large crack sizes that

contribute most to SFPOF (Figure 8). The two curves can be used to bound the SFPOF values calculated with PROF. The parameters for the curves are given in Table 3. The lower bound POD curve being less sensitive should result in higher SFPOF values. So, all PROF analyses for CPs 03, 04, 07, 08, and 09 used the lower bound POD curve unless otherwise noted.

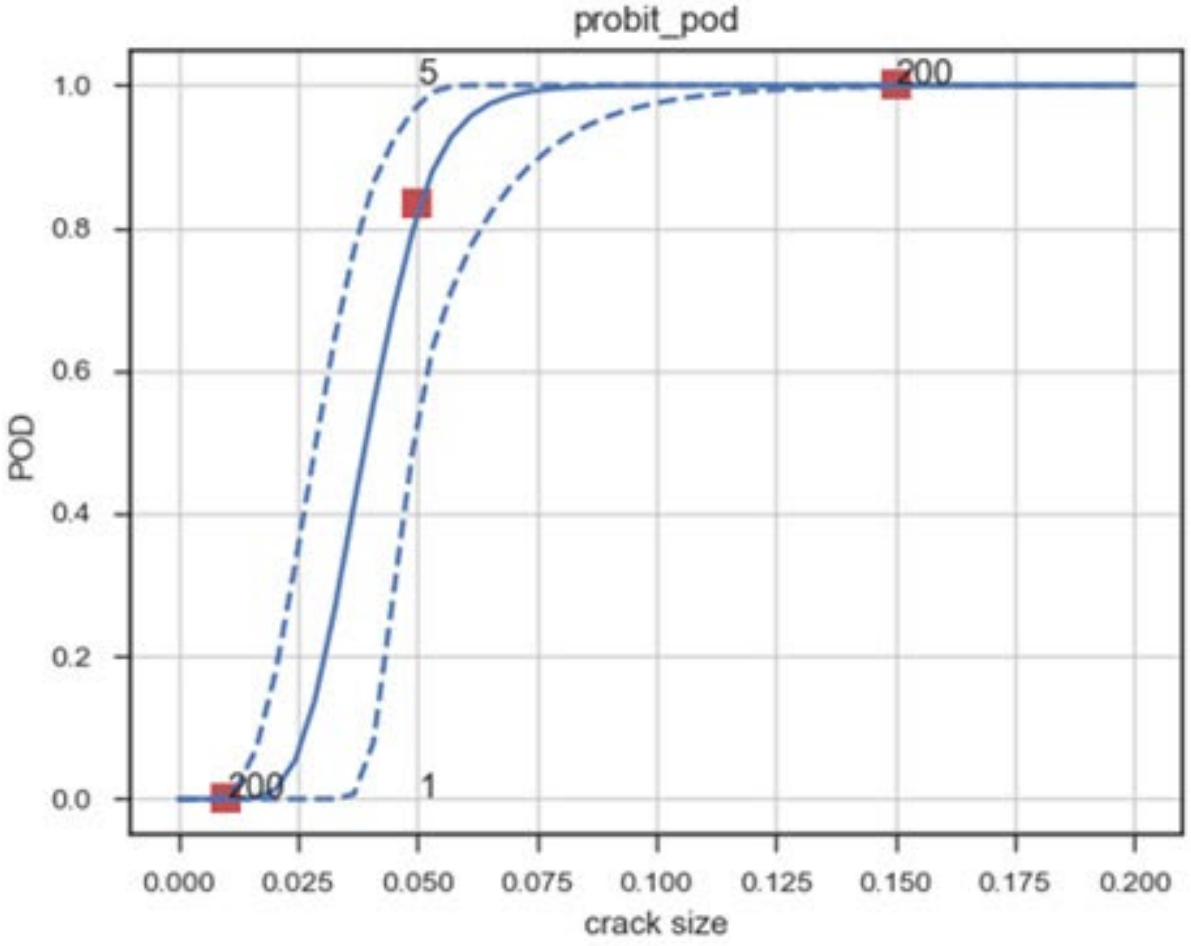

Figure 7. Probit POD Curve and 95% Confidence Bounds for Eddy Current Ring Probe used in P^{2}IAT [3]

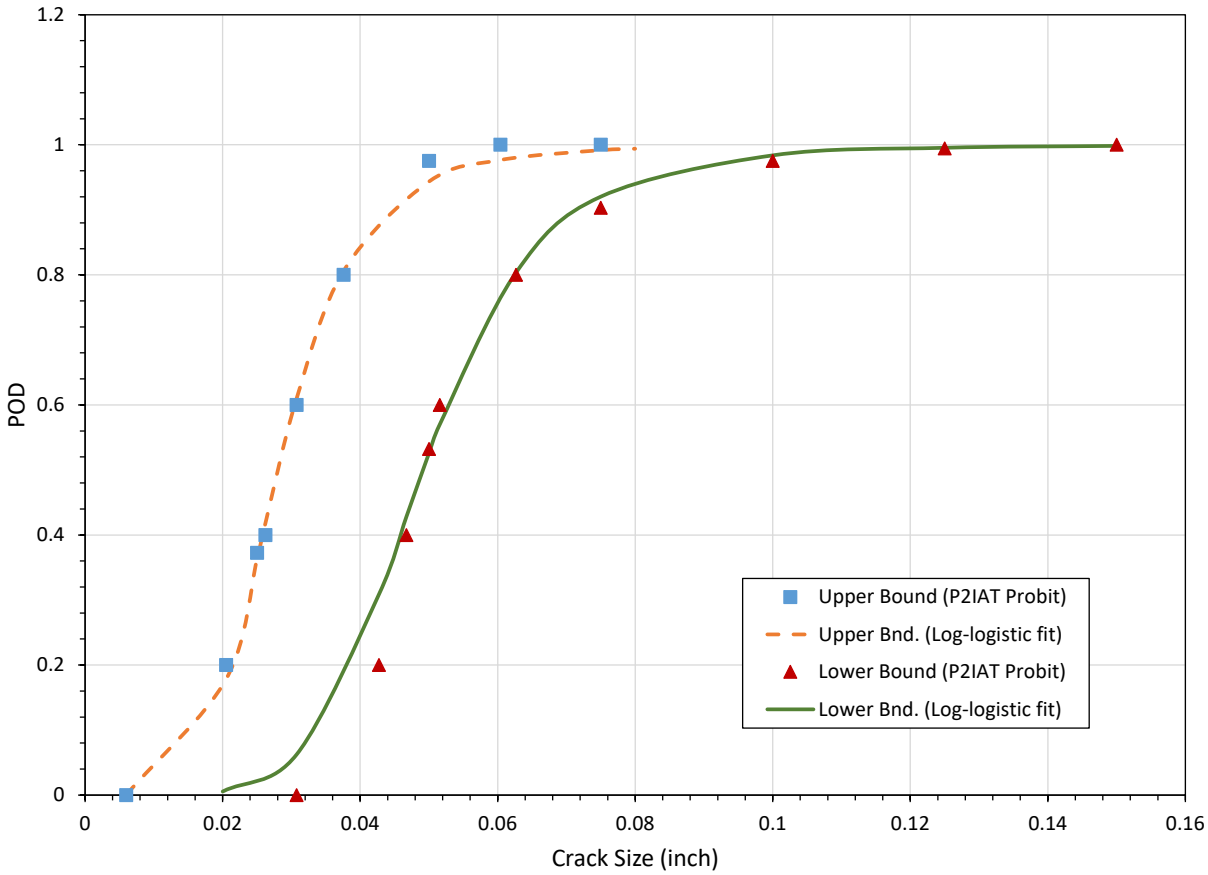

Figure 8. Log-logistic Curve Fit to P²IAT POD Bounds

Table 3. Parameters for Log-logistic Curve Fit to Upper and Lower Bound POD Curves for Eddy Current Ring Probe

Parameter	Upper Bound Curve	Lower Bound Curve
50% Detectable Crack Size (inch)	0.0281	0.0491
Slope	0.3725	0.3138
Minimum Detectable Crack Size (inch)	0	0.0000362

P²IAT used a step function to describe the POD curve for the Jentek eddy current sensors at CP10, CP11, CP12, and CP13 [3]. POD was 0 for a crack size less than 0.999 of the thickness of the part, and 1 for a crack size greater than that. It seems that the rationale for this POD is that the crack originates at the faying surface, remains nearly semicircular as it grows, and is detected when it breaks through to the external surface where the sensor is mounted. The part thickness at each CP and the parameters used to approximate a step function with a log-logistics function are given in Table 4. Using a very steep POD curve at CP10, CP12, and CP13 gave odd results in

PROF. So, upper and lower bound curves that were slight less steep were developed for CP10, CP12, and CP13. The less sensitive lower bound curve was used in all CIAT analyses for these CPs. Plots of the log-logistics step function approximation with these parameters are shown in Figure 9.

Table 4. Log-Logistics POD Parameters for Jentek Eddy Current Sensors

	Thickness, inches	**50% Detectable Crack**	**Slope**	a_{min}	a_{50}	a_{90}
CP10, CP12, CP13 Upper Bound	0.160	0.031	0.018	0.120	0.152	0.159
CP10, CP12, CP13 Lower Bound	0.160	0.031	0.018	0.152	0.183	0.191
CP11	0.080	0.008	0.012	0.071	0.079	0.080

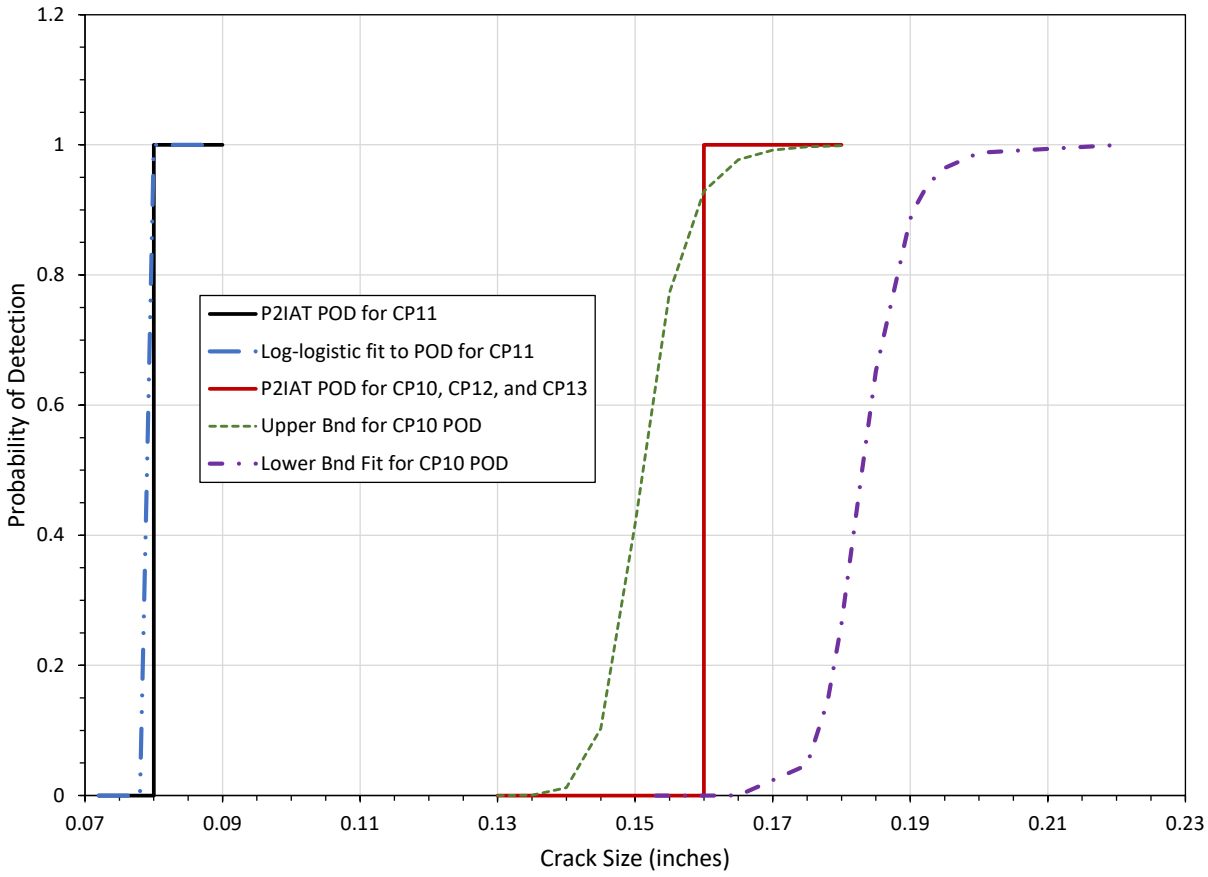

Figure 9. Jentek Eddy Current Sensor POD Curves

3.3.1.4 Crack Growth and Geometry Curves

The crack growth and geometry curves were constructed using AFGROW. CPs 03, 04, 08, 09 and 11 used the standard corner crack at a hole solution (Figure 10) with parameters listed in Table 5. CPs 07, 10, 12, and 13 used the advanced modeling capability in AFGROW to model a corner crack at a fastener hole in flange with two holes. The geometry for CPs 07, 10, and 12 is shown in Figure 11 with parameters in Table 6. CP07 had a step reduction in thickness halfway between the two holes. The larger thickness in which the crack starts was used in the first analysis pass. Since the SFPOF values were above 10^{-7} with the thicker geometry, there was no need for a more accurate geometry as it would have only increased the SFPOF values. The model geometry used for CP13 is shown in Figure 12.

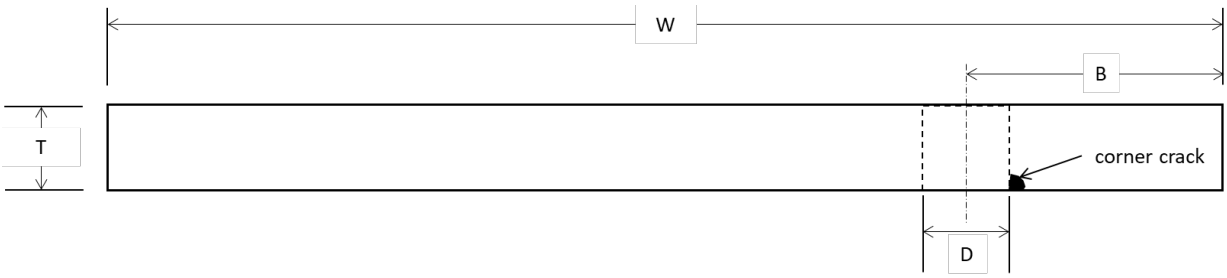

Figure 10. Standard Corner Crack at a Hole Geometry

Table 5. Parameters for AFGROW Standard Corner Crack at a Hole Crack Growth Model

Model Parameter	CP03	CP04	CP08	CP09	CP11
Width (W), inches	2.080	1.100	1.580	1.50	3.00
Thickness (t), inches	0.160	0.075	0.109	0.140	0.080
Hole Diameter (D), inches	0.190	0.190	0.190	0.190	0.500
Hole Offset (B), inches	0.4	0.41	0		0.0
Axial Stress Fraction	0.831	0.968	0.94	0.867	1.0
Bending Stress Fraction	0	0	0	0	0
Bearing Stress Fraction	1.783	0.338	0.5	1.4	0

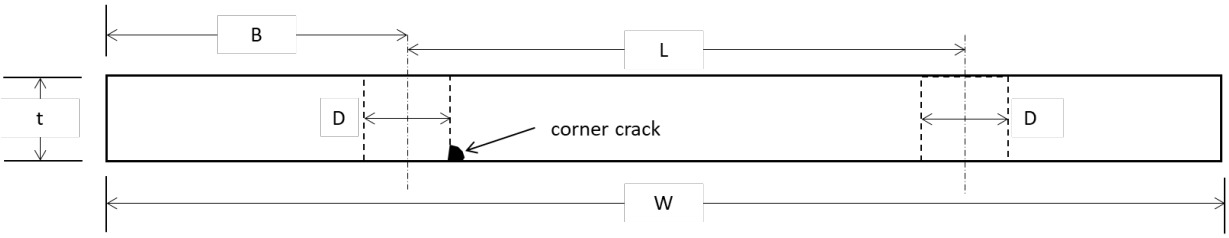

Figure 11. Two Hole Crack Growth Model Geometry

Table 6. Crack Growth Model Parameters for CP07, CP10, and CP12

Model Parameter	CP07	CP10	CP12
Width (W), inches	1.95	1.95	1.95
Thickness (t), inches	0.154	0.160	0.160
Hole Offset (B), inches	0.675	0.770	0.380
Distance between Holes (L), inches	0.895	0.800	0.800
Hole Diameter (D), inches	0.190	0.190	0.190
Axial Stress Fraction	0.95	0.952	0.845
Bearing Stress Fraction	0.53	0.508	0.577

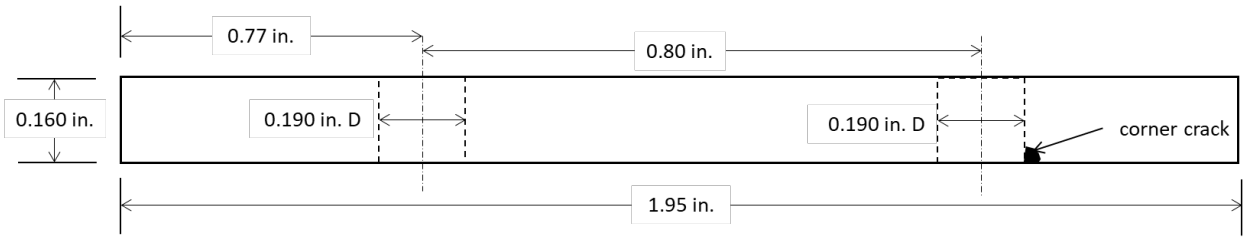

Figure 12. Geometry Model for CP13

3.3.1.4.1 Loading Spectrum

A study was conducted using CP03 RW to determine if a five-week 1,000 SFH block from experimental loading could be used as a repeating spectrum instead of the 8,000 SFH of the experimental loading. PROF is intended to use a repeated loading sequence in the crack growth analysis.

Five-week experimental load spectra blocks of approximately 1,000 SFH were evaluated to find the most and least severe loading, and how they compare to the baseline spectrum. Spectrum severity was based on the crack growth after one pass through the spectrum starting from a semi-circular corner crack. An example of the spectrum evaluation for CP03 RW is shown in Figure 13. The loading for Weeks 21 to 25 was the most severe; the loading for Weeks 6 to 10 least. The severity of the baseline spectrum is slightly more severe than Weeks 6 to10.

Four separate PROF analyses were performed for CP03 RW to determine the effect of loading severity and the ring probe POD confidence bounds on the SFPOF to see what variables need to be included when comparing PROF results to P^2IAT. The four cases were:

1) Weeks 21-25 loading with the upper bound POD,
2) Weeks 21-25 loading with the lower bound POD,
3) Weeks 6-10 loading with the upper bound POD, and
4) Weeks 6-10 loading with the lower bound POD.

The results of these analyses out to 8,400 SFH using conventional IAT and P^2IAT inspection intervals are plotted in Figure 14 and Figure 15. The loading spectrum affects the SFPOF very little for the five-week loading blocks used in the experiment. The different POD curves result in a larger change in SFPOF, and thus a good bound on SFPOF for comparison with P^2IAT. Therefore, the primary PROF analysis for each CP will use the most severe five-week loading spectrum and the lower bound POD curve.

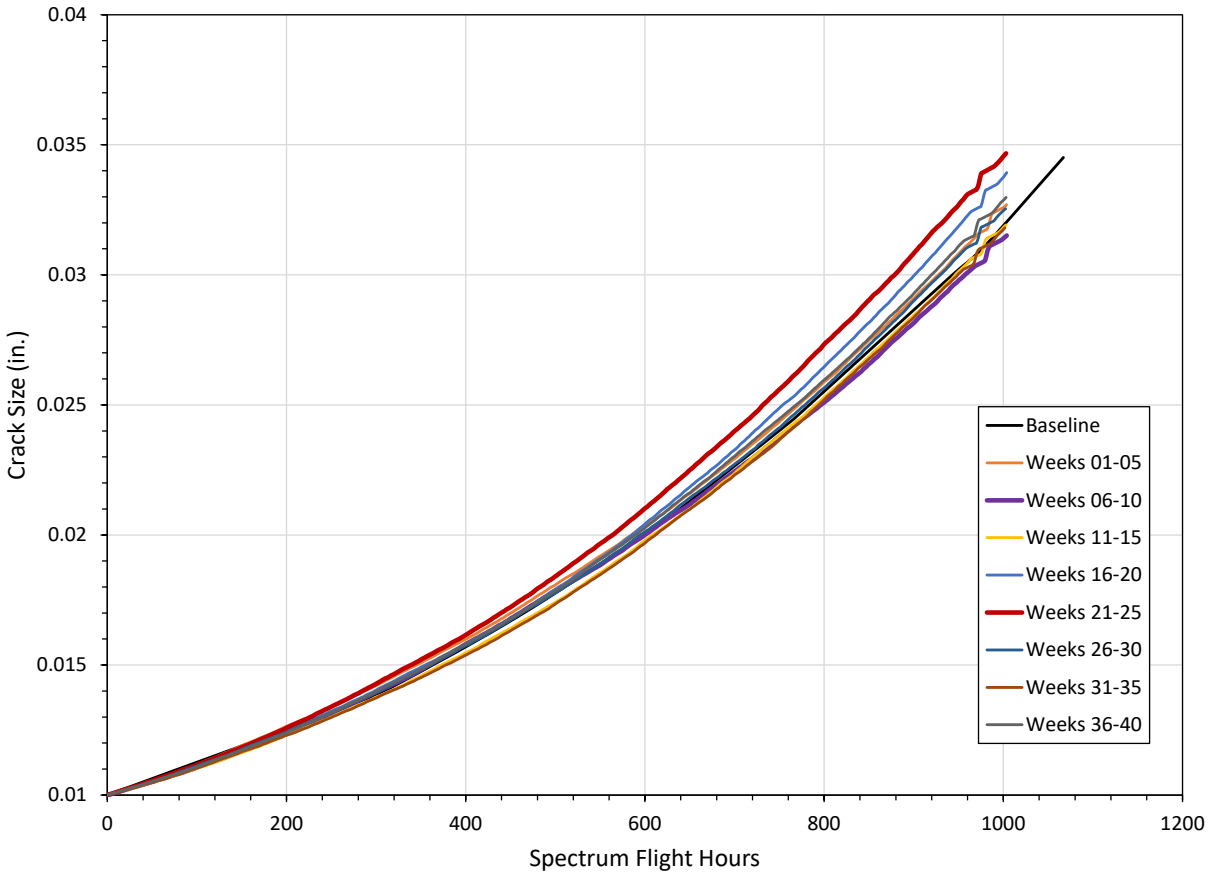

Figure 13. Comparison of Five-Week Loading Severity for CP03 RW

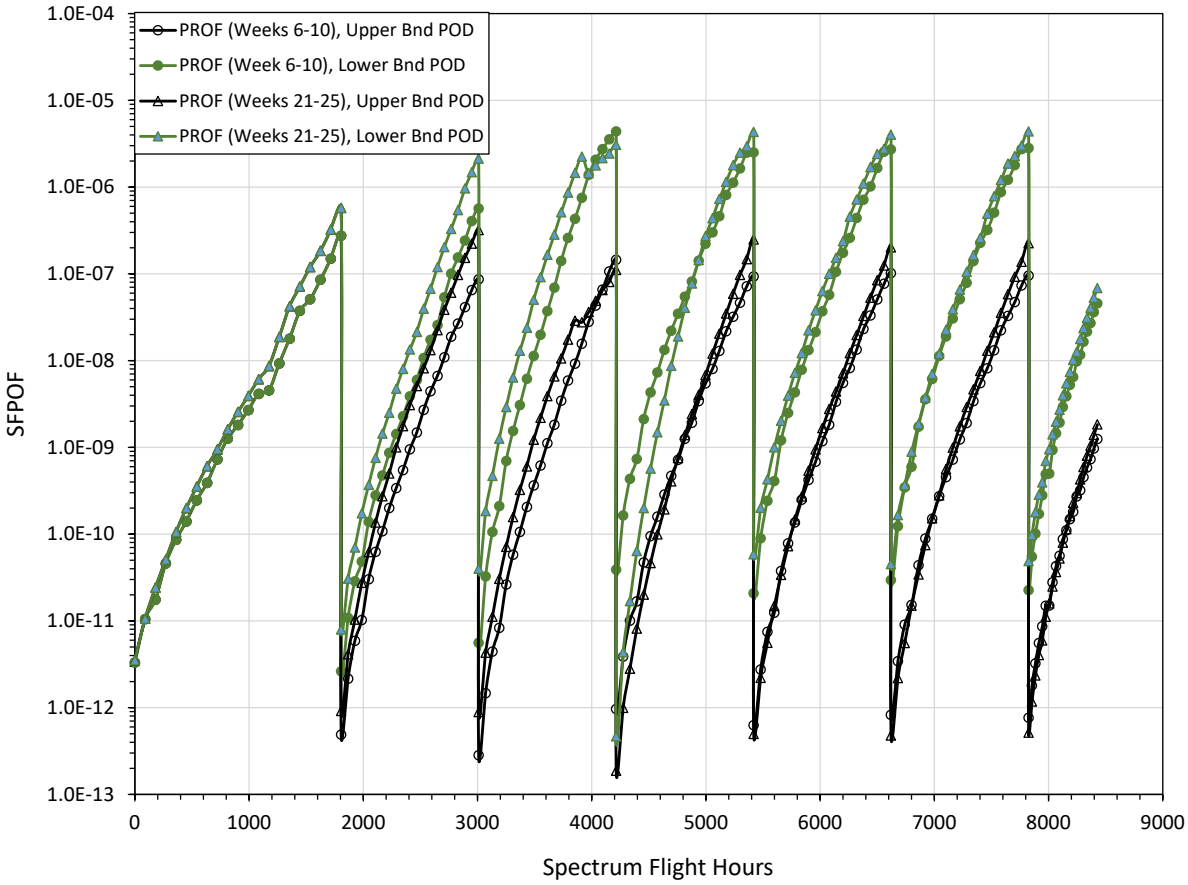

Figure 14. Comparison of the Effect of Loading and POD on SFPOF for CP03 RW, CIAT Inspection Intervals

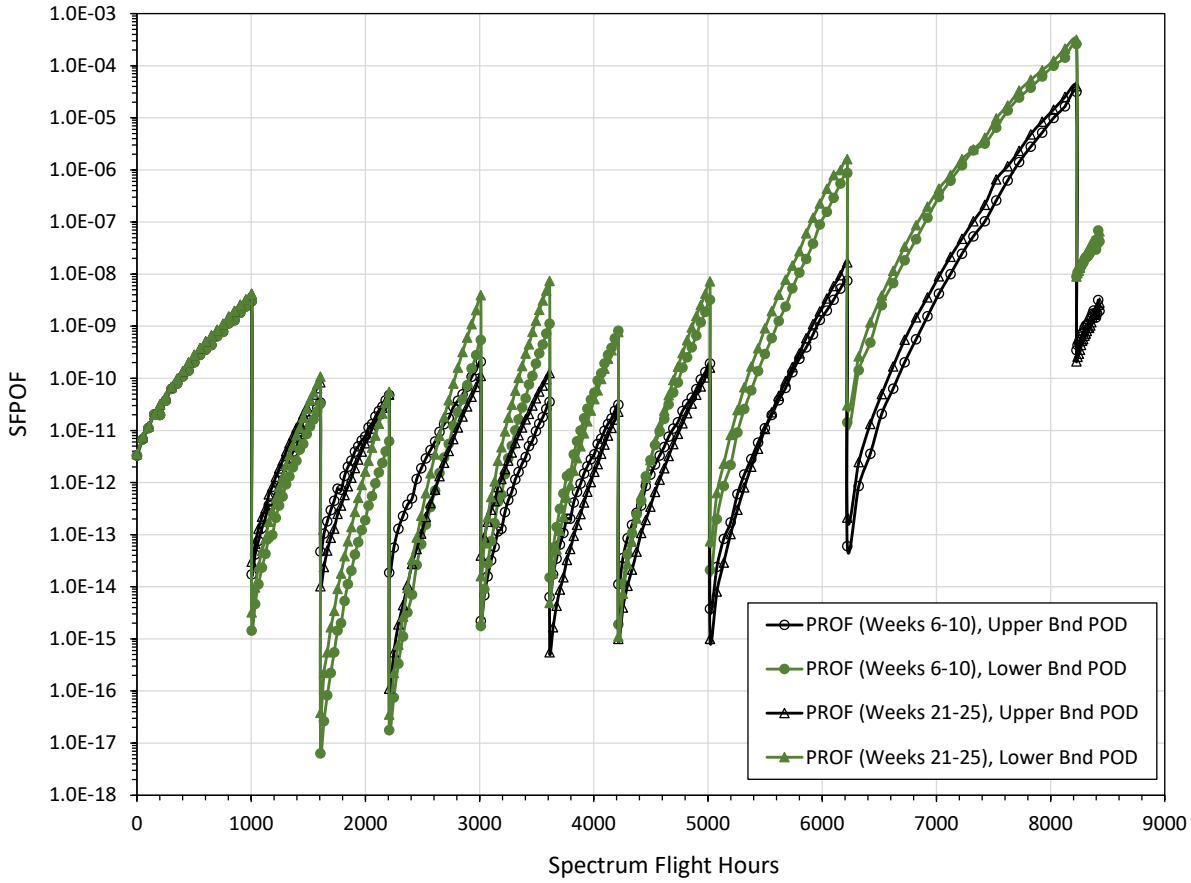

Figure 15. Comparison of the Effect of Loading and POD on SFPOF for CP03 RW, P²IAT Inspection Intervals

Comparisons of five-week loading spectra severity for CP04, CP07, CP08, CP09, CP10, CP11, CP12 and CP13 RW are shown in Figure 16 to Figure 23. The crack growth curves for CP04 RW do not extend to 1,000 SFH because the crack grows to a size that net section yielding occurs around 700 SFH. The loading block for Weeks 21-25 is the most severe for all these CPs, as it was for CP03. This five-week loading block was used as the repeating load spectrum for the crack growth calculations in the PROF analyses for all CPs on the RW.

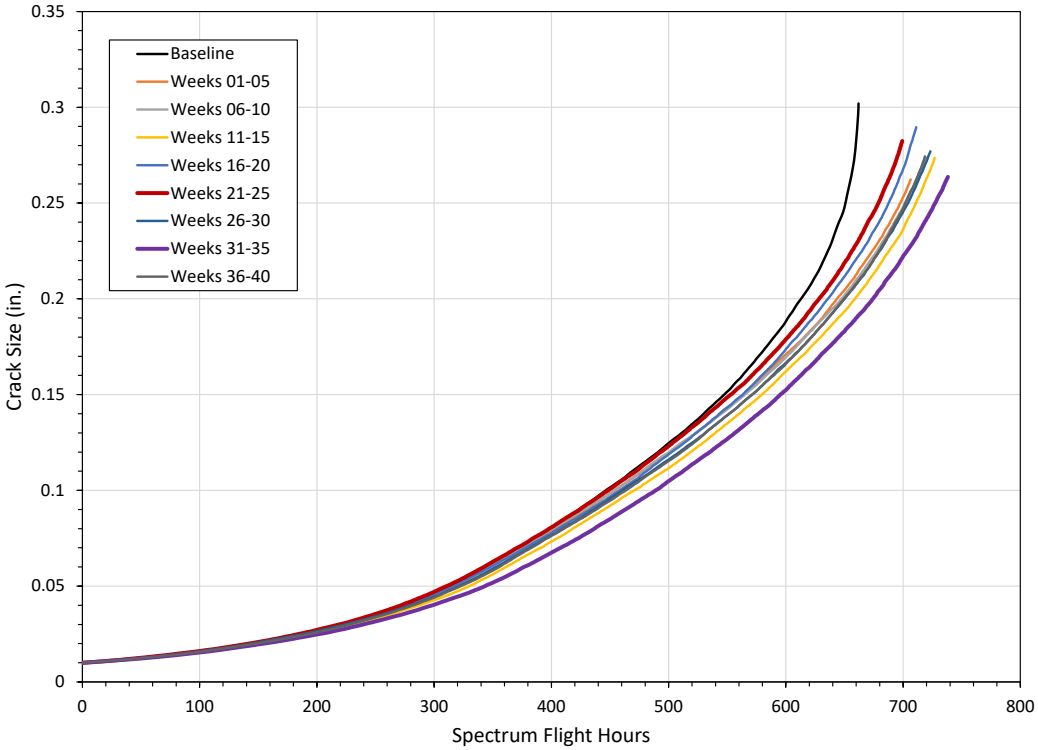

Figure 16. Comparison of Five-Week Loading Severity for CP04 RW

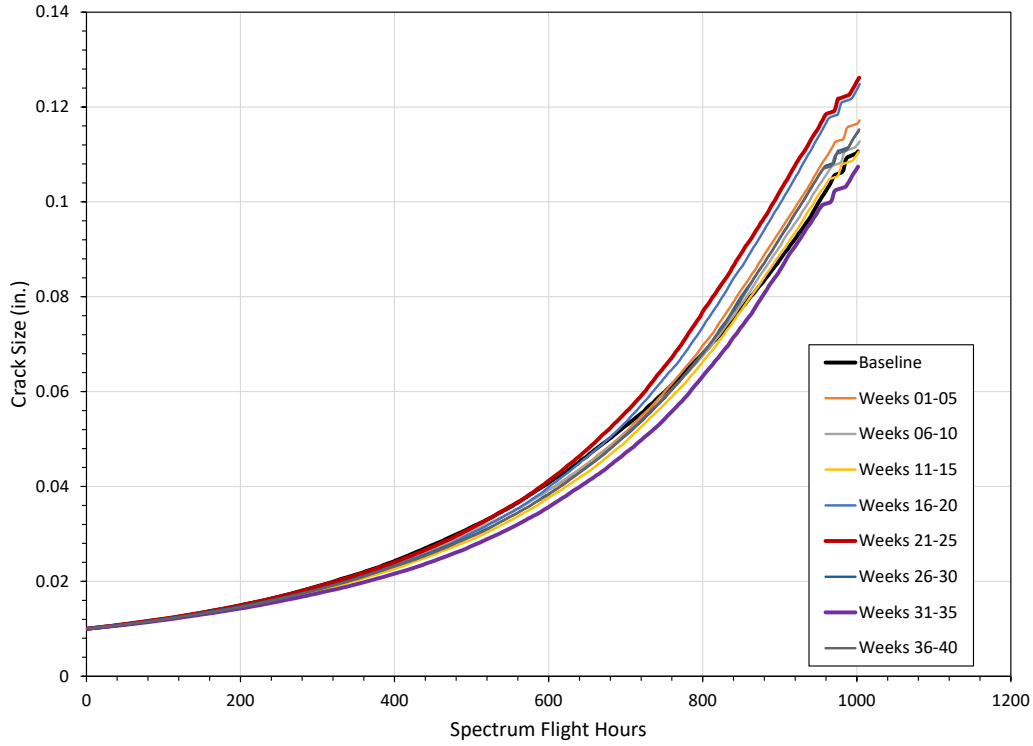

Figure 17. Comparison of Five-Week Loading Severity for CP07 RW

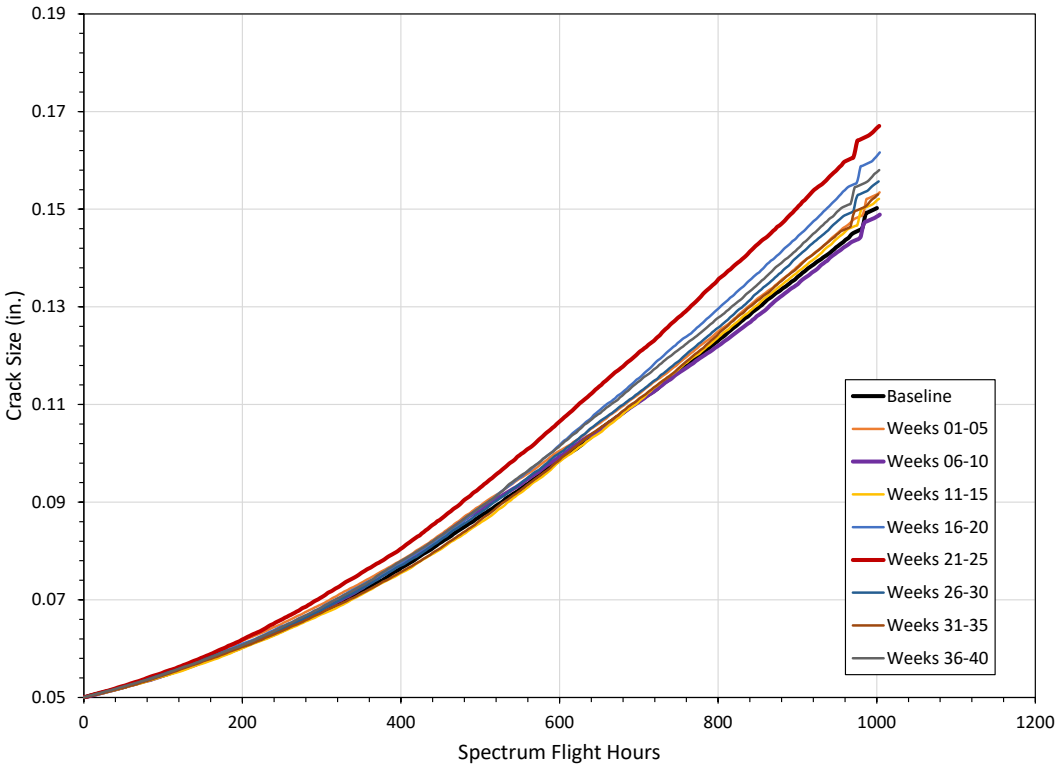

Figure 18. Comparison of Five-Week Loading Severity for CP08 RW

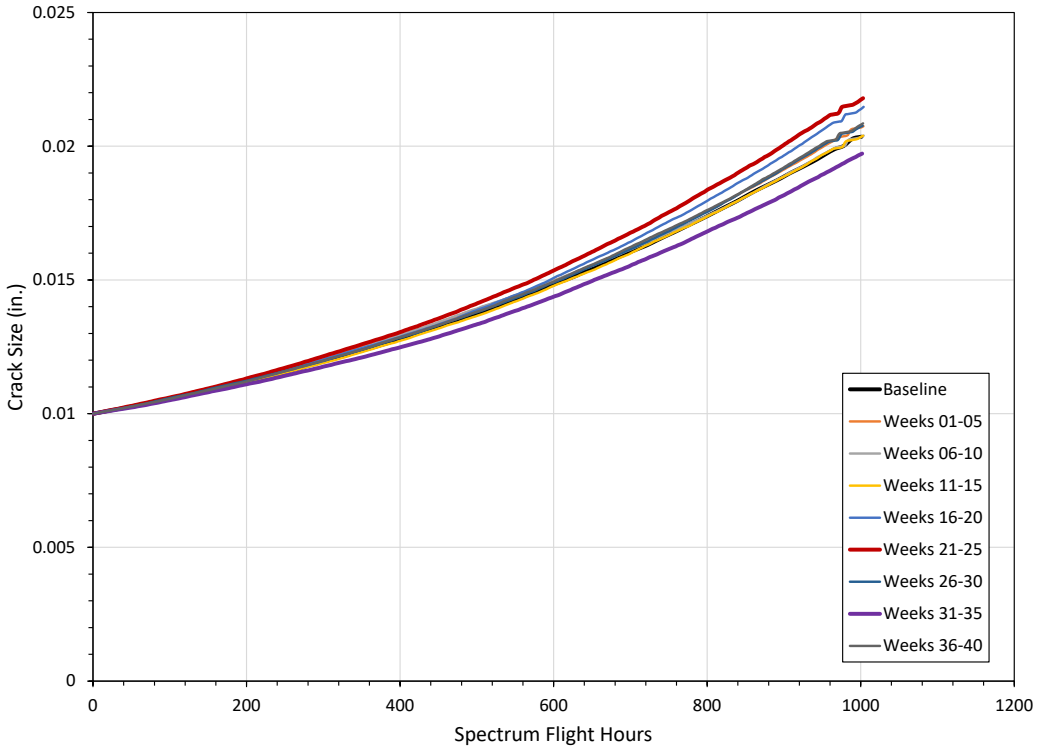

Figure 19. Comparison of Five-Week Loading Severity for CP09 RW

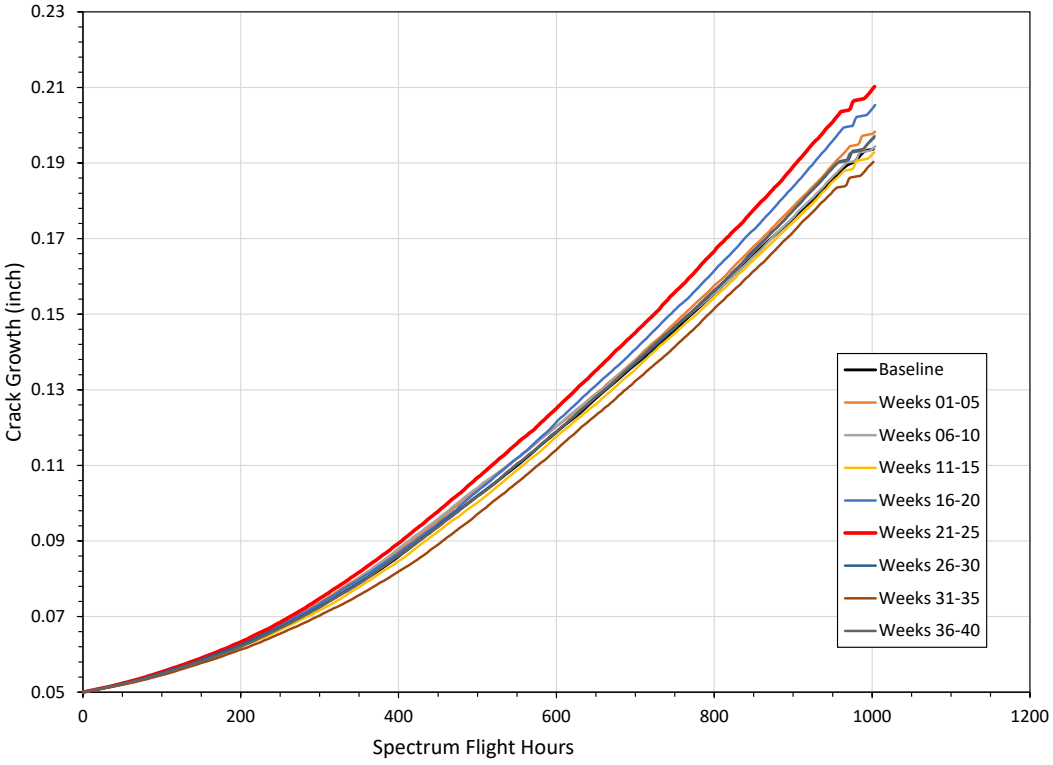

Figure 20. Comparison of Five-Week Loading Severity for CP10 RW

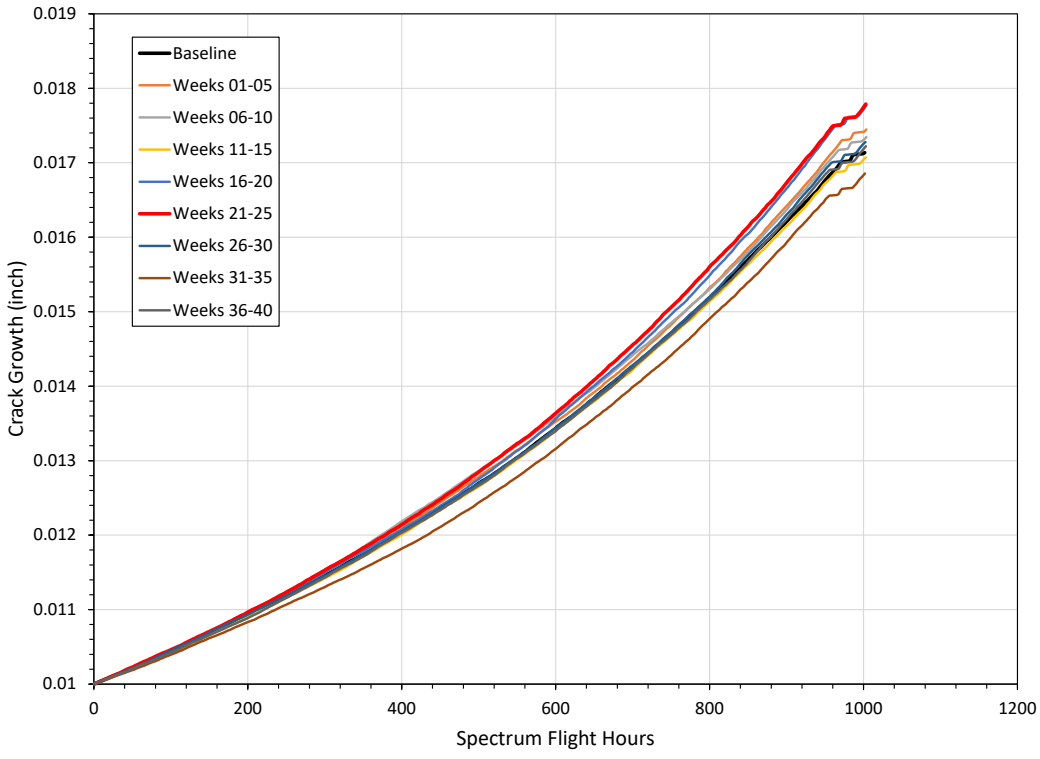

Figure 21. Comparison of Five-Week Loading Severity for CP11 RW

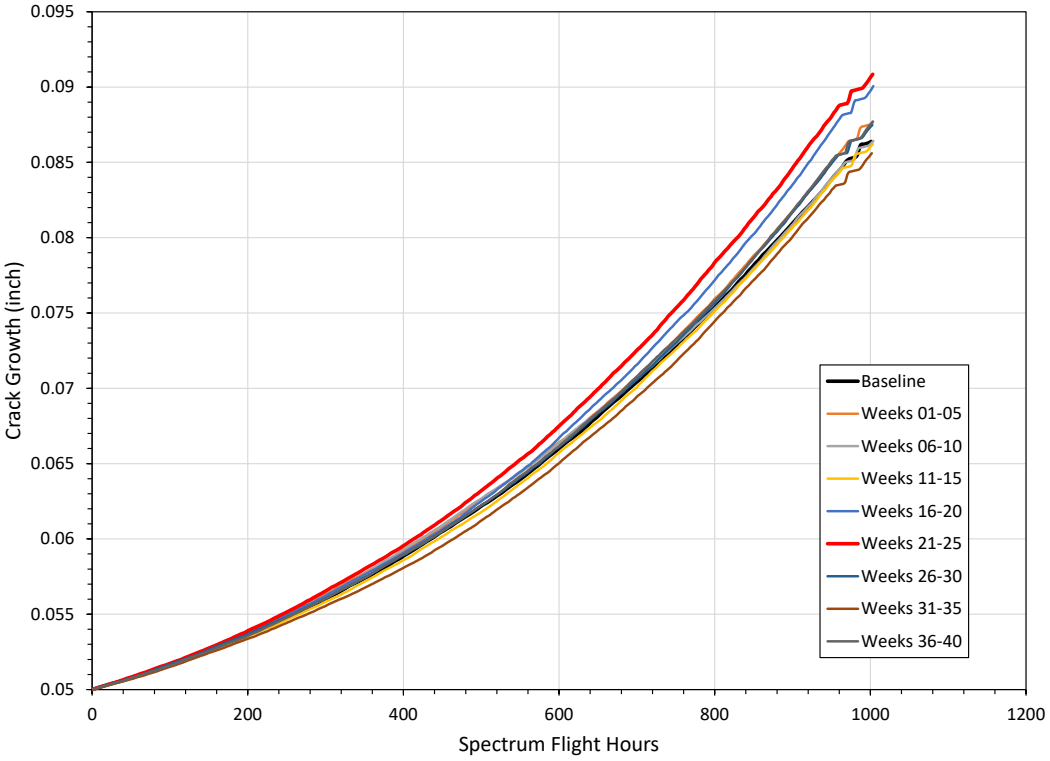

Figure 22. Comparison of Five-Week Loading Severity for CP12 RW

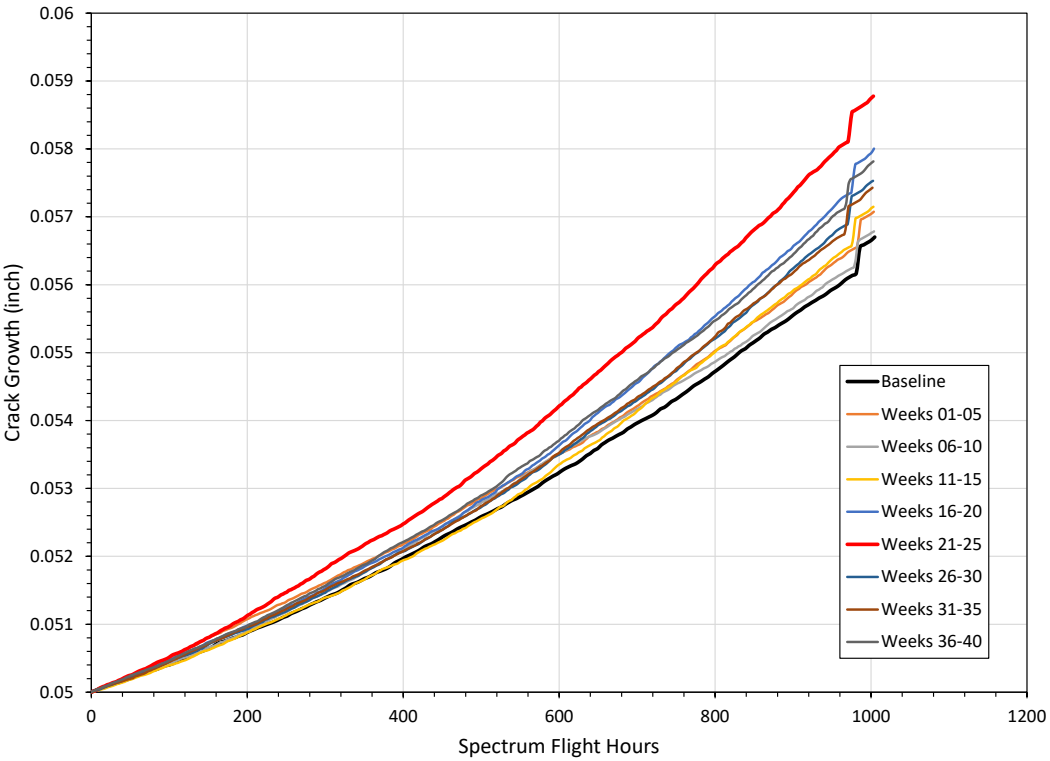

Figure 23. Comparison of Five-Week Loading Severity for CP13 RW

Comparisons of five-week loading spectra severity for CP03, CP04, CP07, CP08, CP09, CP10, CP11, CP12, and CP13 LW are shown in Figure 24 to Figure 32. There is less variation in each of the five-week loading spectra for the LW than the RW, and all the five-week loading spectra are less severe than the baseline spectrum. Weeks 6-10 loading is most severe for CP03, CP07, CP08, CP10, CP12, and CP13 LW. The loading in Weeks 26-30 is the most severe for CP04 LW. Weeks 11-15 are the most severe loading for CP11 LW. Here again, the crack growth curves for CP04 LW do not extend to 1,000 SFH because the crack grew to a size that net section yielding occurred at around 800 SFH in the crack growth analysis.

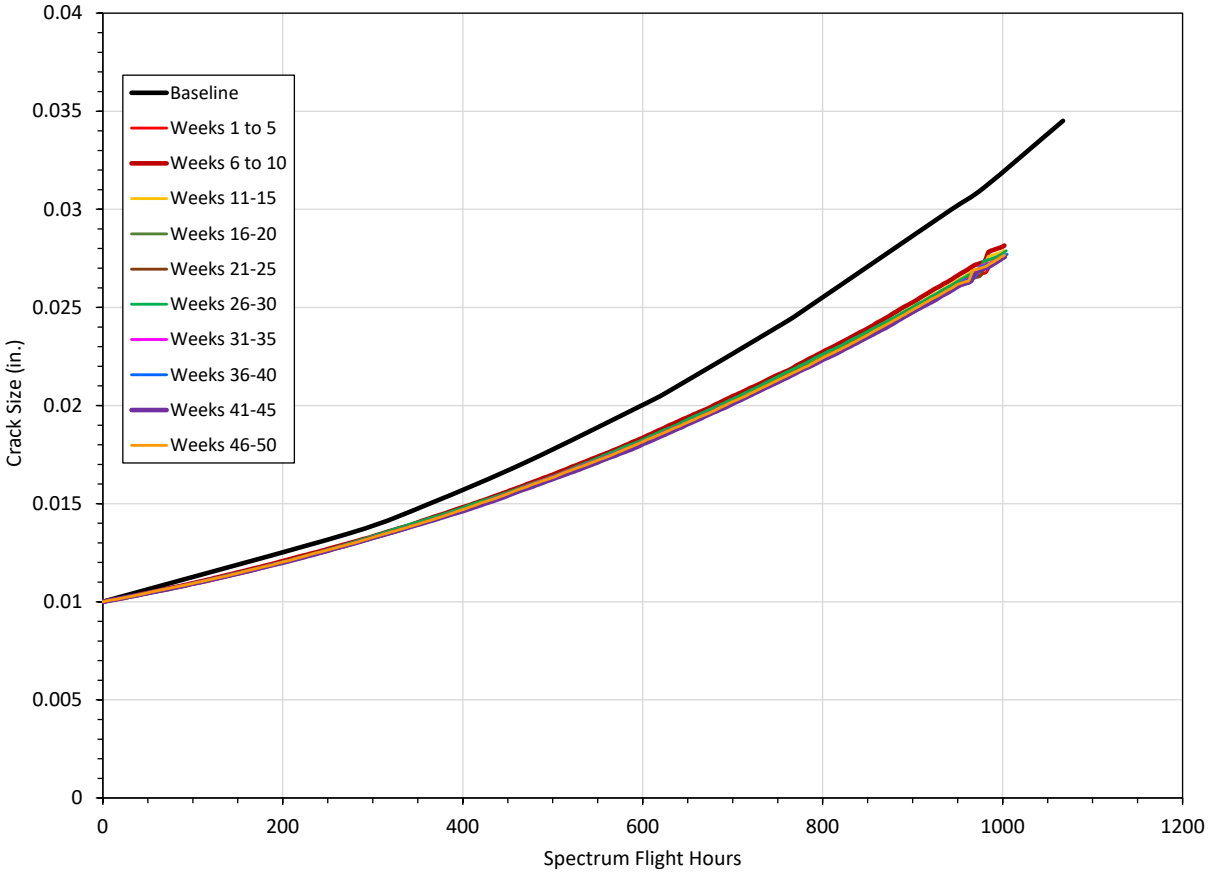

Figure 24. Comparison of Five-Week Loading Severity for CP03 LW

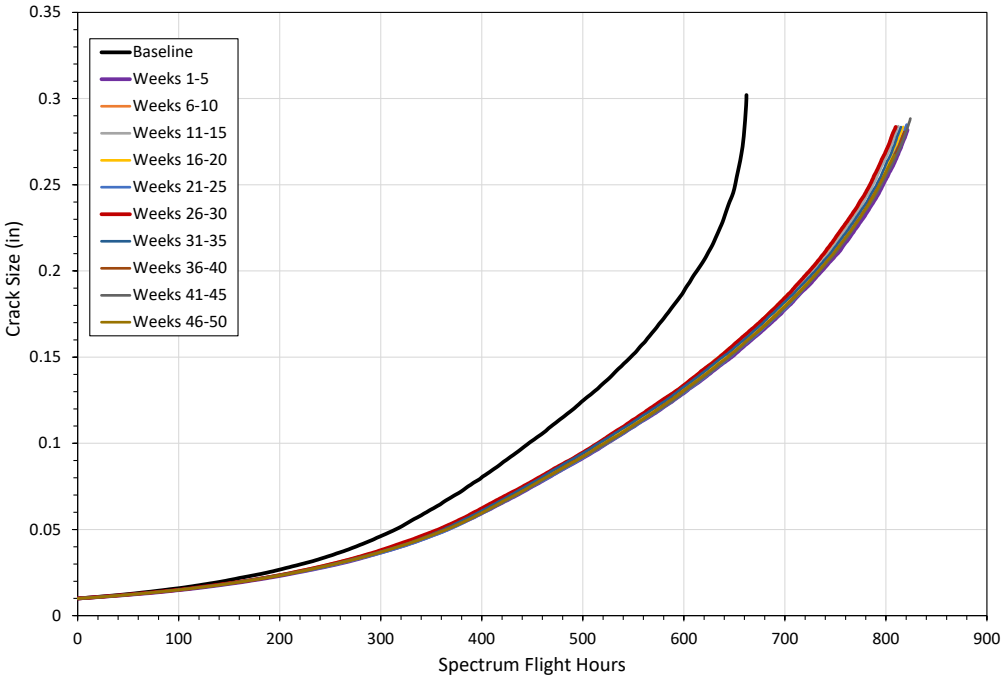

Figure 25. Comparison of Five-Week Loading Severity for CP04 LW

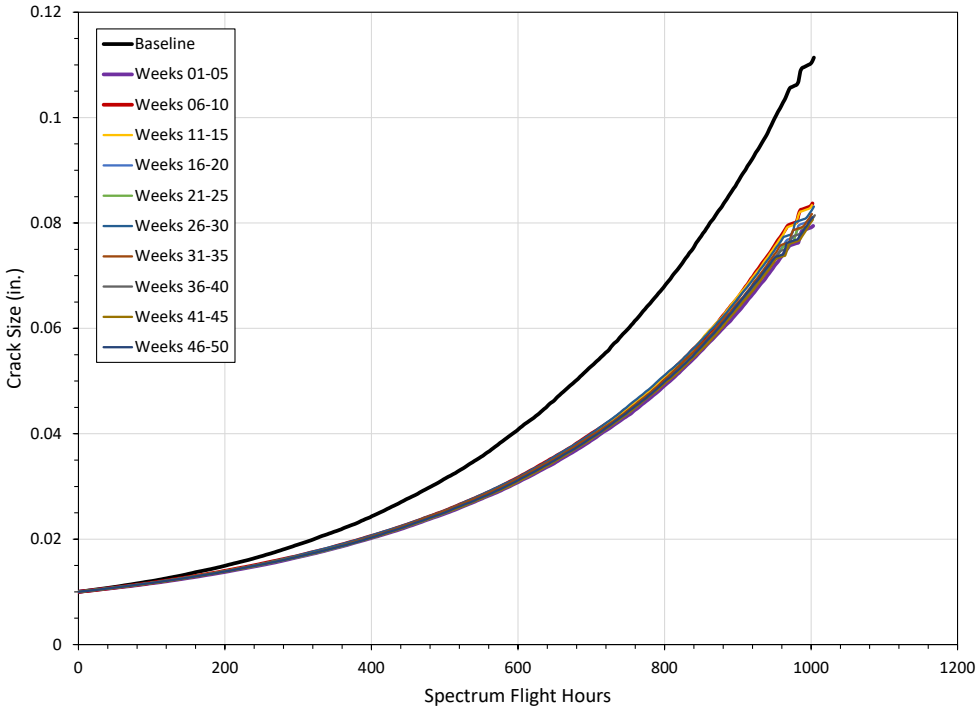

Figure 26. Comparison of Five-Week Loading Severity for CP07 LW

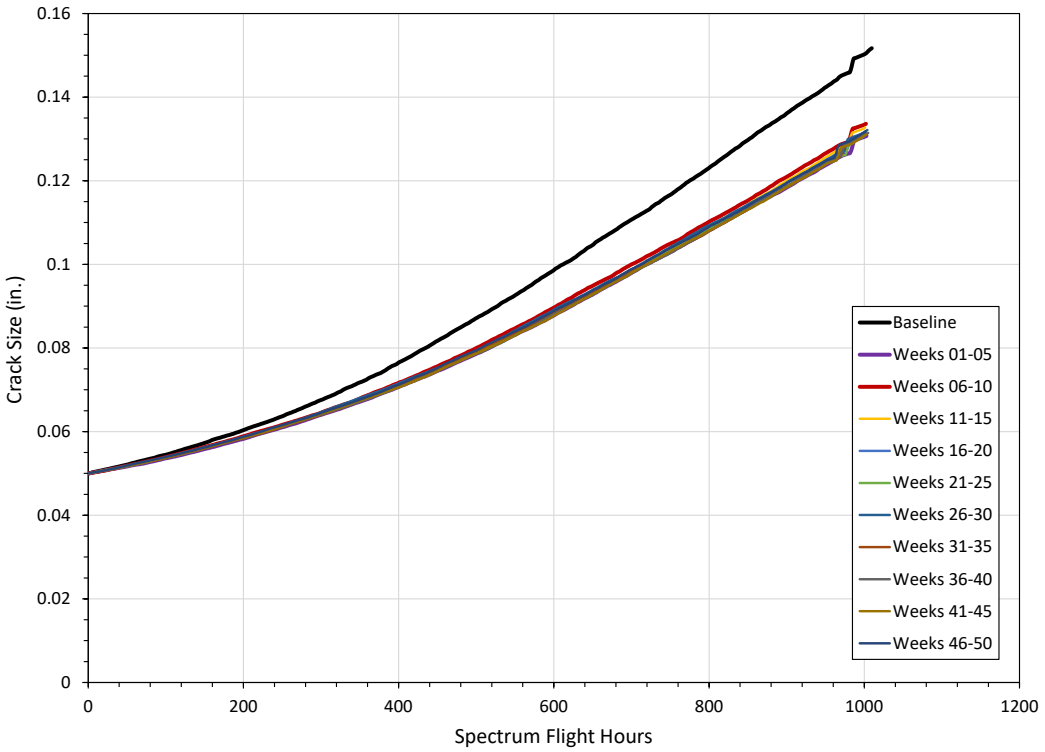

Figure 27. Comparison of Five-Week Loading Severity for CP08 LW

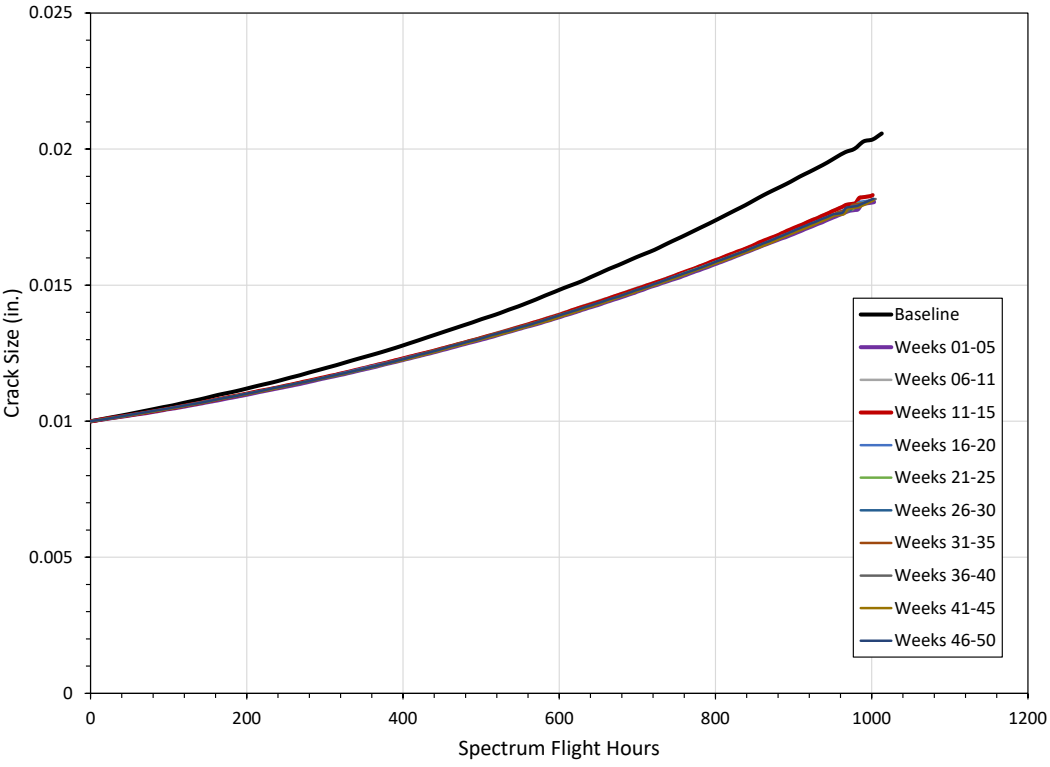

Figure 28. Comparison of Five-Week Loading Severity for CP09 LW

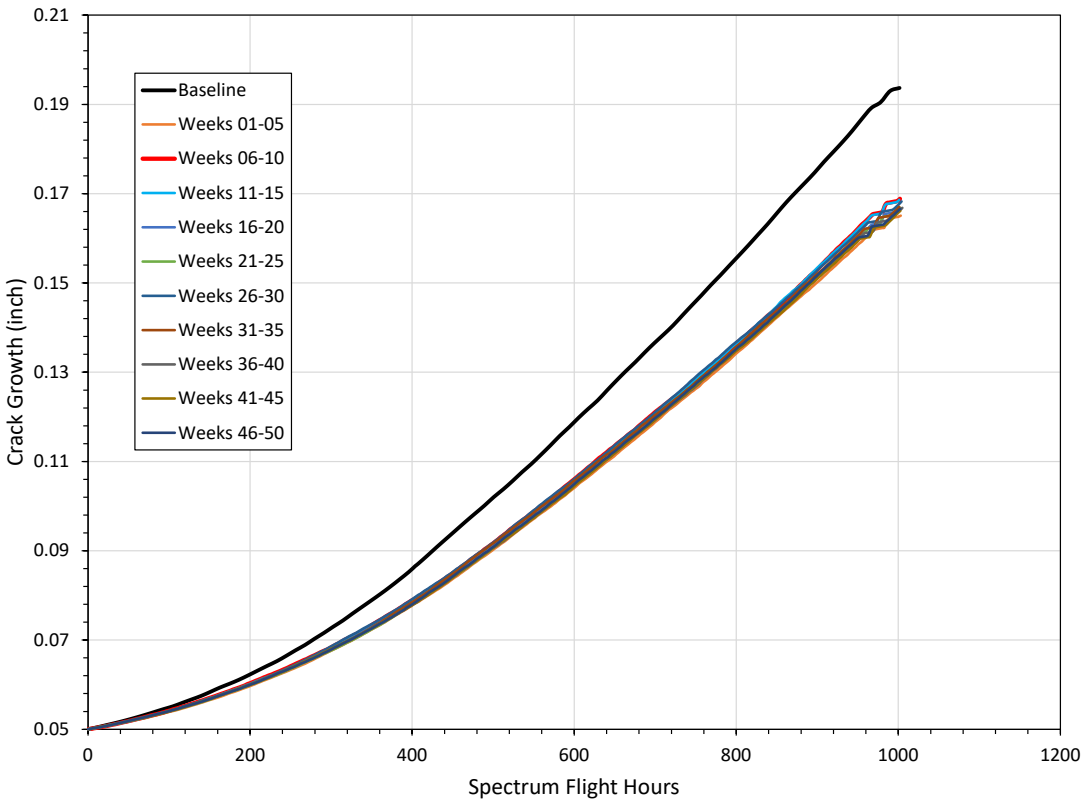

Figure 29. Comparison of Five-Week Loading Severity for CP10 LW

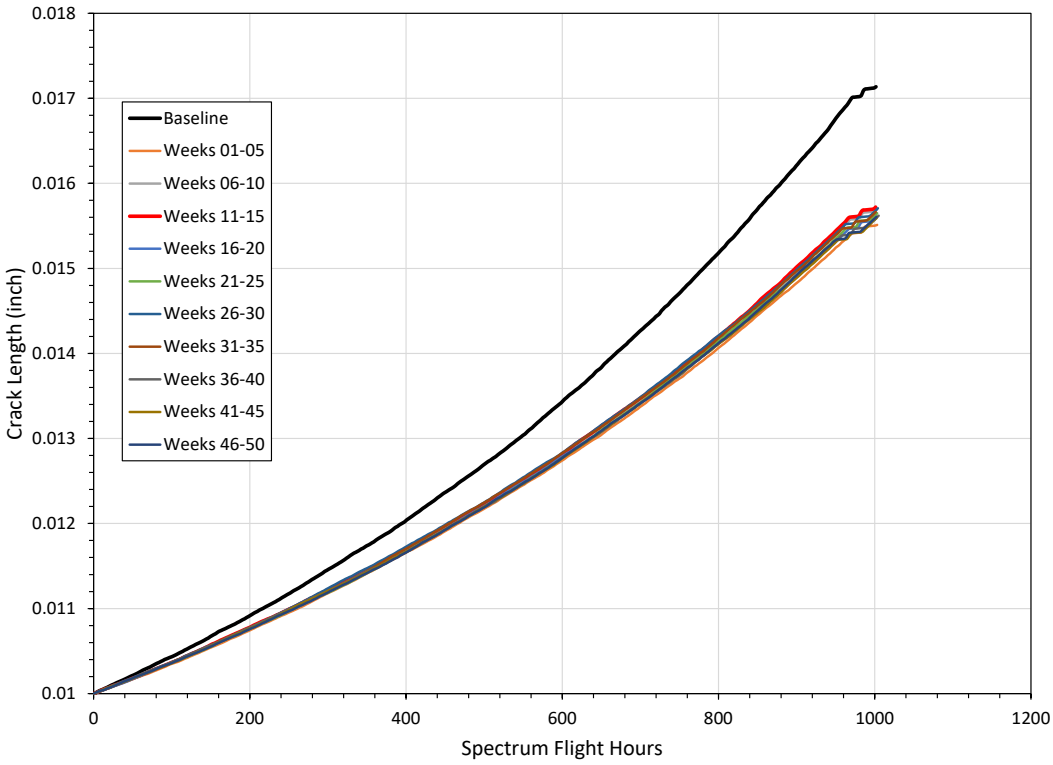

Figure 30. Comparison of Five-Week Loading Severity for CP11 LW

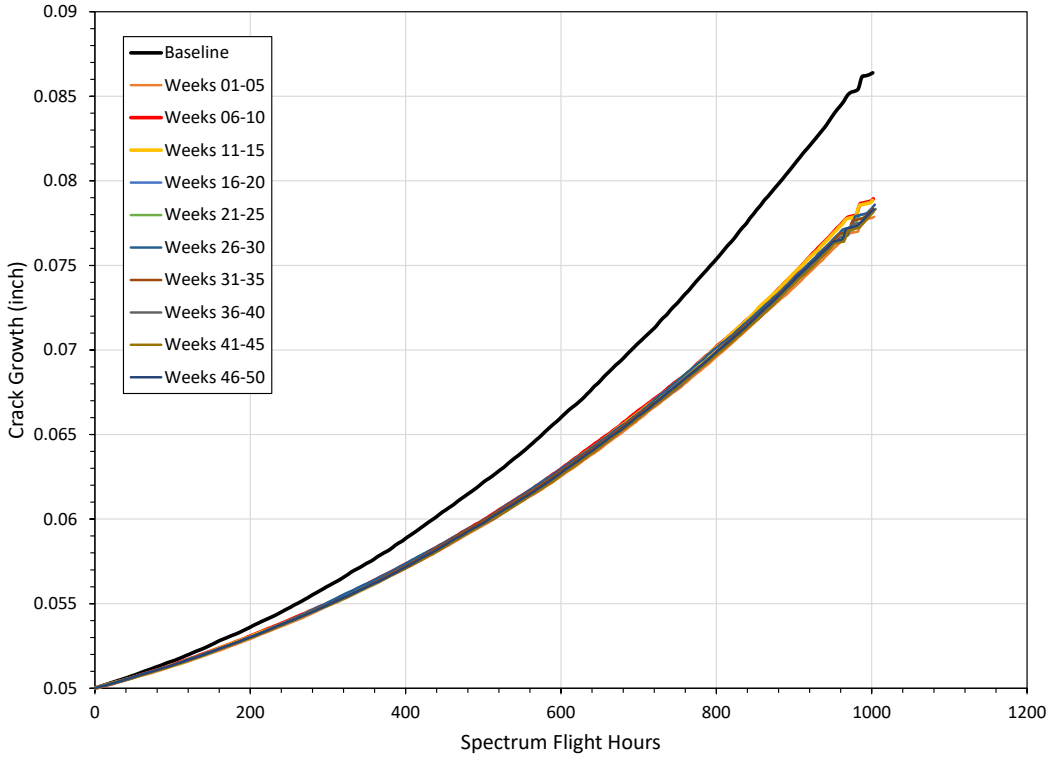

Figure 31. Comparison of Five-Week Loading Severity for CP12 LW

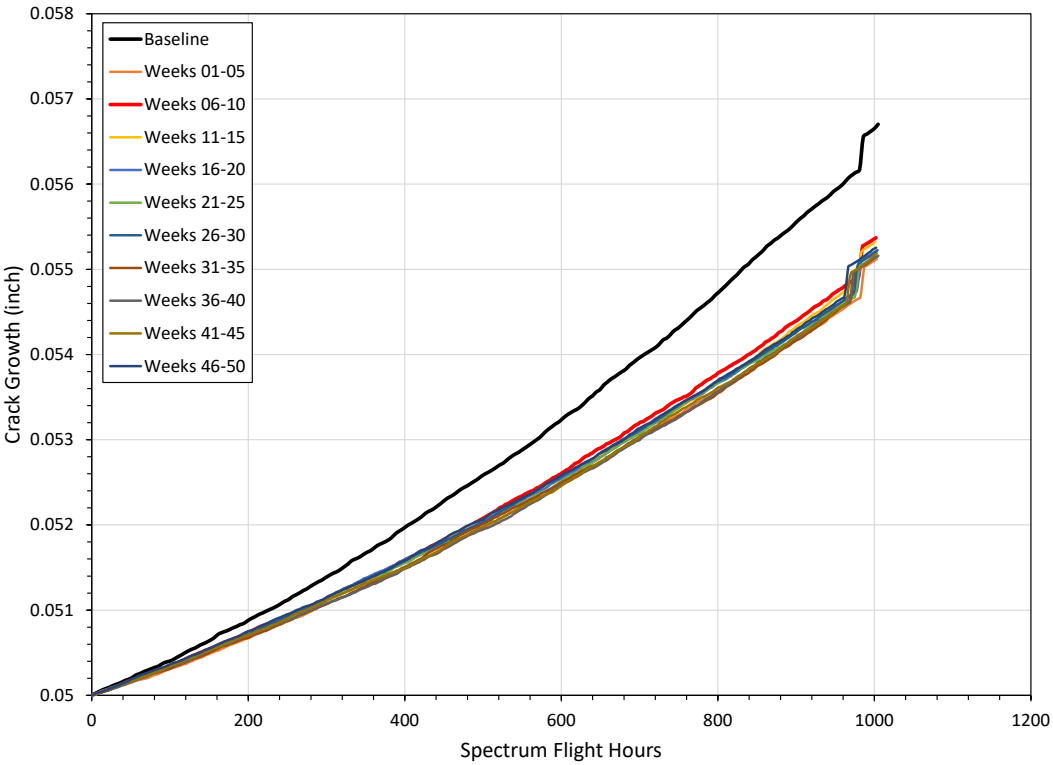

Figure 32. Comparison of Five-Week Loading Severity for CP13 LW

3.4 Comparing PROF Results to P^{2}IAT Results

P^{2}IAT provides SFPOF versus number of flights. This is because as part of its sampling routine, P^{2}IAT chooses flights of different duration for each sample when forecasting. Only when P^{2}IAT is analyzing the applied loading from each week do all the samples have flights of the same duration. PROF, on the other hand, provides SFPOF versus flight hours. In order to compare results from the two programs, the results must have a common basis. P^{2}IAT results for the applied loading were converted to flight hours using the known SFH for each flight.

SFPOF calculated by PROF for the CIAT inspection schedule was compared to SFPOF calculated by P^{2}IAT. If CIAT did not maintain SFPOF at or below 10^{-7}, PROF was run with the P^{2}IAT inspection schedule to see if SFPOF remained below 10^{-7} with the more frequent inspections.

4 RESULTS AND DISCUSSION

The P^{2}IAT software is a prototype code meant to assess and demonstrate the feasibility of a probability of failure-based fatigue tracking approach. As such, some peculiar responses were noted. These will be discussed when comparing P^{2}IAT to CIAT and PROF.

One inefficiency was noted that should be fixed in the next development iteration. When usage (applied loading) is provided at the end of a week, P^{2}IAT analyzes the effect of the applied loads on the fatigue damage in the structure and then makes a forecast of how the fatigue damage will grow 1,000 flights into the future. Before usage from the next week can be analyzed however, the usage from the current IAT reporting period must be re-analyzed, but with forecasting turned off. It seems that if the analysis of the applied loading from the first run could be saved separate from the forecast, the second "no forecasting" run could be eliminated.

Many uncertainties are included in P^{2}IAT that PROF does not consider. Including these uncertainties initially was intended to make P^{2}IAT more representative of the actual wings, a Digital Twin. The thinking was that Bayesian updating of the P^{2}IAT analysis with actual loading data and inspection results would significantly reduce the overall uncertainty and bring consistency to the SFPOF calculations. It is not clear that updating the analysis reduced the uncertainty significantly.

P^{2}IAT is a probabilistic program that relies on sampling to estimate probabilities. The analyst selects the number of samples for each analysis. More samples increases the execution time. Fewer samples reduces the execution time, but too few samples affects the reproducibility of the results. Different answers from the same inputs is unacceptable. When re-running some analyses, the time when an inspection is called for sometimes shifted one IAT reporting period forward or back from a previous analysis. This seemed to happen because of differences in the randomly selected samples in the two runs. Increasing the number of samples used in the analysis ought to eliminate this behavior; however, a thorough study is needed to determine the appropriate number of samples to obtain repeatable results.

In addition, the sampling method and number of samples used in P^{2}IAT gave inconsistent POF results from flight to flight such that a curve fit to the POF for all the flights in an analysis period was needed to estimate the probability of failure and SFPOF [3]. It is not known whether there was any effort to ensure continuity of the POF function across IAT reporting periods (200 SFH blocks) or not. It is very likely that there was not based upon the fact that sampling was used in all POF calculations. It is difficult to ensure that two sets of samples drawn from the same distribution will give the same distribution in reverse unless a large number of samples are drawn. P^{2}IAT used 2,500 samples in most cases here which is not enough. More samples, in the range of 5,000 to 10,000, should be tried to see if more consistent SFPOF values result.

The fatigue crack growth algorithm only used the Region II of the crack growth rate curve (the Paris region) in the crack growth calculations. This enabled easy introduction of variability in the fatigue crack growth rate into P^{2}IAT, but it misses the threshold and asymptotic behavior in Regions I and III. In addition, it was found in [3] that the majority of the variance in the flights to failure is the initial crack size and the marginal distribution of the error term that was added to the crack growth rate on top of the variability. The variability in the crack growth rate curve can

likely be disregarded. In addition, the error term was based upon test data from a few coupons and may not be realistic.

Another peculiarity in the fatigue crack growth model was the crack size distributions for some locations forecasted 95th and higher percentile crack sizes of 100 inches in some reporting periods. The ligament available for crack growth is less than one inch at every CP except CP11. It is not clear if this is a flag to indicate that fracture had occurred, or if this value is used in an actual calculation. If cracks at this percentile and up would cause fracture, how is this handled in drawing samples and calculating the forecasted SFPOF? This makes a big difference when forecasting SFPOF.

4.1 P^{2}IAT Results

The major goal for the P^{2}IAT approach to fatigue tracking was reducing the frequency of structural inspections. There was a sense that inspections in CIAT occurred when the SFPOF was much less than 10^{-7}. Scheduling inspections only when SFPOF is expected to reach 10^{-7} ought to reduce the number of inspections then. However, results from the demonstration were that P^{2}IAT had the same or greater number of inspections than CIAT as shown in Figure 33 and Figure 34.

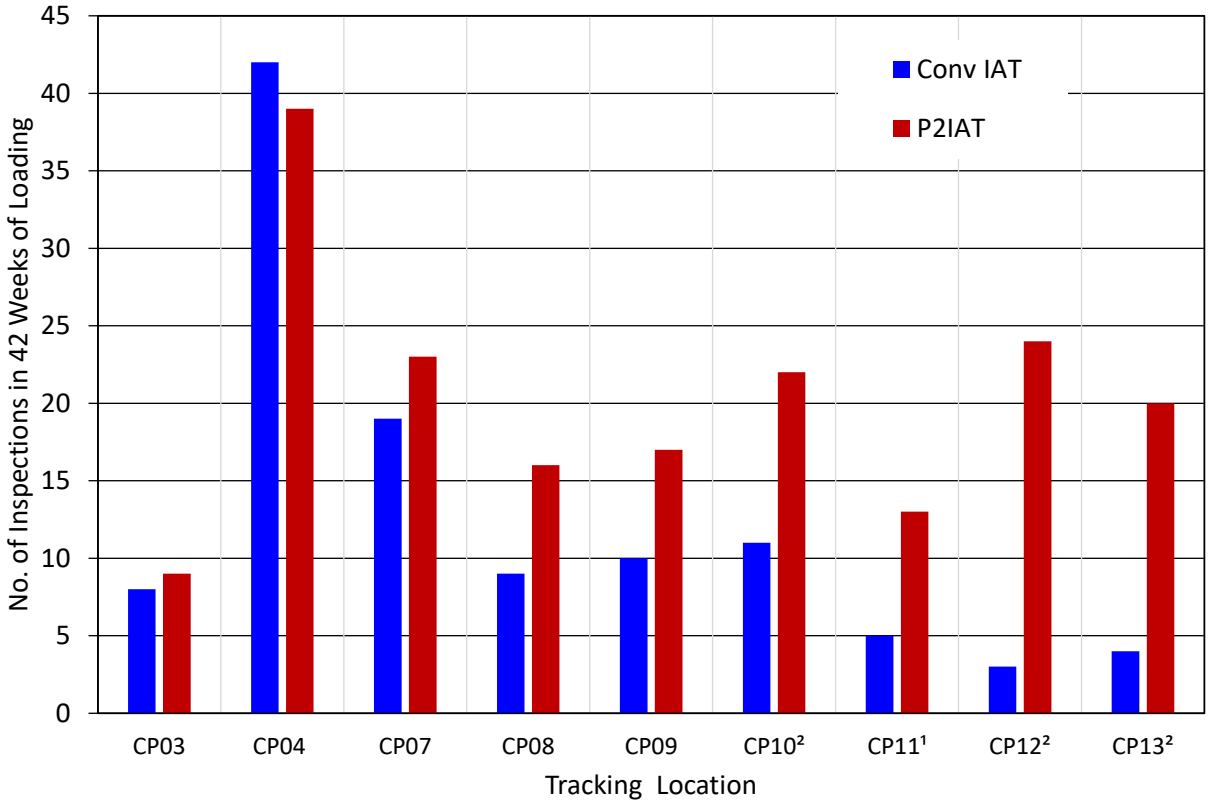

¹ Jentek sensor at CP11 no longer operational after Week 17. IAT stopped at Week 17.
² Jentek system not operational after Week 25. IAT stopped at Week 25.

Figure 33. Number of Inspections for the Right Wing with each IAT Method in 42 Weeks of Loading

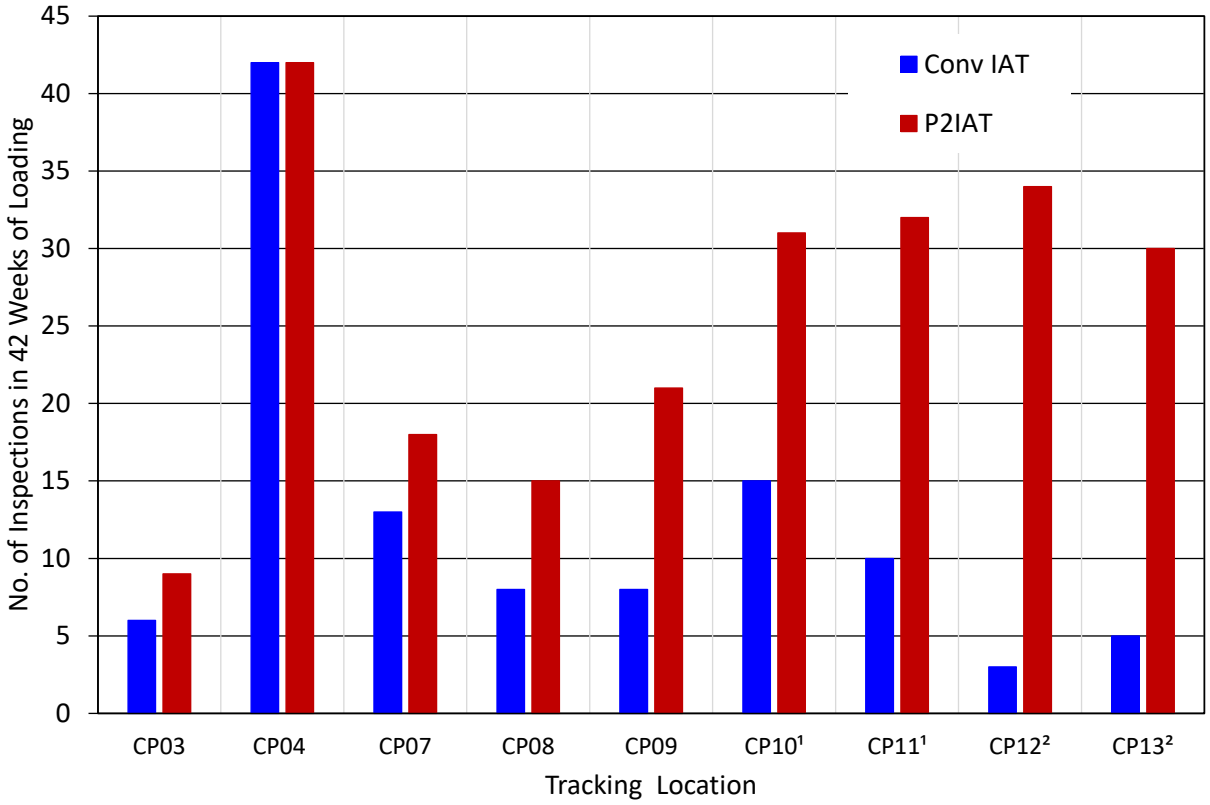

¹ Jentek sensors no longer operational after Week 34. IAT stopped at Week 34.
² Jentek system not operational after Week 36. IAT stopped at Week 36.

Figure 34. Number of Inspections for the Left Wing with each IAT Method in 42 Weeks of Loading

One location on both wings, CP04, required inspections at the end of every week of loading in CIAT. P^{2}IAT required inspections at the end of every week at CP04 LW. Inspections were required by P^{2}IAT at CP04 RW at the end of every week except Weeks 34, 39, and 42. Inspections were not requested after these three weeks because two weeks prior, when the inspection need to be scheduled, the SFPOF was forecasted to not quite reach 10^{-7} as seen in Figure 35, Figure 36, and Figure 37.

Each week of loading was assumed to consist of 200 flights. SFPOF was forecasted for four weeks, or 800 flights, into the future. An inspection was planned at the end of any week that SFPOF exceeds 10^{-7}. If SFPOF equals 9.99×10^{-8} at the end of a week, no inspection is scheduled even though on the next flight SFPOF would likely exceed 10^{-7}. As a result, the SFPOF can reach very high values during the subsequent week. This is undesirable. Setting the threshold for an inspection at a value somewhat less than 10^{-7}, or manually intervening, might be better.

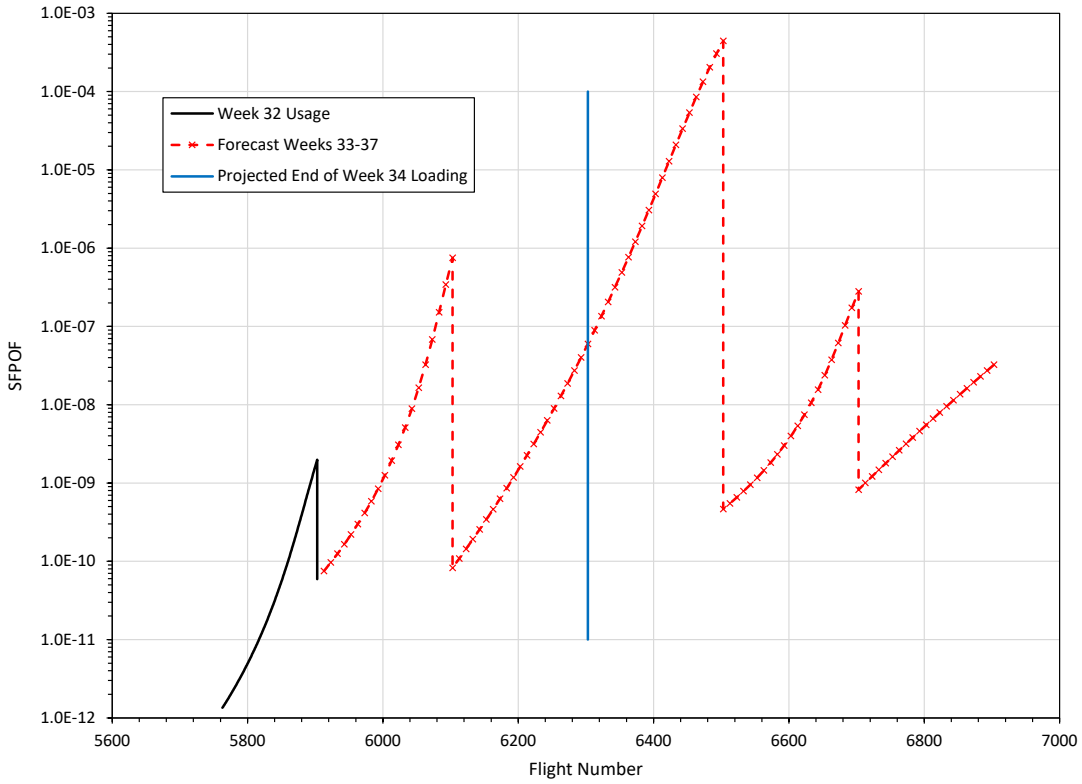

Figure 35. SFPOF Forecast after Week 32 Loading

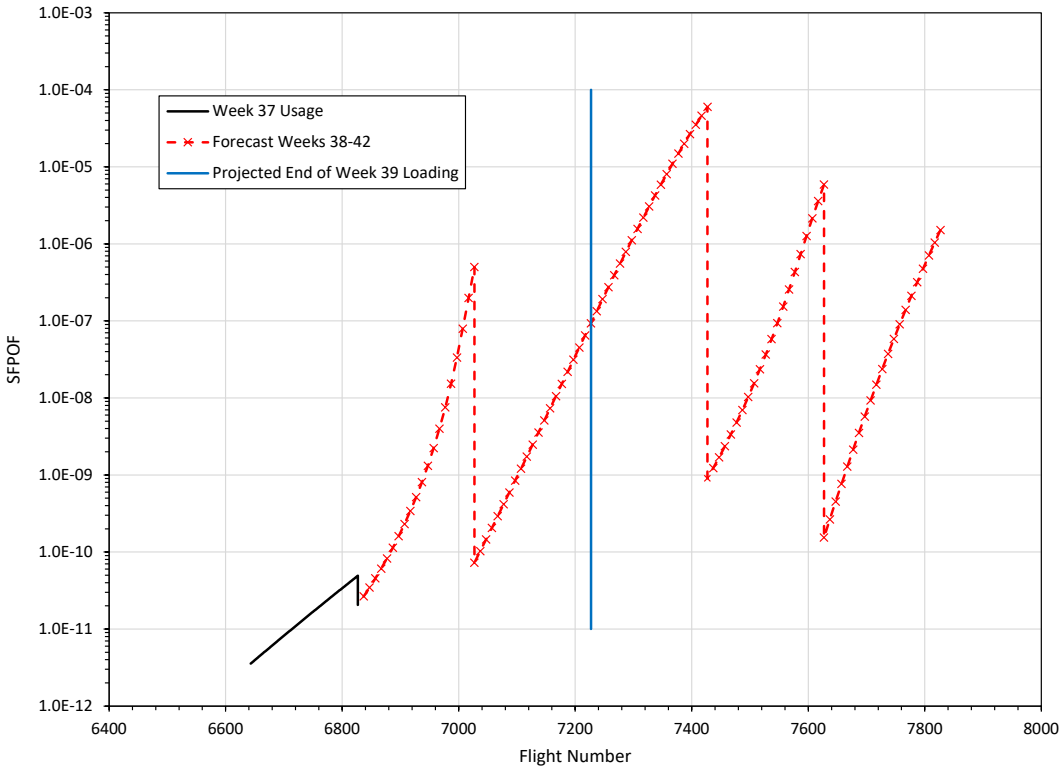

Figure 36. SFPOF Forecast after Week 37 Loading

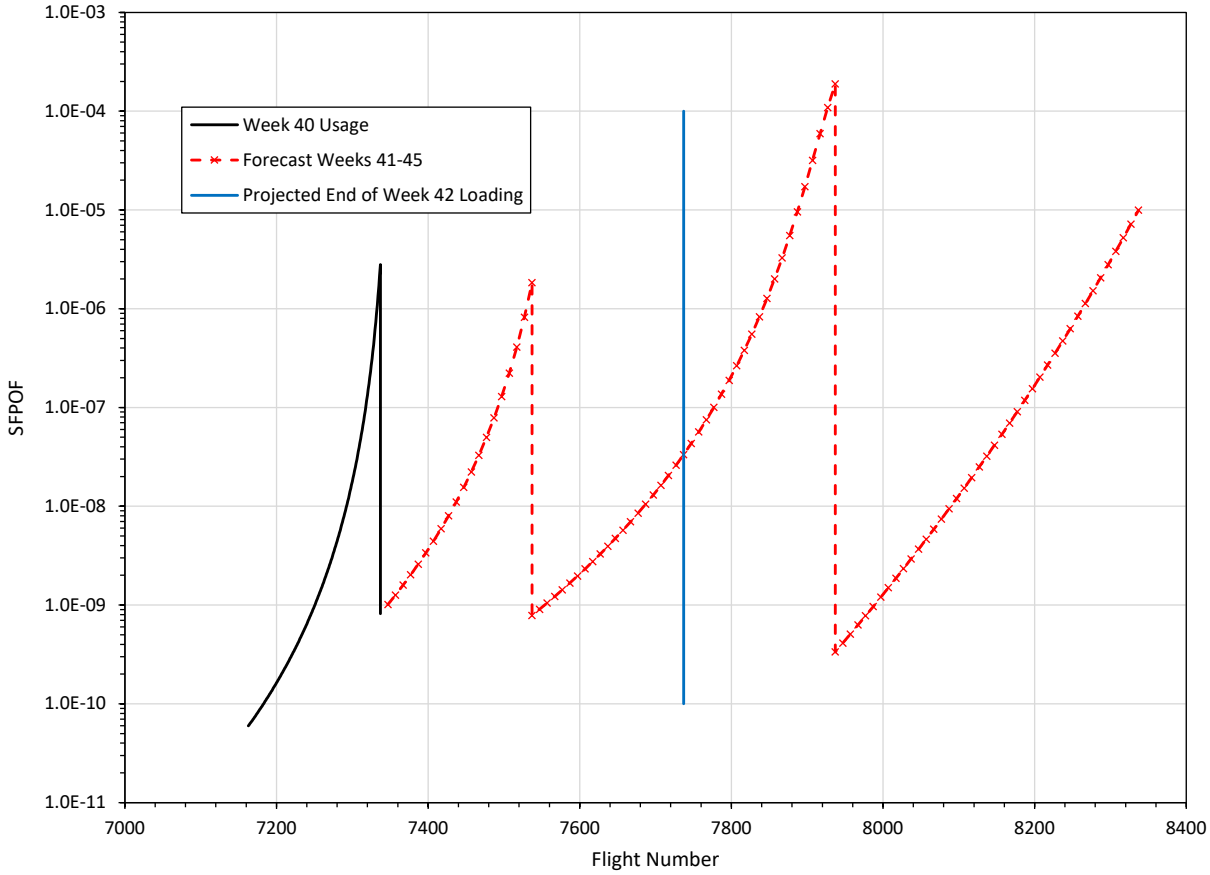

Figure 37. SFPOF Forecast after Week 40 Loading

A question that arises from Figure 33 and Figure 34 is how does SFPOF in the CIAT approach compare to SFPOF in P^{2}IAT? Is the SFPOF at an inspection under CIAT significantly less than 10^{-7}? The next section will compare SFPOF calculated by PROF for the CIAT inspection schedule with SFPOF calculated by P^{2}IAT at its inspections. The SFPOF calculated by PROF for the P^{2}IAT inspection schedule is also examined in select instances where CIAT inspections did not keep SFPOF from exceeding 10^{-7}.

4.2 Comparison of Conventional IAT and P^{2}IAT

SFPOF was determined for the CIAT approach using PROF [12] for CP03, CP04, CP07, CP08, CP10, CP11, CP12, and CP13 on both wings. The details of the procedure were discussed in Section 3.3.1.

4.2.1 Right Wing

4.2.1.1 CP03 RW

There is not much difference in the number of inspections between P^{2}IAT and CIAT for CP03 RW. P^{2}IAT calls for nine inspections while CIAT calls for eight as seen in Figure 38. Vertical lines in the graph represent inspections. The only exception is the vertical line in the P^{2}IAT curve at approximately 6,800 SFH, which is the result of an artificial decrease in SFPOF due to changes in the samples between weeks.

As shown in Figure 38, CIAT does not keep SFPOF below 10^{-7}. SFPOF is below 10^{-7} at only two CIAT inspections, though the remaining SFPOF peaks remain below the unacceptable SFPOF level of 10^{-5} [9]. After the first three inspections, P^{2}IAT does not keep SFPOF below 10^{-7} either. SFPOF exceeds 10^{-5} at 4,200 SFH with P^{2}IAT.

The SFPOF curve calculated by PROF using the P^{2}IAT inspection times in Figure 39 is about two orders of magnitude lower than the P^{2}IAT curve until about 5,500 SFH. Then as the time between P^{2}IAT inspections increases, SFPOF from the PROF analysis increases to equal and exceed the P^{2}IAT values. Using the P^{2}IAT inspections in PROF keeps SFPOF below 10^{-7} until about 6,000 SFH. After 5,000 SFH, P^{2}IAT inspections are at intervals of 1,200 SFH and 2,000 SFH instead of the previous 600 to 800 SFH interval. According to the PROF analysis, inspections every 600 to 800 SFH are necessary to keep SFPOF from exceeding 10^{-7}.

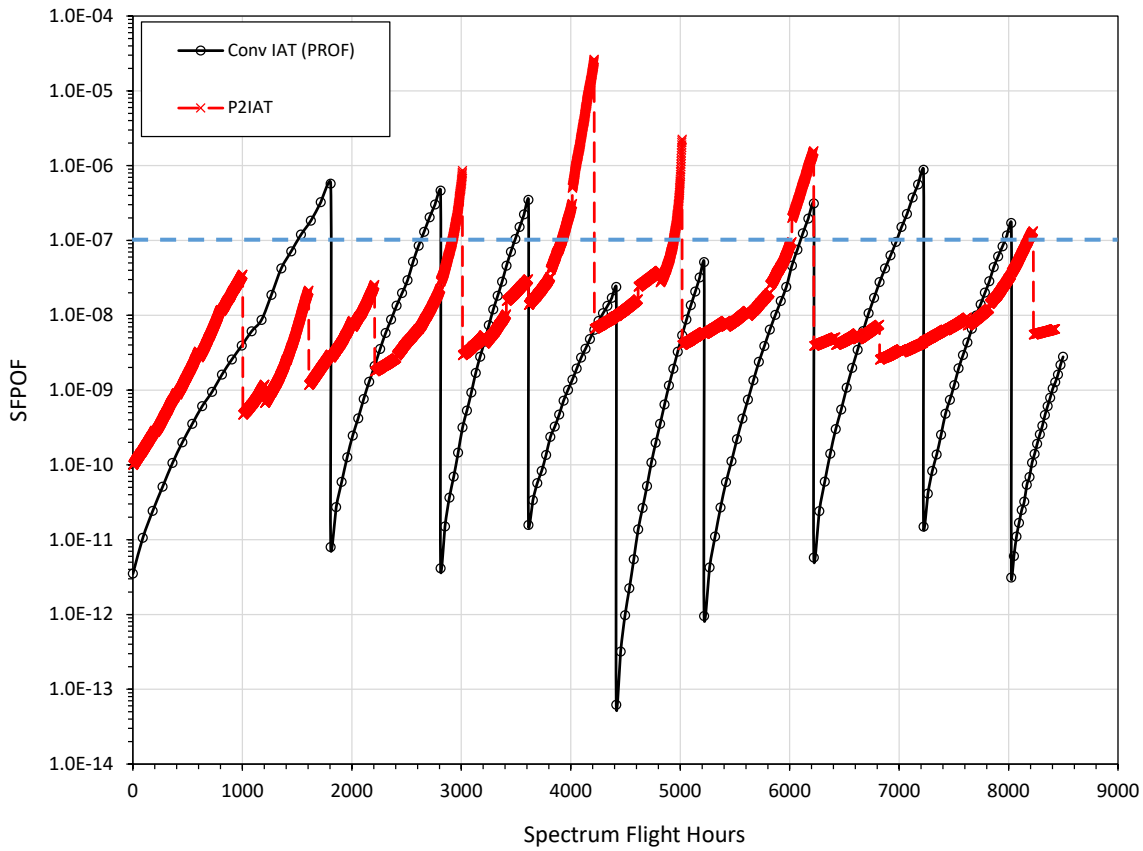

Figure 38. SFPOF for CIAT and P^{2}IAT Inspections, CP03 RW

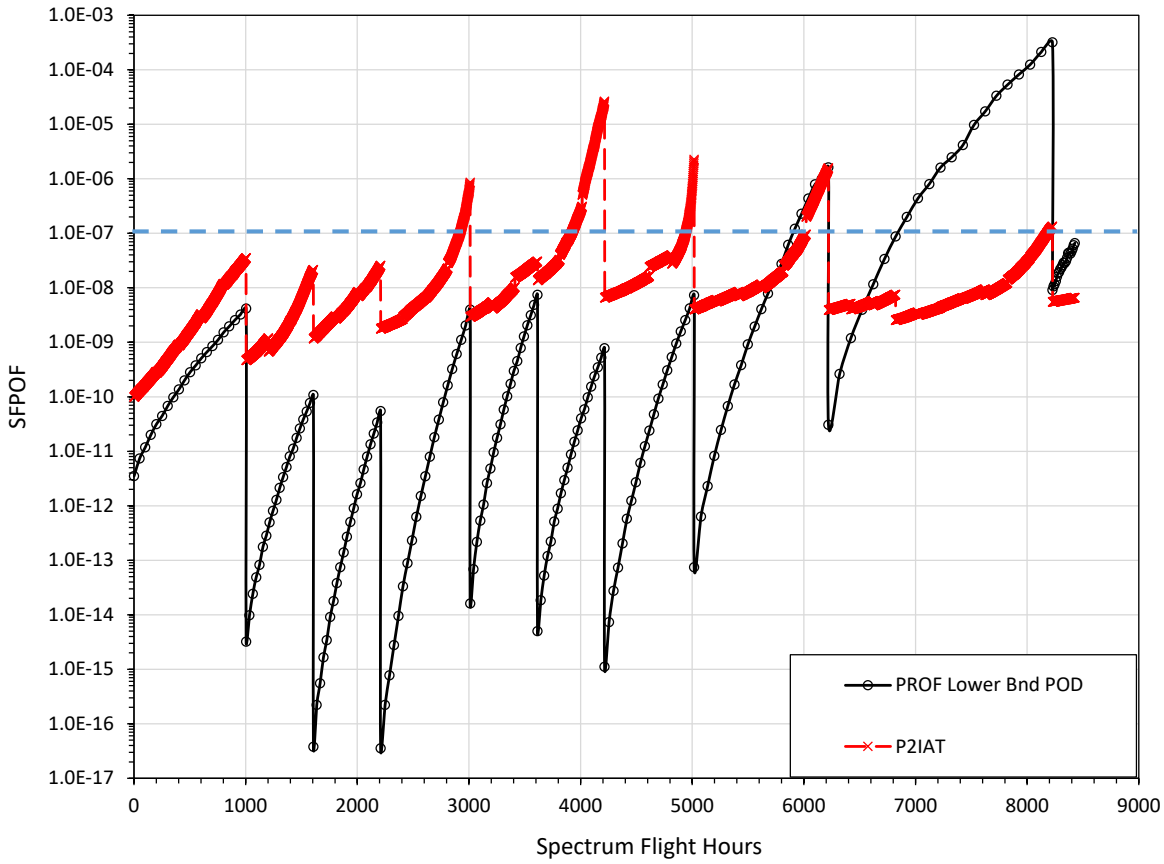

Figure 39. SFPOF with the P²IAT Inspection Intervals, CP03 RW

4.2.1.2 CP04 RW

CIAT and P²IAT give essentially the same number of inspections for CP04 RW; both IAT methods call for inspections as often as possible – approximately every 200 SFH (end of every week). P²IAT does not have inspections after 6,800, 7,800, and 8,400 SFH as explained in Figure 35, Figure 36, and Figure 37. According to the PROF calculations, CIAT is not able to keep SFPOF below 10^{-7} even with inspections every week as shown in Figure 40. SFPOF is initially below 10^{-7} in CIAT, but increases with each inspection stabilizing around 10^{-5}. In contrast, SFPOF in P²IAT is initially above 10^{-7} for the first eight inspections. Then drops below 10^{-7} for all subsequent inspections, except the ones at 4,000 SFH and 8,000 SFH. The spike in SFPOF at 8,000 SFH comes after not inspecting at 7,800 SFH as explained in Figure 36. Since CIAT/PROF and P²IAT started with the same EIDS distribution and have inspections every 200 SFH, it is apparent from Figure 41 that the methods used to calculate SFPOF in PROF and P²IAT give different results.

Since the CIAT curve in Figure 40 used the lower bound POD curve from Table 3, it was decided to see how using the upper bound POD curve would affect SFPOF. Figure 41 shows that SFPOF decreases with the more sensitive inspection, but still does not stabilize below 10^{-7}.

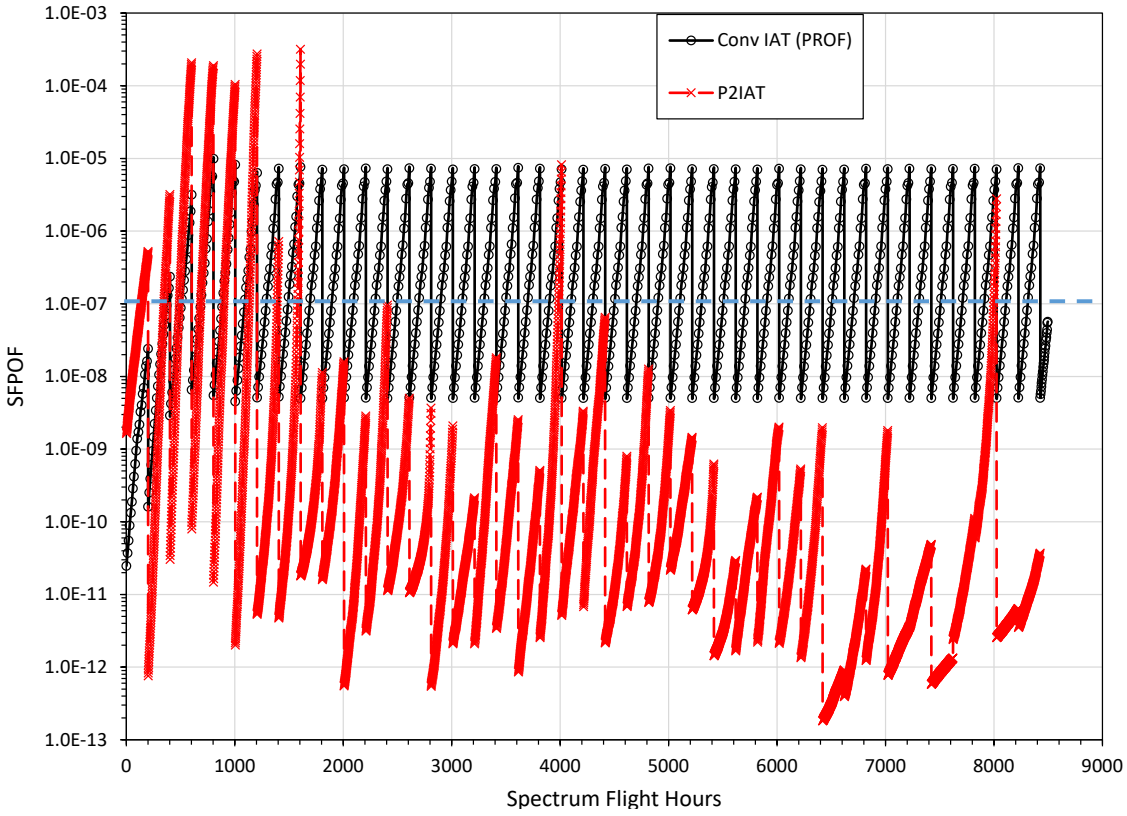

Figure 40. SFPOF for CIAT and P²IAT Inspections, CP04 RW

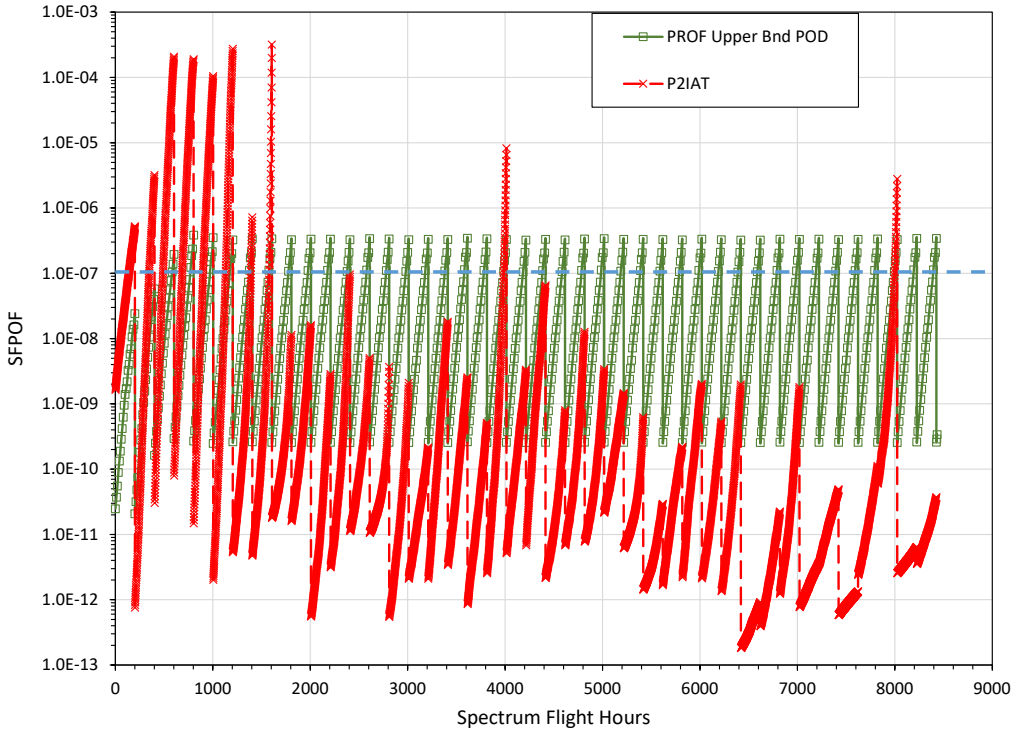

Figure 41. SFPOF for CIAT with Upper Bound POD Curve, CP04 RW

4.2.1.3 CP07 RW

There is a difference of only four inspections between P^{2}IAT and CIAT at CP07 RW. P^{2}IAT calls for 23 inspections while CIAT calls for 19 as seen in Figure 42. The maximum SFPOF with CIAT is reasonably stable at about 10^{-6}. All but eight of SFPOF peaks in P^{2}IAT are below 10^{-7}. The more frequent inspections in P^{2}IAT are effective at keeping the SFPOF near 10^{-7}, but not below.

Introducing the P^{2}IAT inspection intervals into PROF results in more variation in the SFPOF peaks as shown in Figure 43. Eight of the SFPOF peaks do not exceed 10^{-7}, but two are now above 10^{-5}. The other 13 SFPOF peaks are between 10^{-6} and 10^{-5}. Using PROF to calculate SFPOF results in even more inspections than P^{2}IAT calls for being needed to keep the SFPOF peaks from exceeding 10^{-7} at CP07 RW.

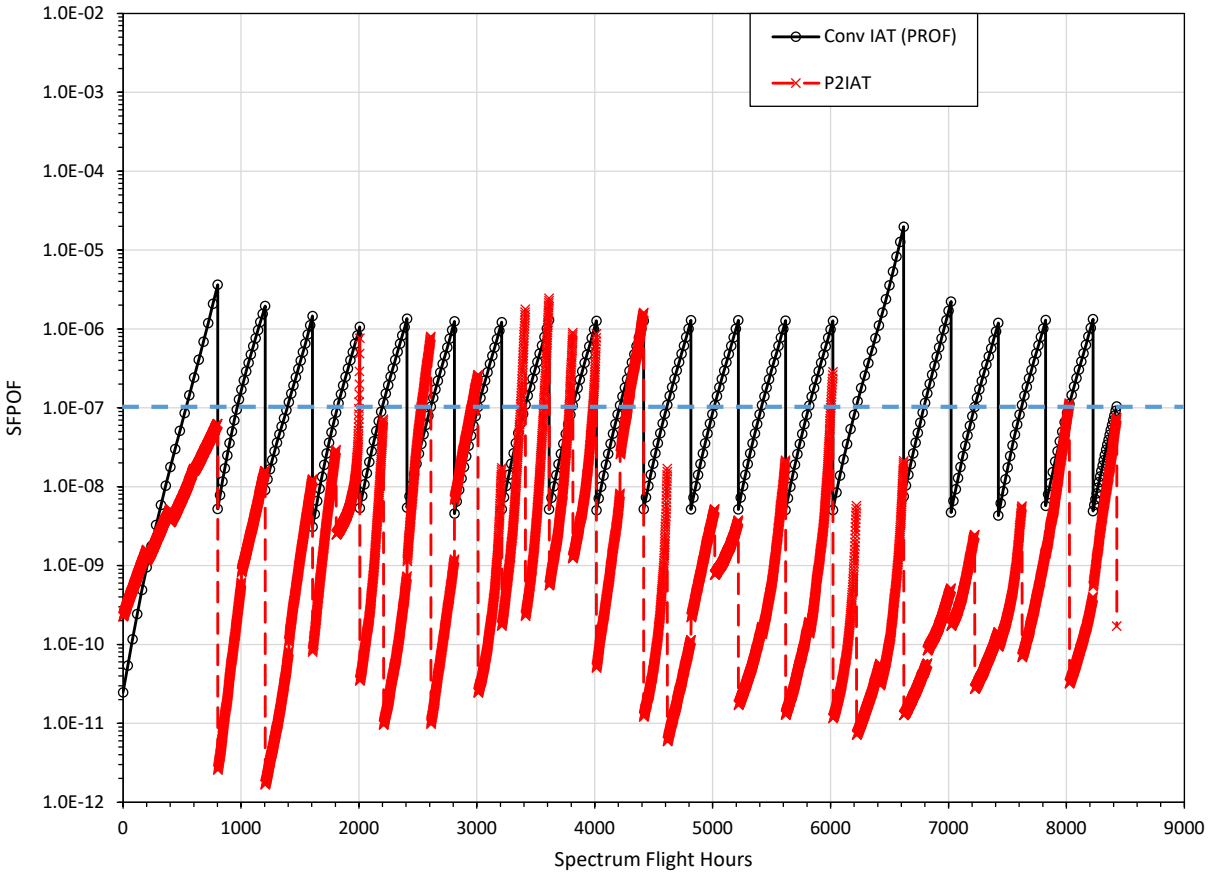

Figure 42. SFPOF for CIAT and P^{2}IAT Inspections, CP07 RW

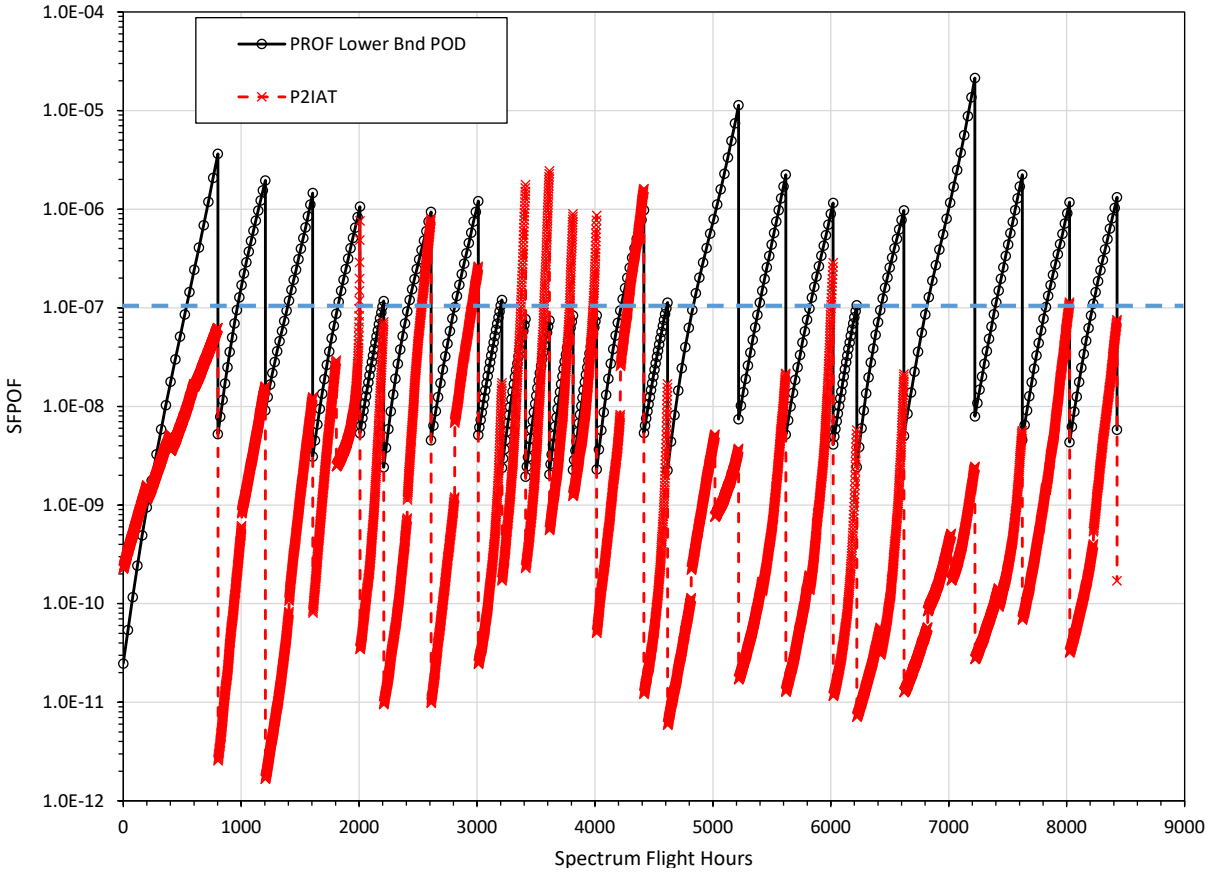

Figure 43. SFPOF with the P²IAT Inspection Intervals, CP07 RW

4.2.1.4 CP08 RW

CIAT calls for one more than half the number of inspections that P²IAT does for CP08 RW. P²IAT calls for sixteen inspections while CIAT calls for nine as seen in Figure 44. In CIAT, only one SFPOF peak is below 10^{-7}, the first inspection. In addition, one SFPOF peak in the curve for CIAT reaches the unacceptable region, greater than 10^{-5}. In contrast, P²IAT has eight SFPOF peaks at or below 10^{-7}. Only two SFPOF peaks are significantly greater than 10^{-7} with P²IAT. More frequent inspections than CIAT calls for are needed if SFPOF peaks are not to exceed 10^{-7}.

PROF calculations of SFPOF with the P²IAT inspection intervals results in but two of the SFPOF peaks being below 10^{-7} as seen in Figure 45. The PROF calculated SFPOF values track the P²IAT calculated values closely except in the range from 3,400 to 4,200 SFH. Inspections from 3,200 to 3,800 SFH used an eddy current pencil probe as the eddy current ring probe failed and it took several weeks to obtain a new one. The pencil probe is less sensitive than the ring probe, which is reflected in the respective POD curves. This resulted in the high SFPOF values for P²IAT 4,200 SFH. After inspections with the ring probe resumed, SFPOF came back down in P²IAT.

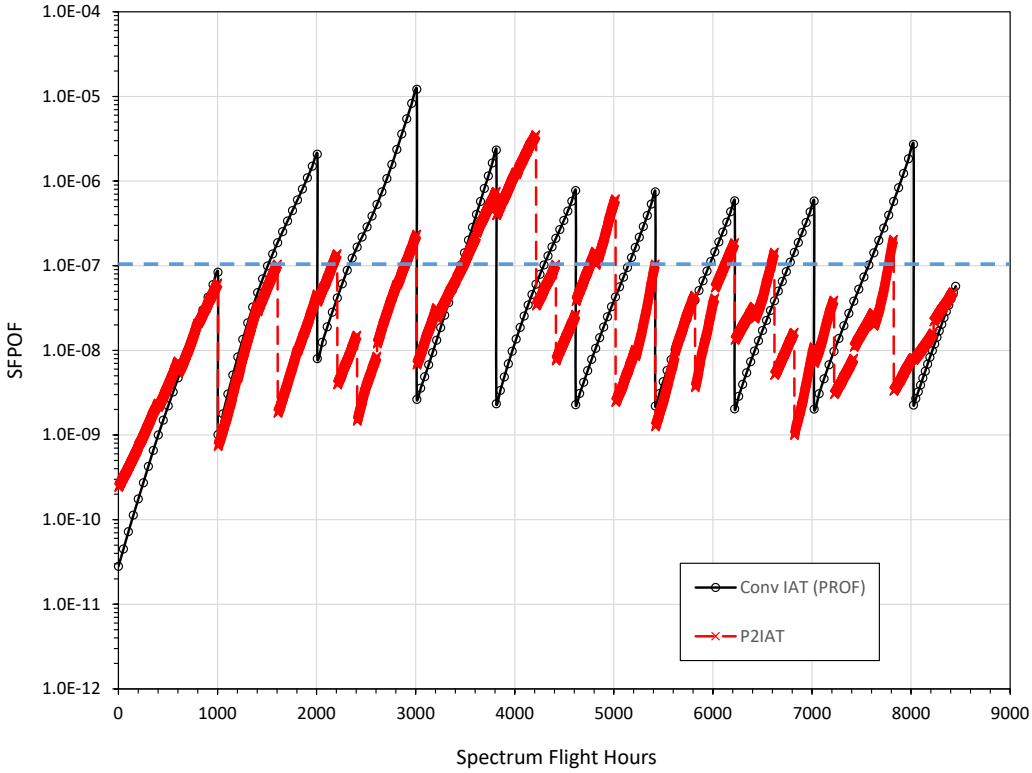

Figure 44. SFPOF for CIAT and P²IAT Inspections, CP08 RW

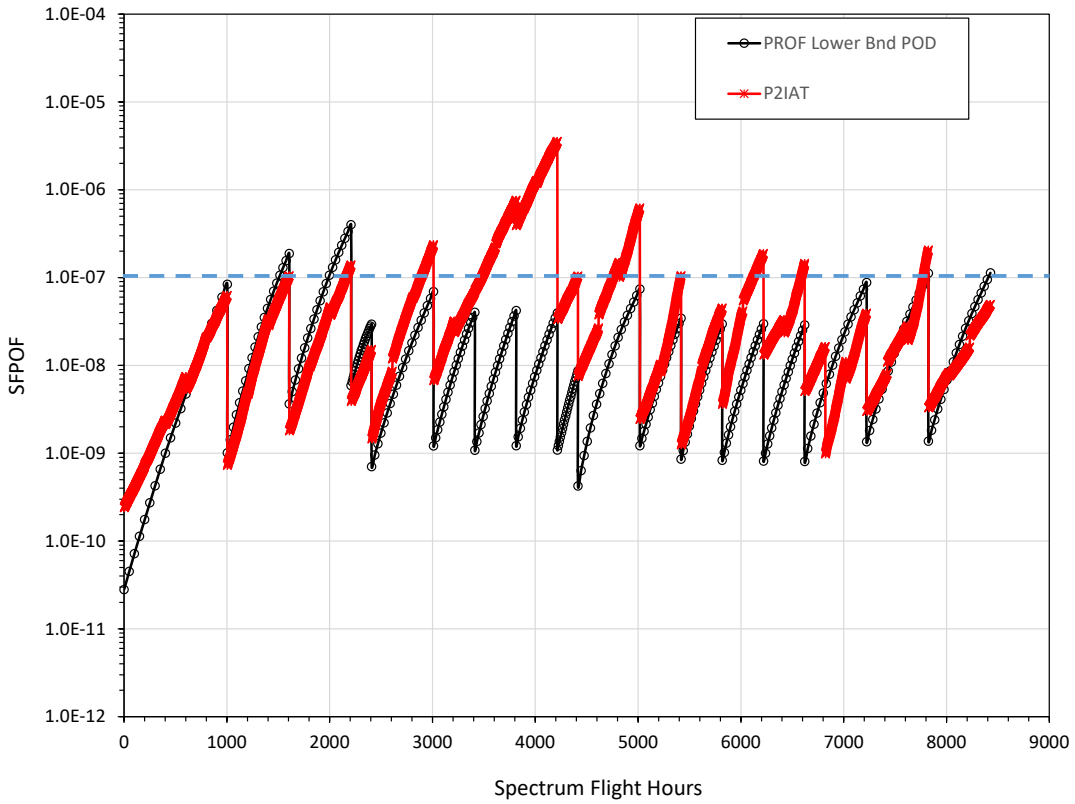

Figure 45. SFPOF with the P²IAT Inspection Intervals, CP08 RW

4.2.1.5 CP09 RW

P^2IAT calls for seventeen inspections at CP09 RW while CIAT calls for ten as seen in Figure 46. While only three of the SFPOF peaks for CIAT are below 10^{-7}, the other seven remain close to 10^{-7}. P^2IAT has half of the SFPOF peaks at or below 10^{-7}, but the other half of the SFPOF peaks are in the same range as the CIAT peaks.

Adding a couple more inspections into the CIAT plan would likely maintain the SFPOF peaks below 10^{-7}. However, an additional seven inspections are not needed as the plot of SFPOF calculated by PROF using the P^2IAT inspections illustrates in Figure 47. SFPOF stays well below 10^{-7} for the PROF calculations.

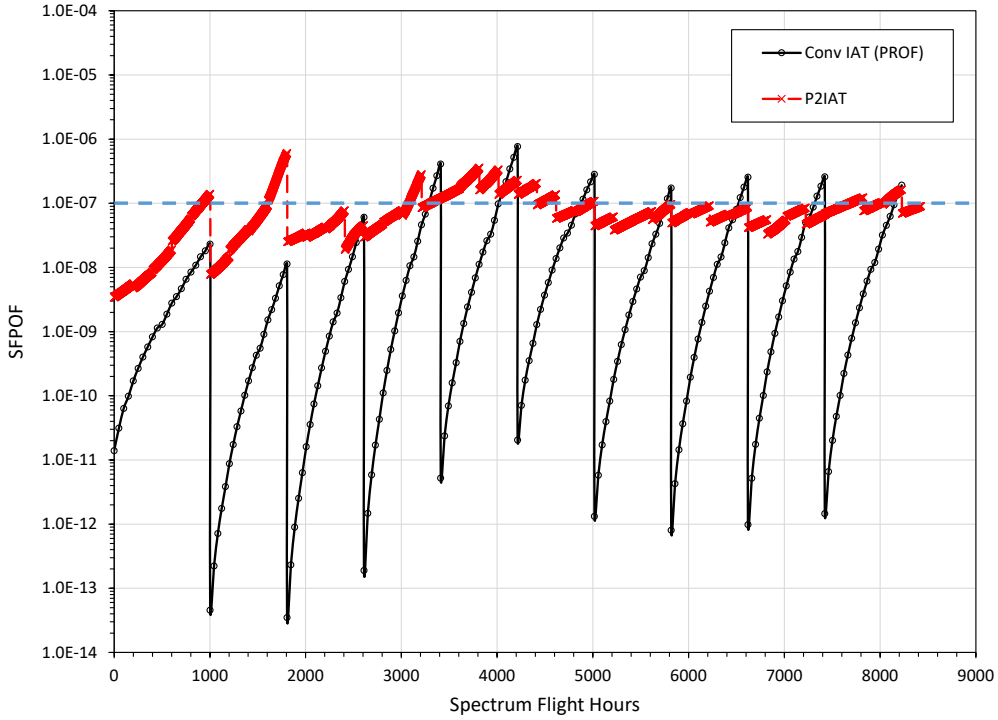

Figure 46. SFPOF for CIAT and P^2IAT Inspections, CP09 RW

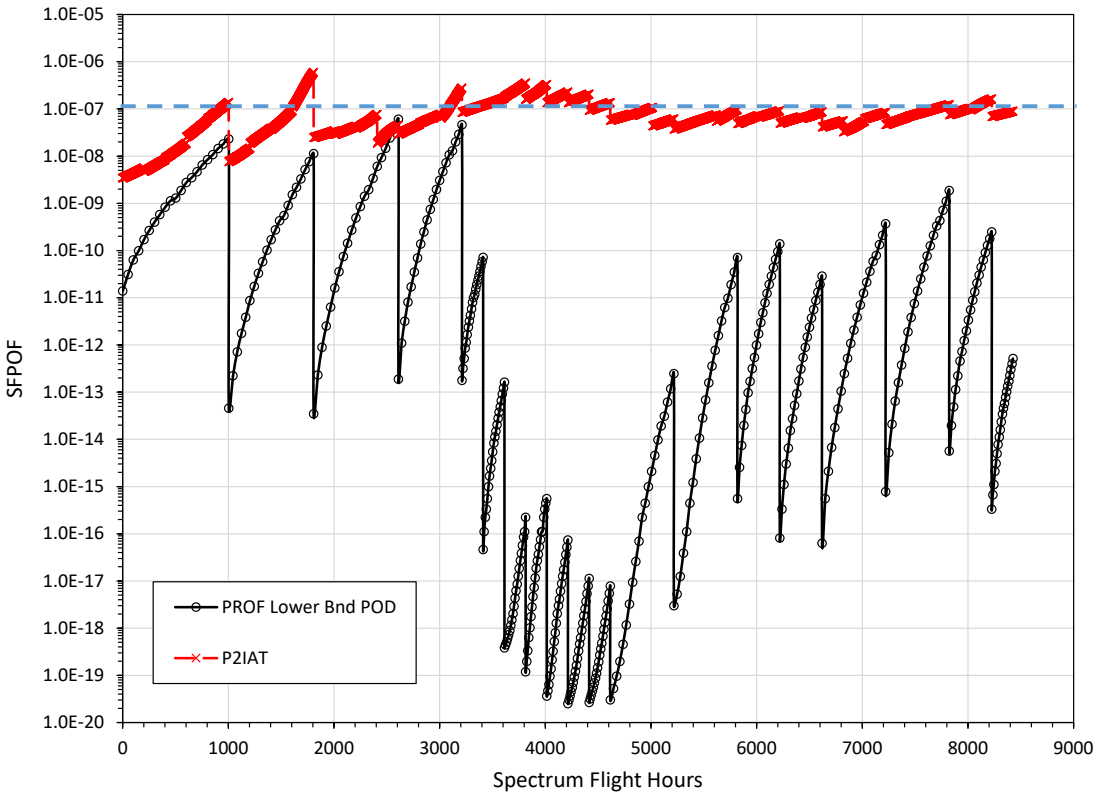

Figure 47. SFPOF with the P²IAT Inspection Intervals, CP09 RW

4.2.1.6 CP10 RW

P²IAT has twice as many inspections for CP10 RW as does CIAT. P²IAT calls for 22 inspections while CIAT calls for eleven as shown in Figure 48. CIAT keeps SFPOF below 10^{-7} for every inspection, even using the less sensitive POD curve (a_{50} = 0.183 inches, a_{90} = 0.191 inches) than P²IAT (POD(a) = 0 for a < 0.160; POD(a) = 1 for a ≥ 0.160). Note that PROF truncates low SFPOF values at 10^{-20}, so the flat portions of the conventional IAT curve at 10^{-20} indicate that SFPOF was less than or equal to 10^{-20} during these intervals. P²IAT calculates much higher values for SFPOF than does PROF, which drives the need for more inspections in P²IAT.

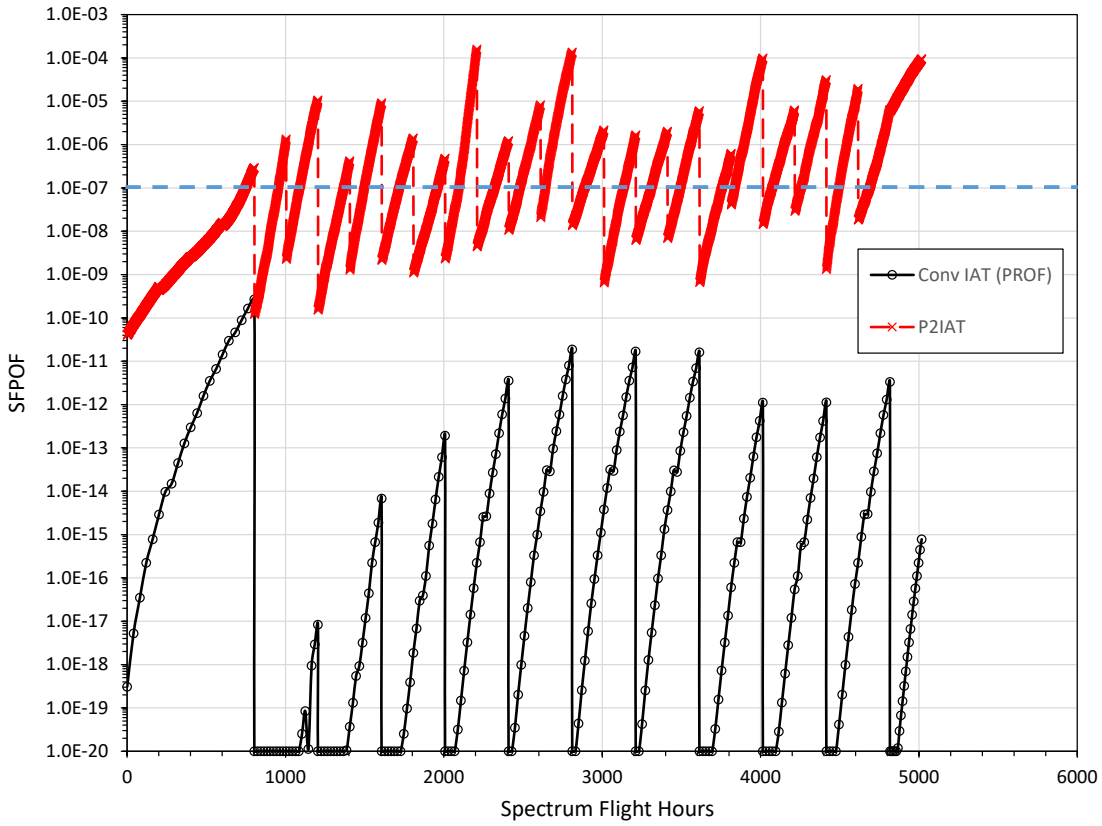

Figure 48. SFPOF for CIAT and P^{2}IAT Inspections, CP10 RW

4.2.1.7 CP11 RW

P^{2}IAT calls for thirteen inspections at CP11 RW while CIAT calls for five. CIAT calculates lower SFPOF values than P^{2}IAT as seen in Figure 49. Neither CIAT nor P^{2}IAT keep SFPOF peaks below 10^{-7} however. Utilizing the P^{2}IAT inspections in PROF results in SFPOF peaks remaining very near 10^{-7} as shown in Figure 50.

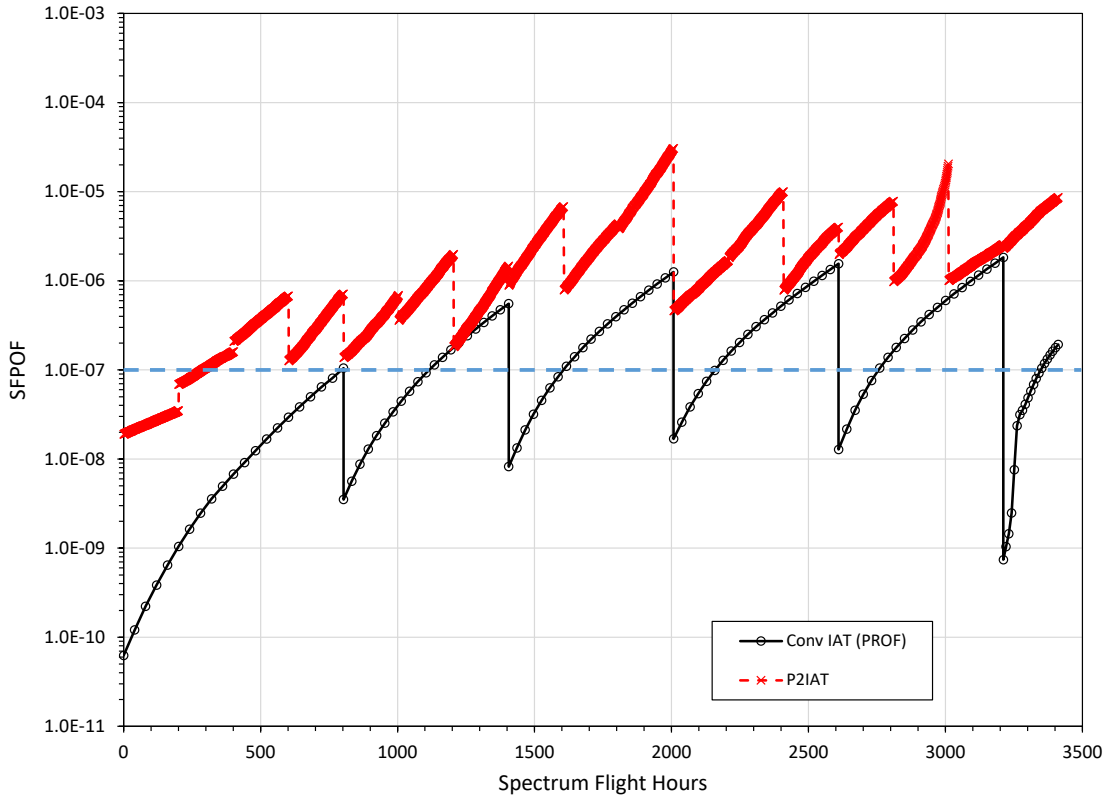

Figure 49. SFPOF for CIAT and P²IAT Inspections, CP11 RW

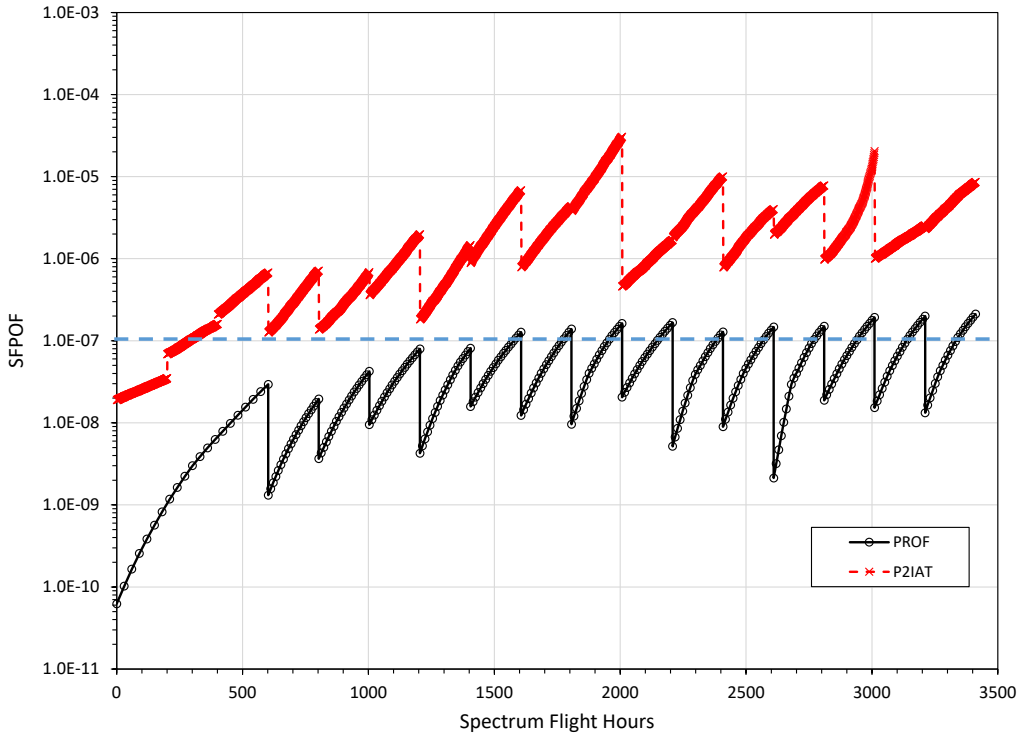

Figure 50. SFPOF with the P²IAT Inspection Intervals, CP11 RW

4.2.1.8 CP12 RW

P^{2}IAT calls for eight times more inspections at CP12 RW than does CIAT. P^{2}IAT has 24 inspections while CIAT has only three inspections as shown in Figure 51. CIAT inspections are unable to keep SFPOF below 10^{-7}. P^{2}IAT calculations also do not maintain SFPOF below 10^{-7}, even though after 400 SFH (Week 2) inspections were performed every 200 SFH (every week). Applying the P^{2}IAT inspection schedule in PROF results in SFPOF values well below 10^{-7} as shown in Figure 52. PROF needs more than the three inspections from CIAT, but less than the 24 from P^{2}IAT, to keep SFPOF below 10^{-7}.

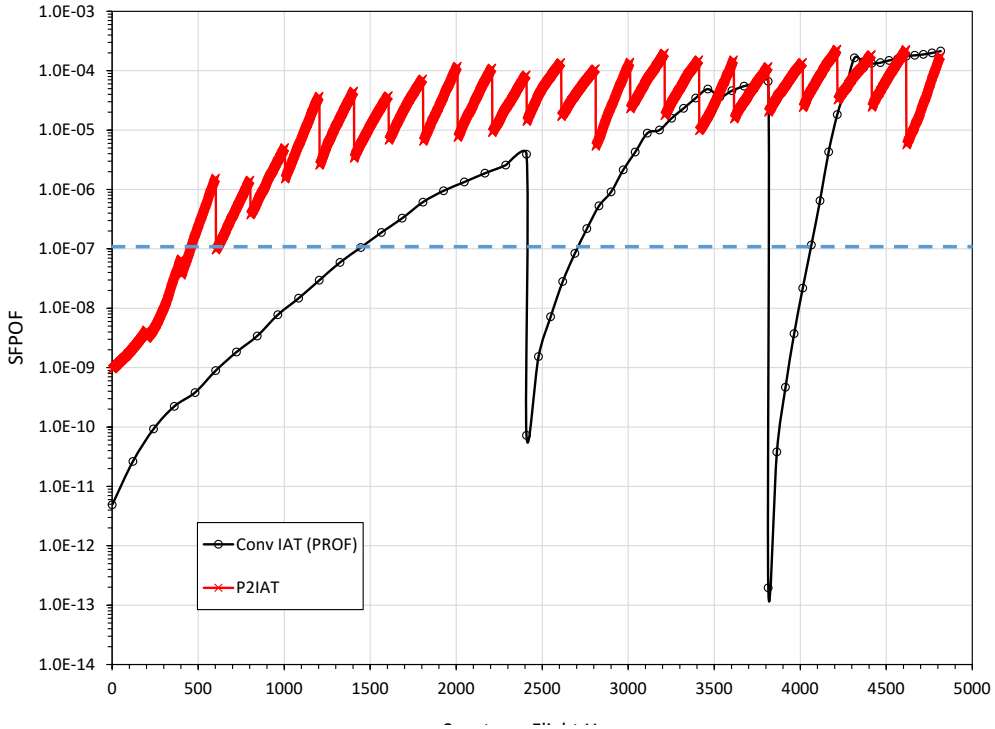

Figure 51. SFPOF for CIAT and P^{2}IAT Inspections, CP12 RW

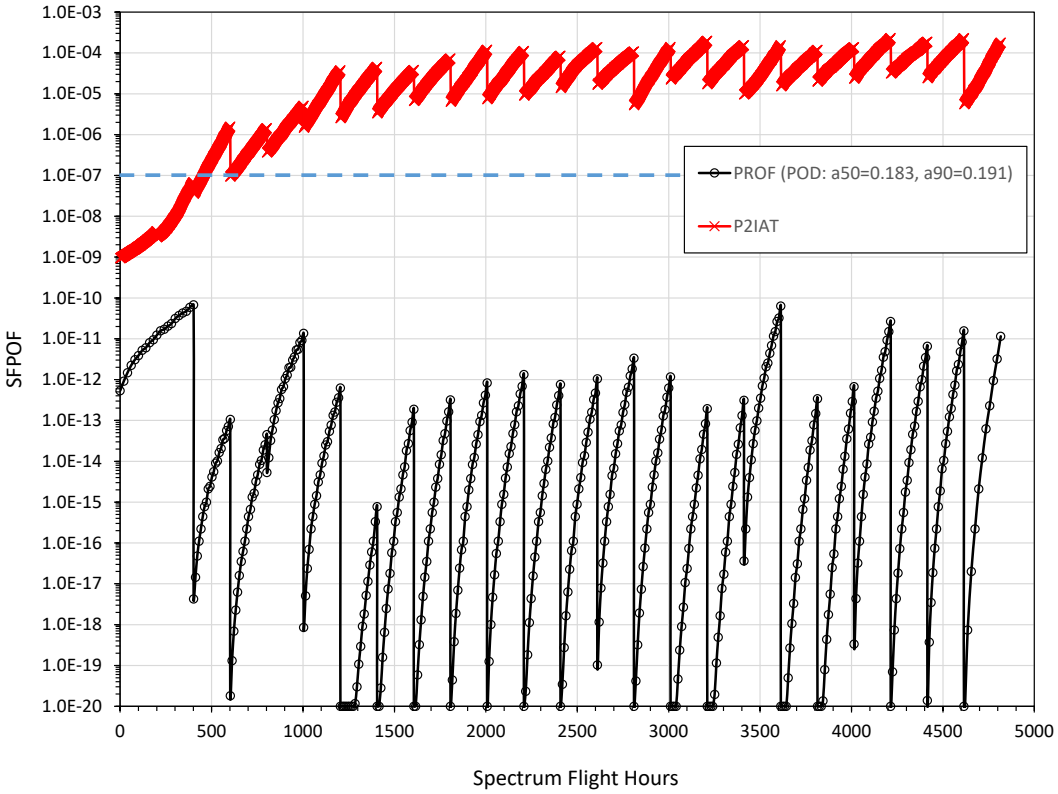

Figure 52. SFPOF with the P²IAT Inspection Intervals, CP12 RW

4.2.1.9 CP13 RW

P²IAT calls for twenty inspections at CP12 RW while CIAT calls for four inspections as shown in Figure 53. CIAT inspections are able to keep SFPOF, calculated by PROF, below 10^{-7} while using the less sensitive POD curve (a_{50} = 0.183 inches, a_{90} = 0.191 inches). P²IAT calculates much higher SFPOF values resulting in more frequent inspections.

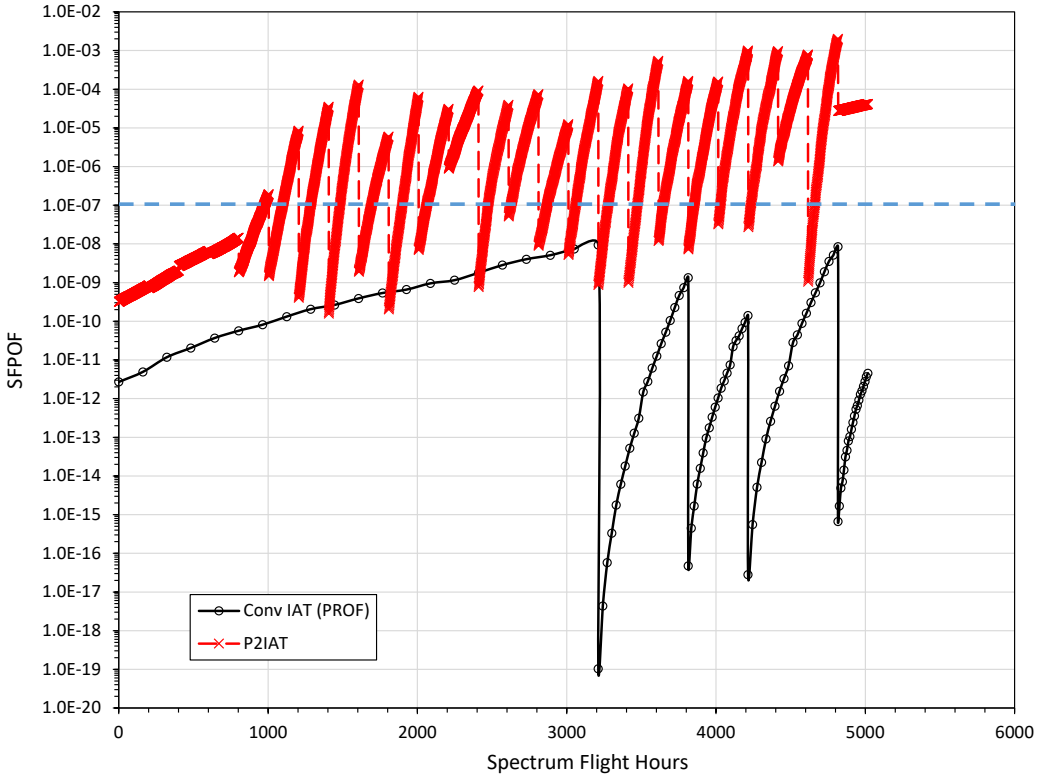

Figure 53. SFPOF for CIAT and P²IAT Inspections, CP13 RW

4.2.2 Left Wing

4.2.2.1 CP03 LW

CIAT requires three fewer inspections than P²IAT at CP03 LW. P²IAT calls for nine inspections while CIAT calls for six as shown in Figure 54. There are only eight inspections (vertical lines) evident in the P²IAT curve. The inspection at 1,000 SFH does not significantly reduce SFPOF. P²IAT does not keep SFPOF below 10^{-7} for almost half of its inspections. SFPOF exceeds 10^{-6} in two instances.

SFPOF is equal to or less than 10^{-7} for all of the CIAT inspections except two. At these two inspections, SFPOF is only slightly above 10^{-7}. An additional inspection or two in the CIAT inspection schedule would likely keep SFPOF from exceeding 10^{-7}.

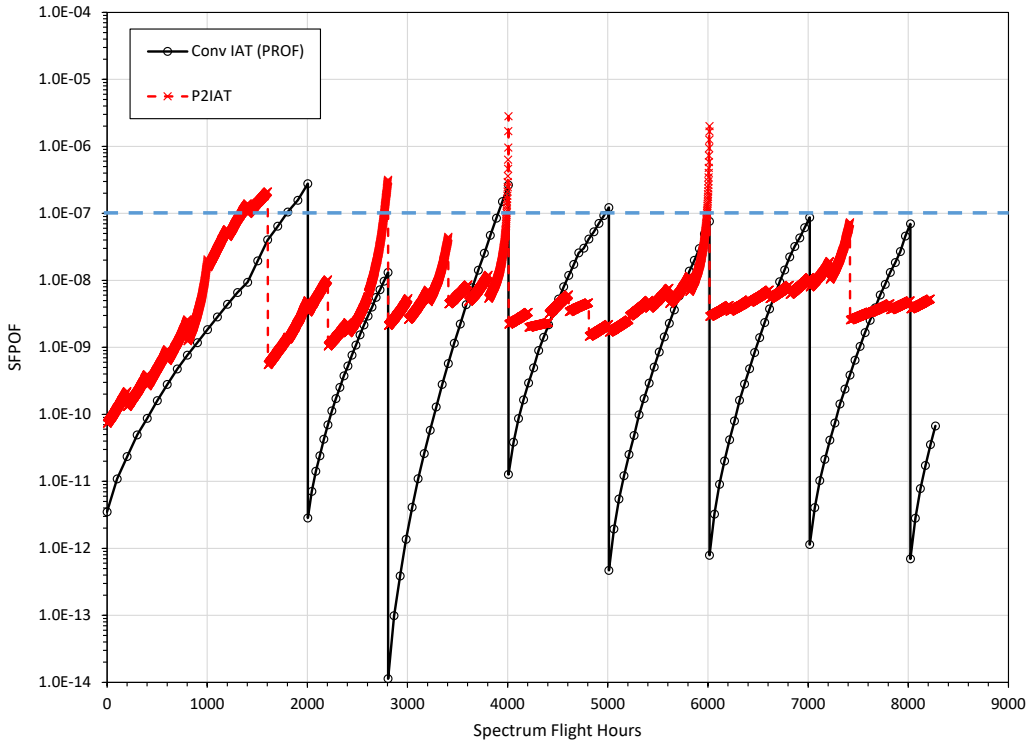

Figure 54. SFPOF for CIAT and P^{2}IAT Inspections, CP03 LW

4.2.2.2 CP04 LW

P^{2}IAT and CIAT call for the same number of inspections, 42, for CP04 LW as shown in Figure 55. Both methods call for inspections every 200 SFH. However, P^{2}IAT and PROF give very different SFPOF values. SFPOF peaks increase with each week in PROF until they reach a steady state of about 10^{-6}. P^{2}IAT, in contrast, starts at high SFPOF peaks and decreases towards the end of the history, never reaching a steady state. The PROF analysis leads the conclusion that inspections are needed more often than every 200 SFH to keep SFPOF at or below 10^{-7}. P^{2}IAT indicates that inspecting every 200 SFH is sufficient to maintain SFPOF below 10^{-7} in the long run.

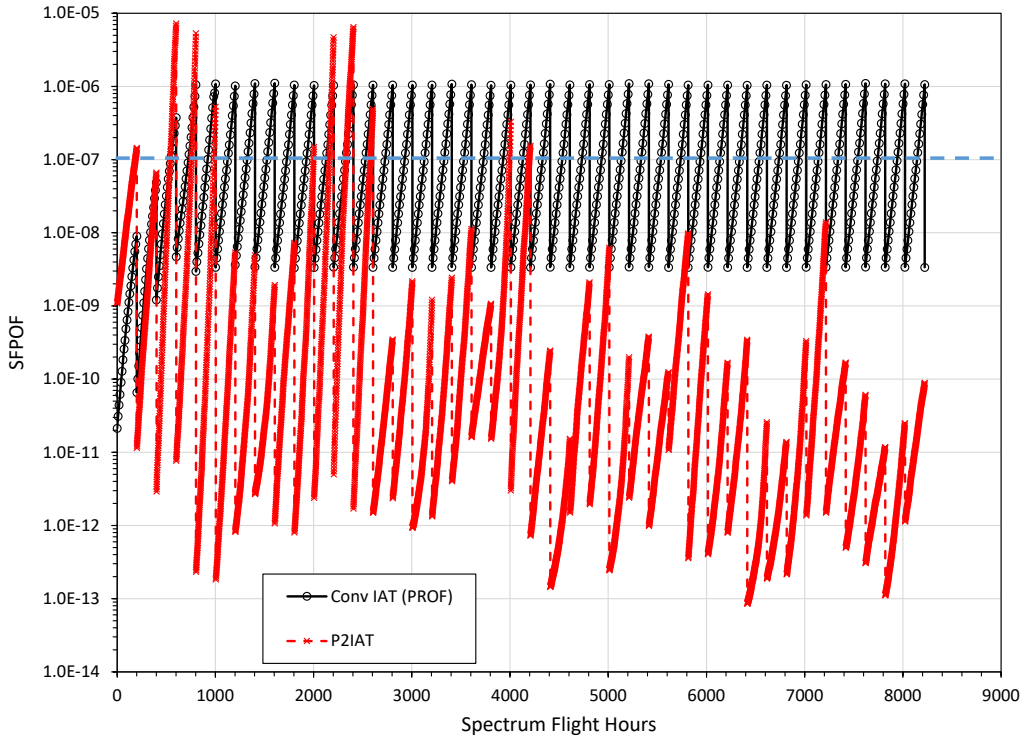

Figure 55. SFPOF for CIAT and P^{2}IAT Inspections, CP04 LW

4.2.2.3 CP07 LW

P^{2}IAT calls for eighteen inspections at CP07 LW, while CIAT calls for thirteen. SFPOF for CIAT reaches 10^{-5} before every inspection as shown in Figure 56. P^{2}IAT keeps SFPOF below 10^{-7} before each inspection except for three instances. When the P^{2}IAT inspection times are used in PROF as in Figure 57, the SFPOF peaks decrease to around 10^{-6} but still do not drop below 10^{-7}.

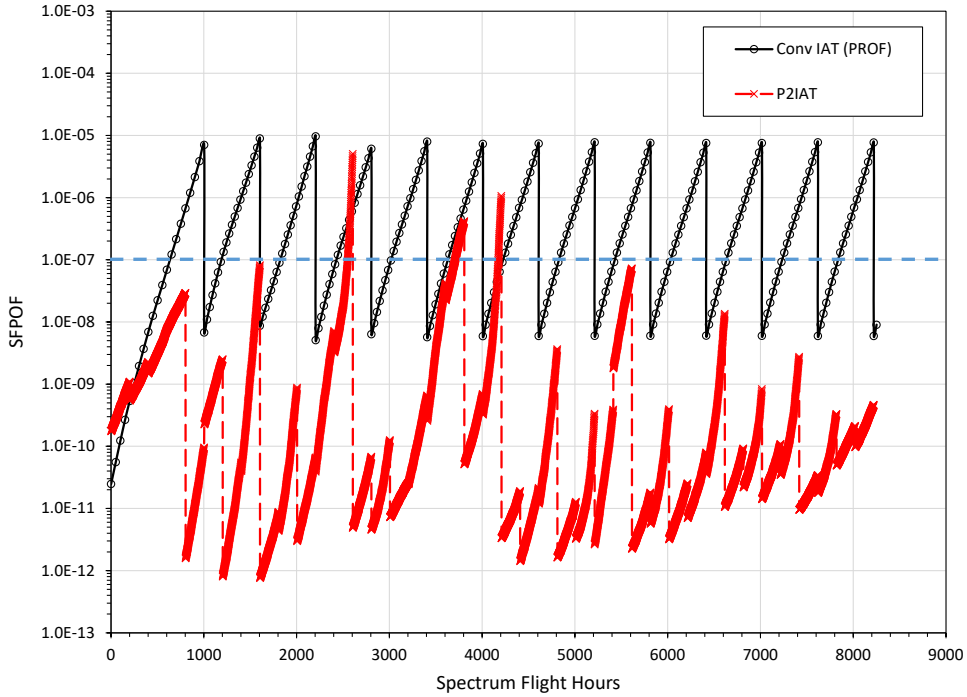

Figure 56. SFPOF for CIAT and P²IAT Inspections, CP07 LW

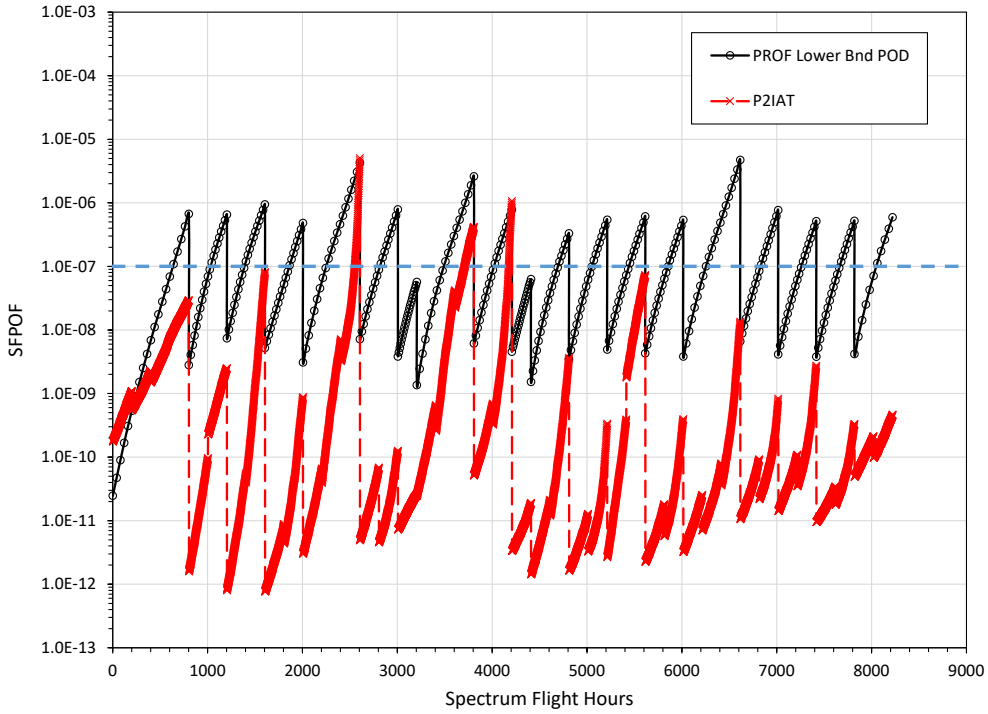

Figure 57. SFPOF with the P²IAT Inspection Intervals, CP07 LW

4.2.2.4 CP08 LW

P^2IAT calls for fifteen inspections at CP08 LW, while CIAT calls for eight. Peak SFPOF values for CIAT are around 10^{-6} in Figure 58. P^2IAT maintains maximum SFPOF values below 10^{-7} except for inspections in the range 3,200 to 3,800 SFH when pencil probe inspections were performed instead of ring probe inspections. When the P^2IAT inspection times are used in PROF, SFPOF values track the P^2IAT values closely as shown in Figure 59.

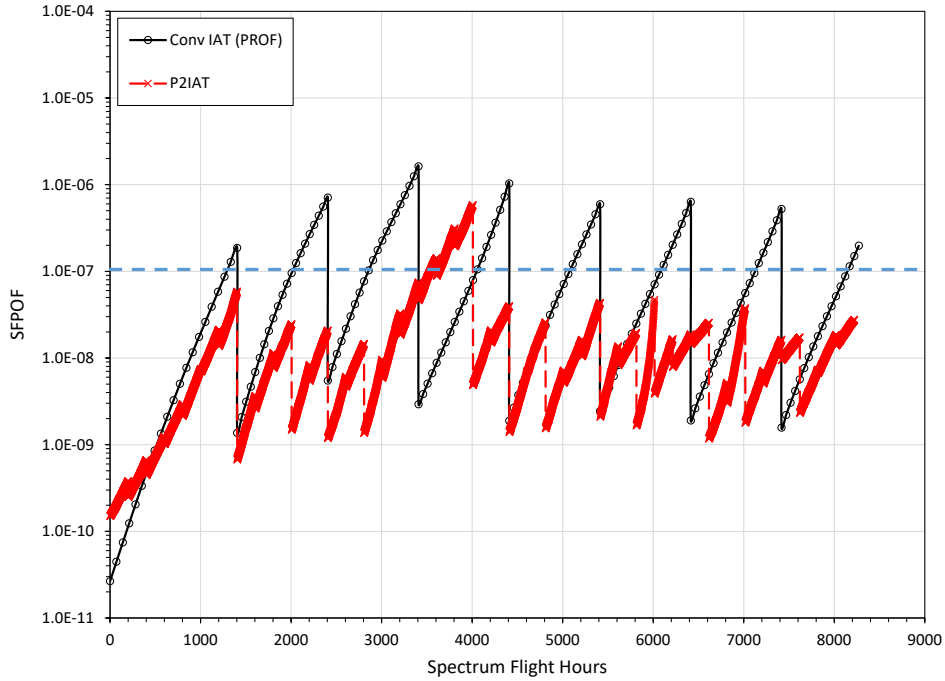

Figure 58. SFPOF for CIAT and P^2IAT Inspections, CP08 LW

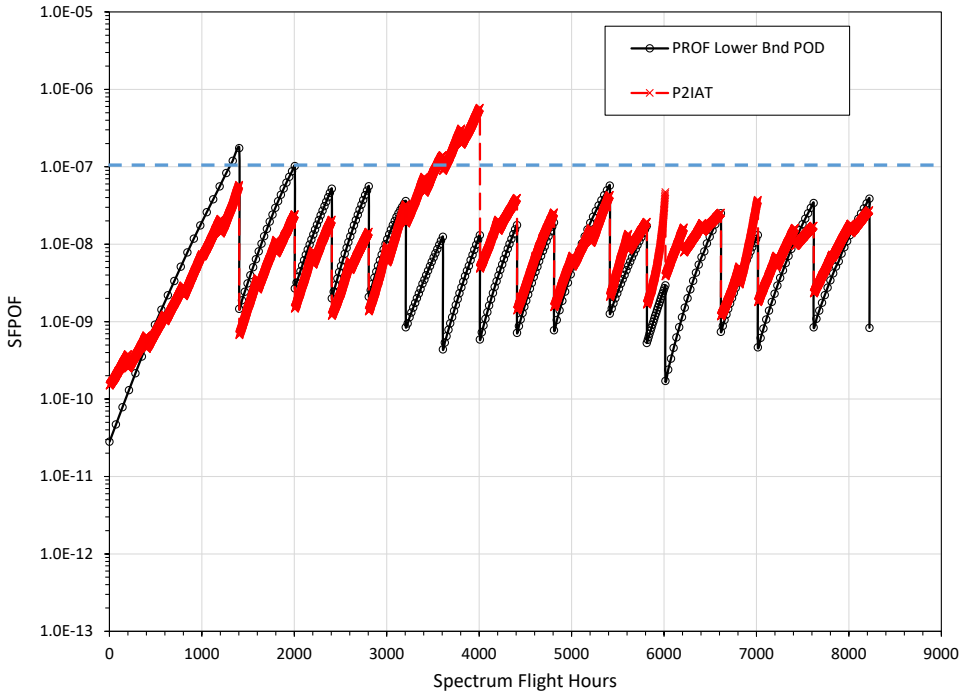

Figure 59. SFPOF with the P^{2}IAT Inspection Intervals, CP08 LW

4.2.2.5 CP09 LW

P^{2}IAT calls for twenty-one inspections at CP09 LW, while CIAT calls for eight. CIAT and P^{2}IAT have similar peak SFPOF values of around 10^{-7} in Figure 60. PROF has much lower SFPOF values after inspections for conventional IAT.

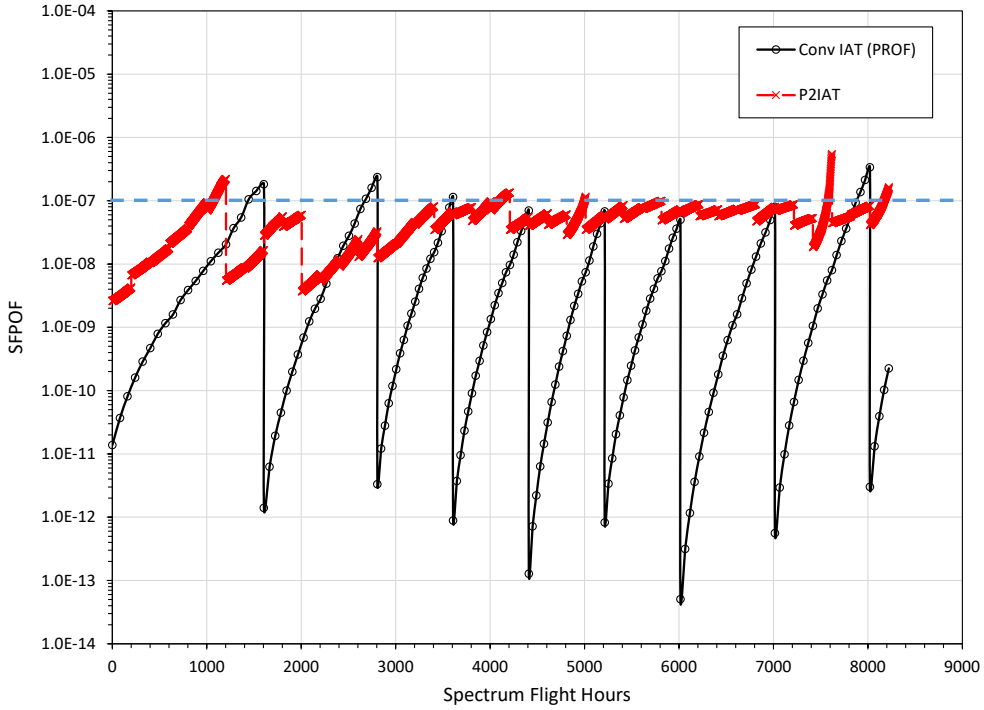

Figure 60. SFPOF for CIAT and P²IAT Inspections, CP09 LW

4.2.2.6 CP10 LW

P²IAT calls for 31 inspections at CP10 LW, while CIAT calls for fifteen, as seen in Figure 61. CIAT using PROF to calculate SFPOF with the least sensitive POD curve from **Error! Reference source not found.** (a_{50} = 0.183 inches, a_{90} = 0.191 inches) results in SFPOF well below 10^{-7}. P²IAT calculates much higher SFPOF values. As a result, P²IAT is not able to maintain SFPOF below 10^{-7}, even though inspections occur every 200 SFH after the first 800 SFH.

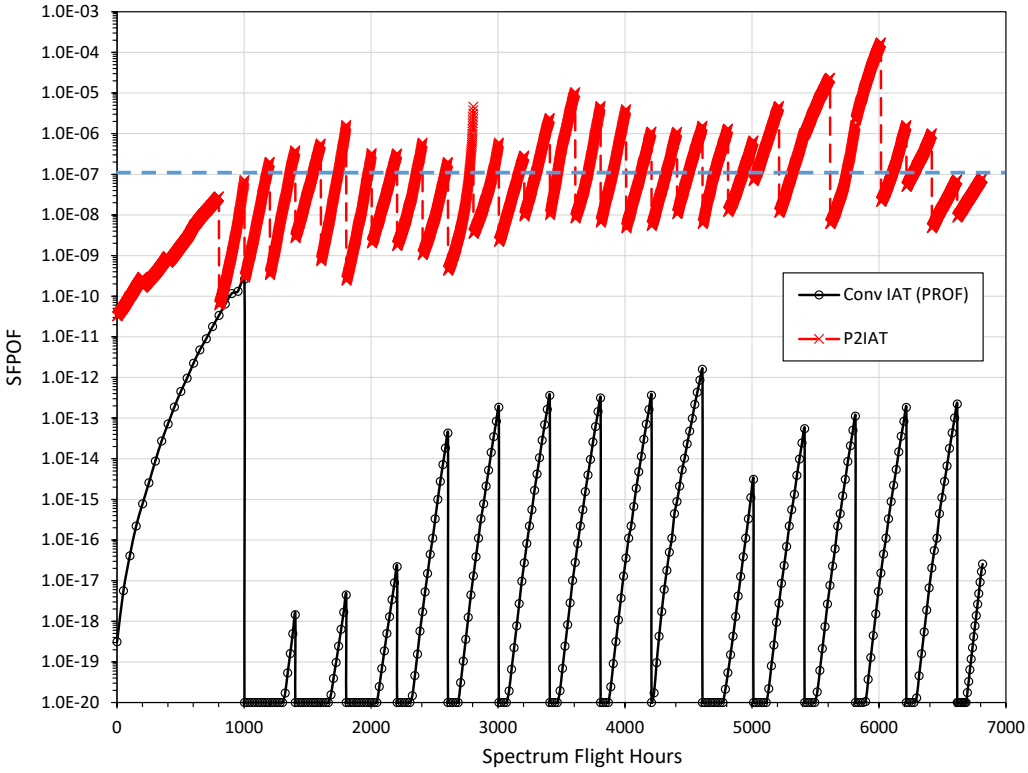

Figure 61. SFPOF for CIAT and P^{2}IAT Inspections, CP10 LW

4.2.2.7 CP11 LW

P^{2}IAT calls for 32 inspections at CP11 LW, while CIAT calls for ten, as shown in Figure 62. Both IAT methods result in peak SFPOF values of about 10^{-6}. The first two inspection in P^{2}IAT occur at 400 SFH and 800 SFH. Subsequent inspections occur every 200 SFH, as often as possible. SFPOF calculated with PROF starts lower, but eventually the PROF-calculated SFPOF stabilizes in the same range as P^{2}IAT calculations. Using P^{2}IAT inspection times in PROF results in maximum SFPOF values around 10^{-7} as shown in Figure 63.

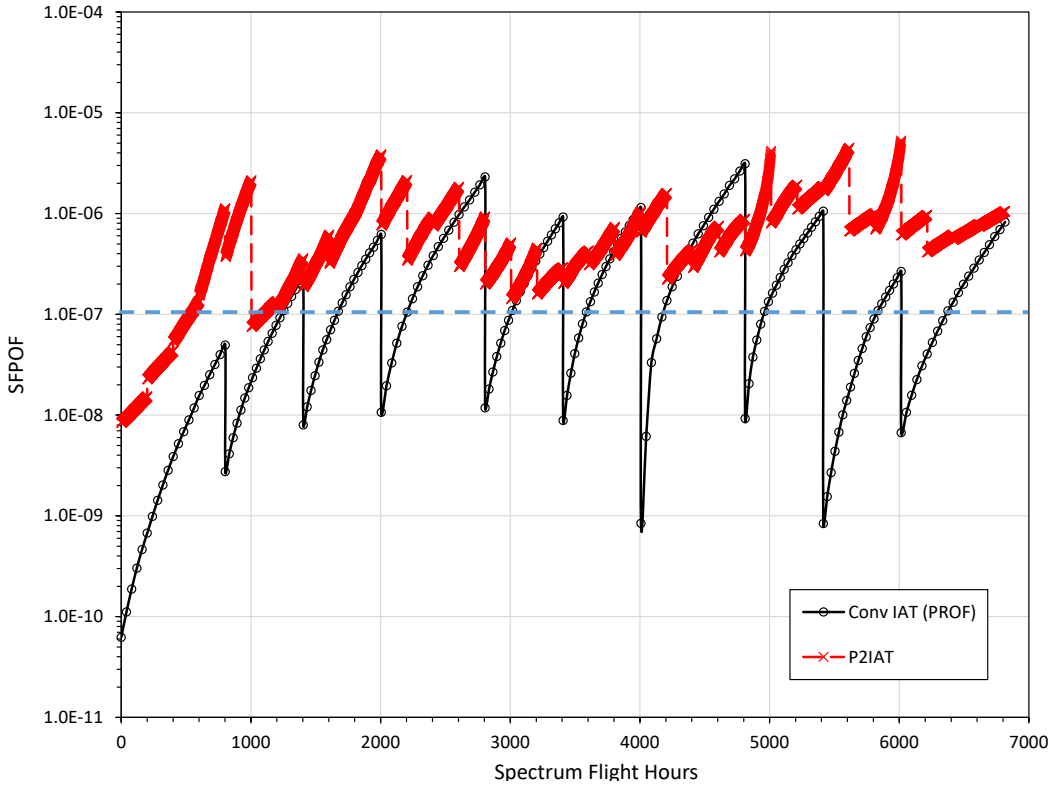

Figure 62. SFPOF for CIAT and P²IAT Inspections, CP11 LW

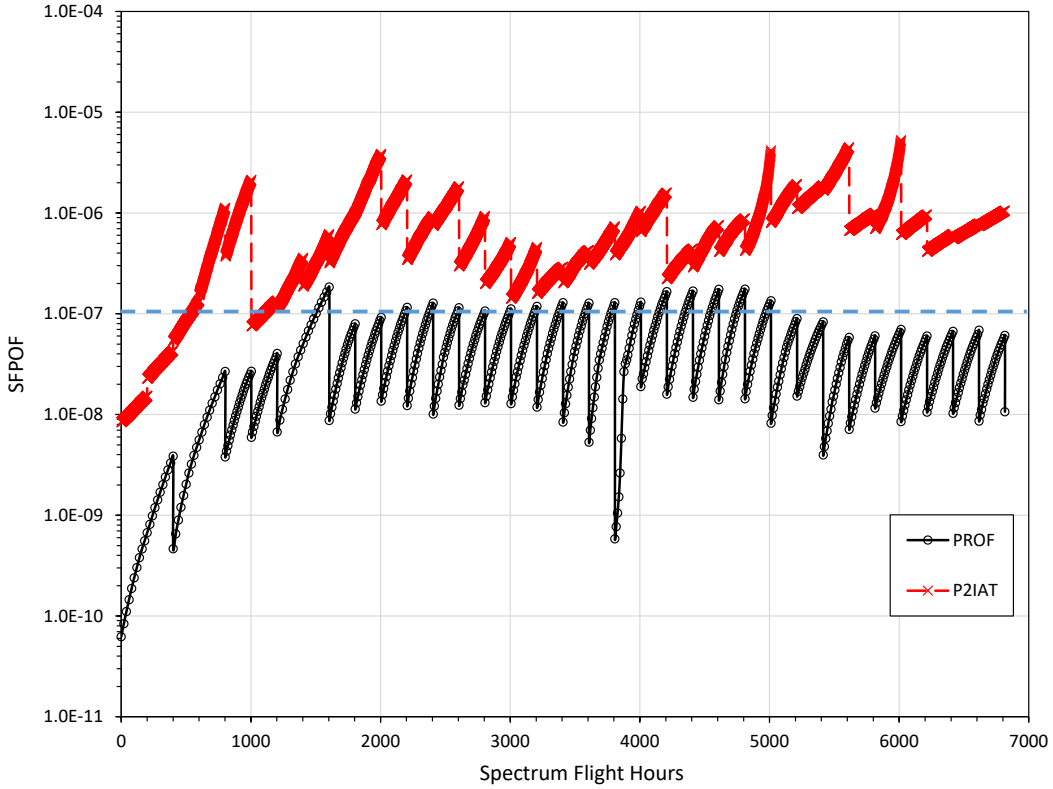

Figure 63. SFPOF with the P²IAT Inspection Intervals, CP11 LW

4.2.2.8 CP12 LW

P^{2}IAT calls for 34 inspections at CP12 LW, while CIAT calls for three, as seen in Figure 64. As with CP11 LW, neither IAT method keeps SFPOF from exceeding 10^{-7}. After 600 SFH, P^{2}IAT inspections occur as often as possible, every 200 SFH. SFPOF values calculated with PROF in CIAT start off much lower than the P^{2}IAT values. Eventually, the peak SFPOF values for CIAT rise into the range of the P^{2}IAT values. However, if the P^{2}IAT inspection times are used in the PROF calculations as in Figure 65, SFPOF stays well below 10^{-7}.

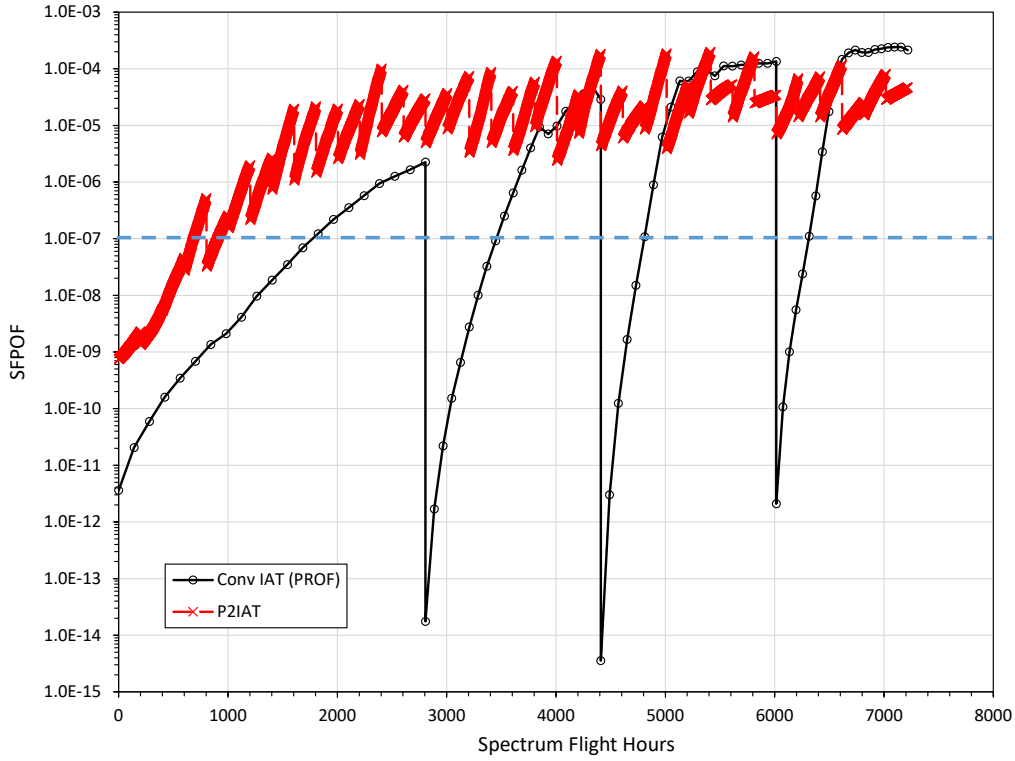

Figure 64. SFPOF for CIAT and P^{2}IAT Inspections, CP12 LW

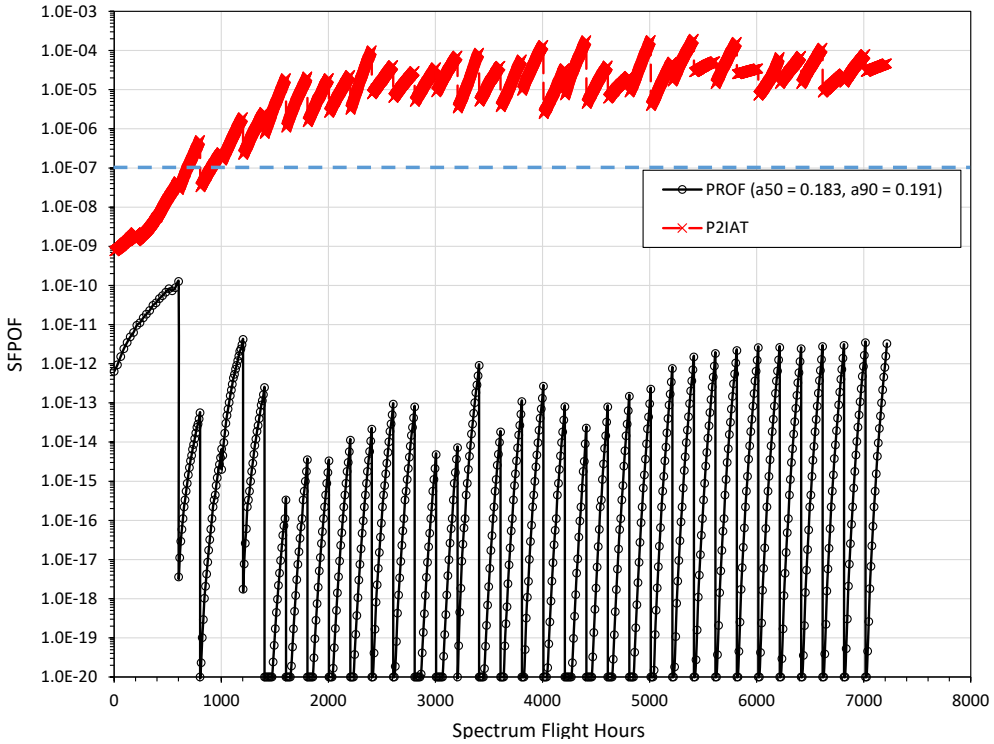

Figure 65. SFPOF with the P^{2}IAT Inspection Intervals, CP12 LW

4.2.2.9 CP13 LW

P^{2}IAT calls for 30 inspections at CP13 LW, while CIAT calls for five, as shown in Figure 66. The peak SFPOF values for CIAT remain well below 10^{-7}, while P^{2}IAT is unable to maintain the peak SFPOF below 10^{-7} even with inspections occurring every 200 SFH after 1,200 SFH.

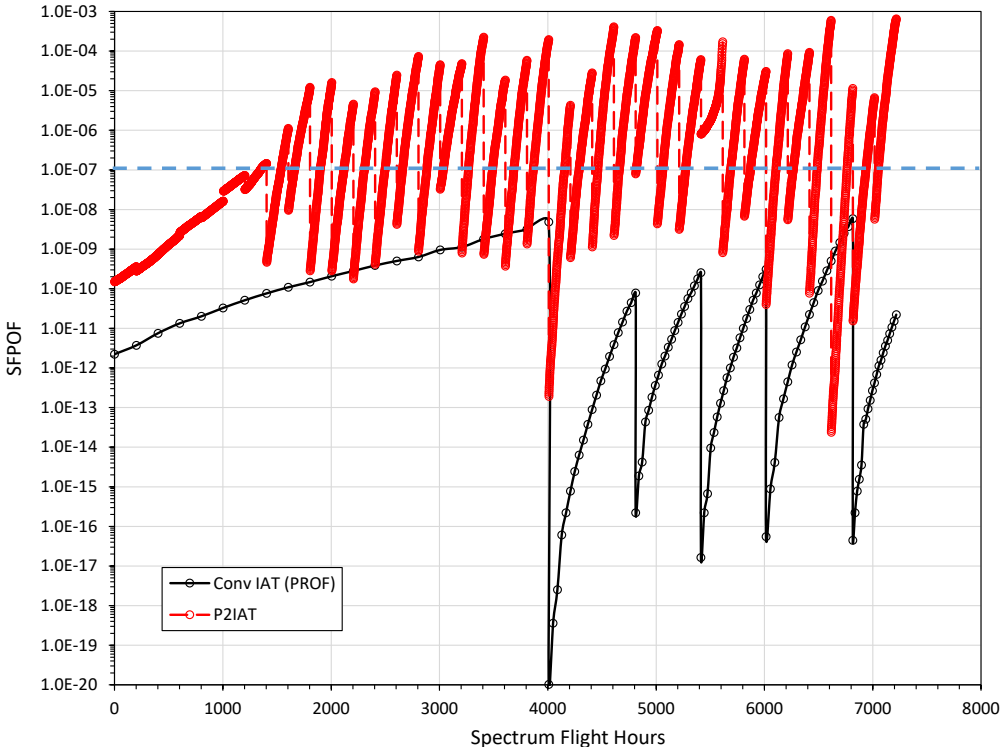

Figure 66. SFPOF for CIAT and P²IAT Inspections, CP13 LW

4.3 Comparing P²IAT and PROF Calculations

From Section 4.2, it is observed that P²IAT and PROF very seldom calculate similar SFPOF values. The change in SFPOF after an inspection is also very different. It is difficult to say that one calculation is more accurate than the other without actual data which is hard to obtain for rarely occurring structural failures. However, the differences between P²IAT and PROF calculations can be documented to inform potential users.

Besides the difference in methods for calculating SFPOF, the biggest differences between P²IAT and PROF are the evolution of the crack size distribution due to crack growth and post-inspection modification of the crack size distribution. These differences will be illustrated using results from CP08 LW. P²IAT and PROF analyses gave very similar SFPOF values, when the P²IAT inspection intervals were used in PROF, for this CP as Figure 59 shows.

4.3.1 Crack Size Distribution Evolution

The evolution of the 90th, 99th, and 99.9th percentiles of the crack size distribution up to the first inspection at 1,400 SFH is shown in Figure 67, Figure 68, and Figure 69, respectively. PROF and P²IAT start with the same EIDS distribution, but P²IAT determines the percentiles for the EIDS distribution from the samples drawn for the probabilistic analysis. Drawing a few thousand samples makes it difficult for P²IAT to accurately reproduce the high percentile EIDS of the underlying distribution. Hence, there is a difference between EIDS values for PROF and P²IAT.

Estimates of the crack size distribution as a function of flight hours in PROF are based on deterministic projections of the percentiles of the EIDS using a table lookup from the crack growth curve [12]. The Particle Filter and Sequential Importance Resampling used in P^{2}IAT [3] result in a more complex evolution of the crack size distribution. This may be one reason why the crack sizes for these percentiles do not change rapidly with flight hours in P^{2}IAT.

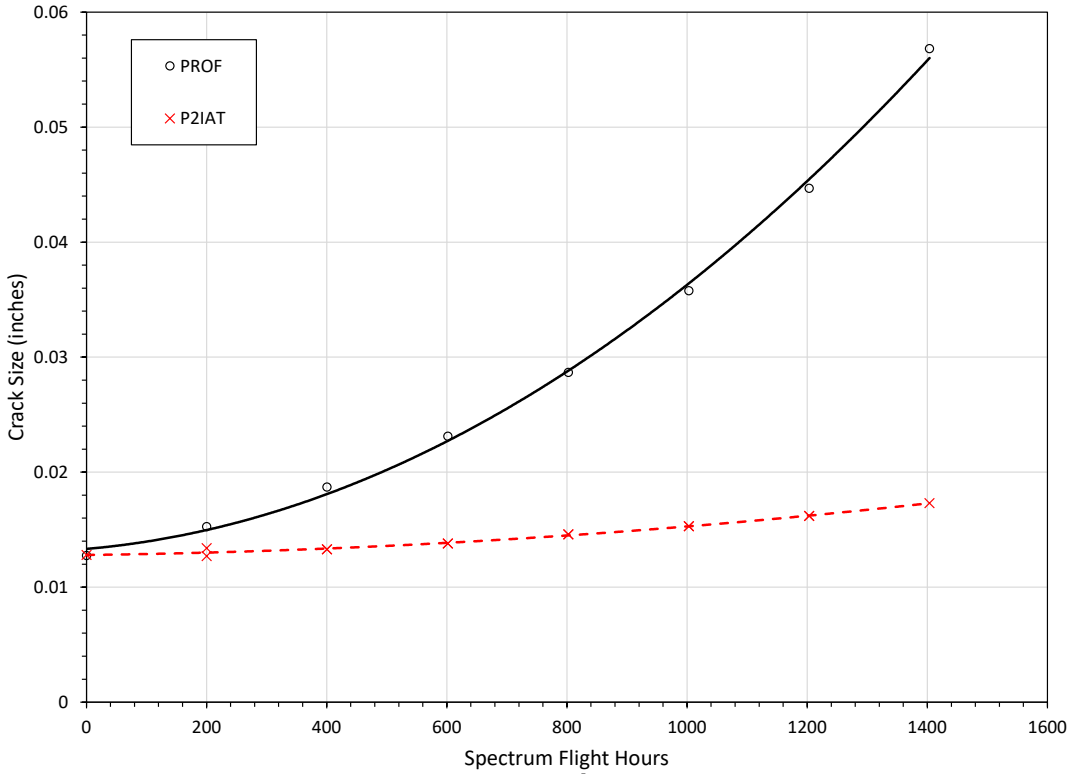

Figure 67. Growth of 95th Percentile EIDS

It is surprising that P^{2}IAT would have approximately the same SFPOF as PROF with such small crack sizes in the large crack tail of the distribution. The critical crack size at CP08 LW is over 0.5 inch. However, even with smaller initial crack sizes at all these percentiles, SFPOF on the first flight in Figure 59 is slightly higher for P^{2}IAT than PROF. This seems to indicate that all of the uncertainties considered in P^{2}IAT are contributing to higher SFPOF values.

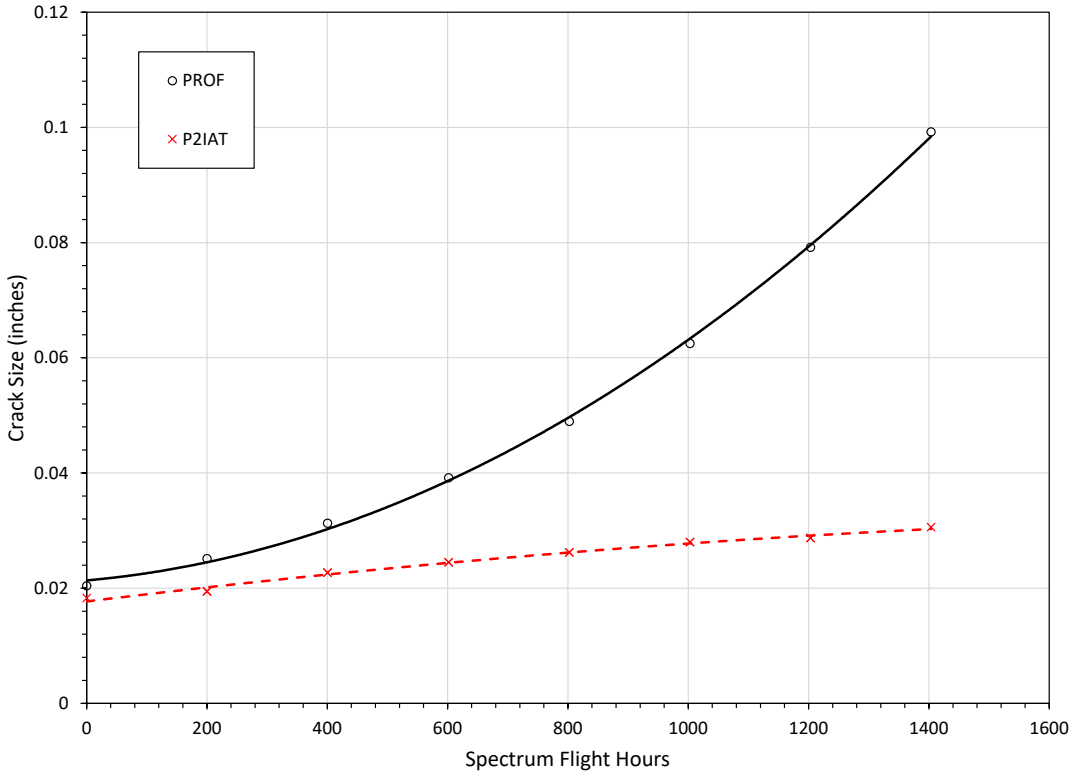

Figure 68. Growth of 99th Percentile EIDS

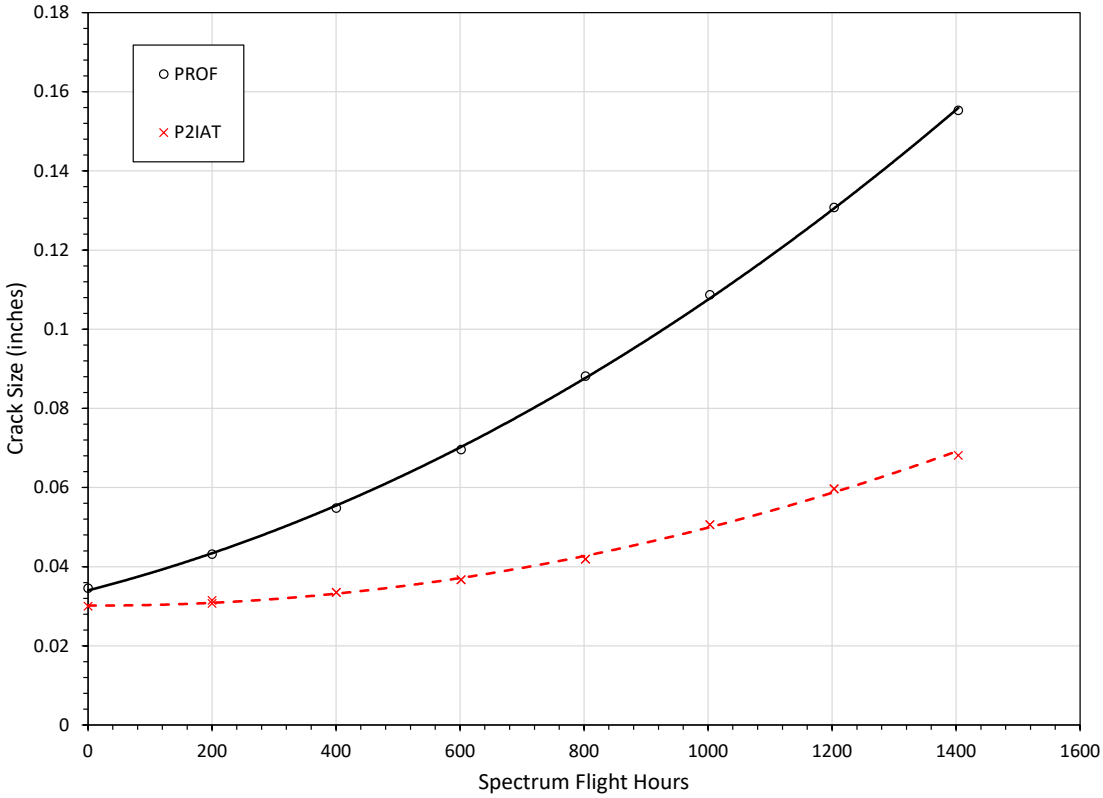

Figure 69. Growth of 99.9th Percentile EIDS

4.3.2 Post-Inspection Modification of the Crack Size Distribution

The tail of the crack size distribution is most affected by the results of inspections. The larger the cracks in the tail of the distribution, the greater the impact of the inspection since larger cracks are more likely to be found by an inspection. An inspection with no findings should reduce the probability of there being a large crack more than the probability of a small crack.

The large crack tail of the crack size distribution calculated by P^{2}IAT for CP08 LW before and after the inspections at 1,400 SFH and 7,600 SFH are presented in Figure 70. The modifications to the tail of the crack size distribution post-inspection in P^{2}IAT are relatively small. This is partially because of the small crack sizes in P^{2}IAT distribution, but is also due to the approach used to update the crack size distribution. P^{2}IAT uses the Bayes Network to adjust the crack size distribution based upon the likelihood of the inspection result, in this case no finding, given the POD curve in Figure 7. The details of how the crack size distribution is updated using inspection results is not explained well in [3] except to note that it is all done via sampling of an underlying distribution.

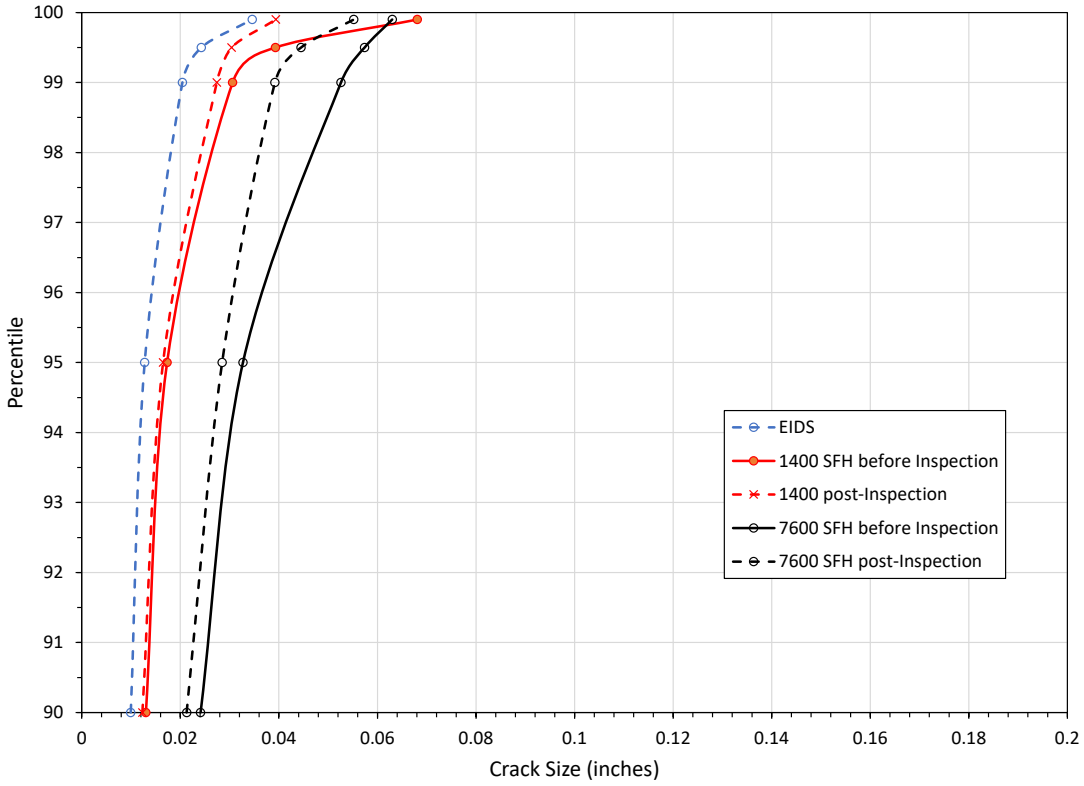

Figure 70. Tail of Crack Size Distribution in P^{2}IAT at 1,400 and 7,600 SFH

The large crack tail of the crack size distribution calculated by PROF for CP08 LW before and after the inspections at 1,400 SFH and 7,600 SFH are presented in Figure 71. The tail of the crack size distribution is changed much more in PROF. The crack size distribution extends to much larger crack in PROF. PROF does not take inspection results as an input. Instead, PROF assumes that cracks of a given size are found in proportion to the POD and the found cracks are

repaired to smaller cracks. PROF calculates the percentage of cracks, P, expected to be found by the inspection as

$$P = \int_0^\infty POD(c) \cdot f_{before}(c) dc \quad (3)$$

where *POD(c)* is the POD curve as a function of crack size *c*, and $f_{before}(c)$ if the probability density function of crack size before the inspection. The crack size density function after the inspection, $f_{after}(c)$, is

$$f_{after}(c) = P \cdot f_R(c) + [1 - POD(c)] \cdot f_{before}(c) \quad (4)$$

where $f_R(c)$ is the probability density function for the repaired crack sizes. [13]

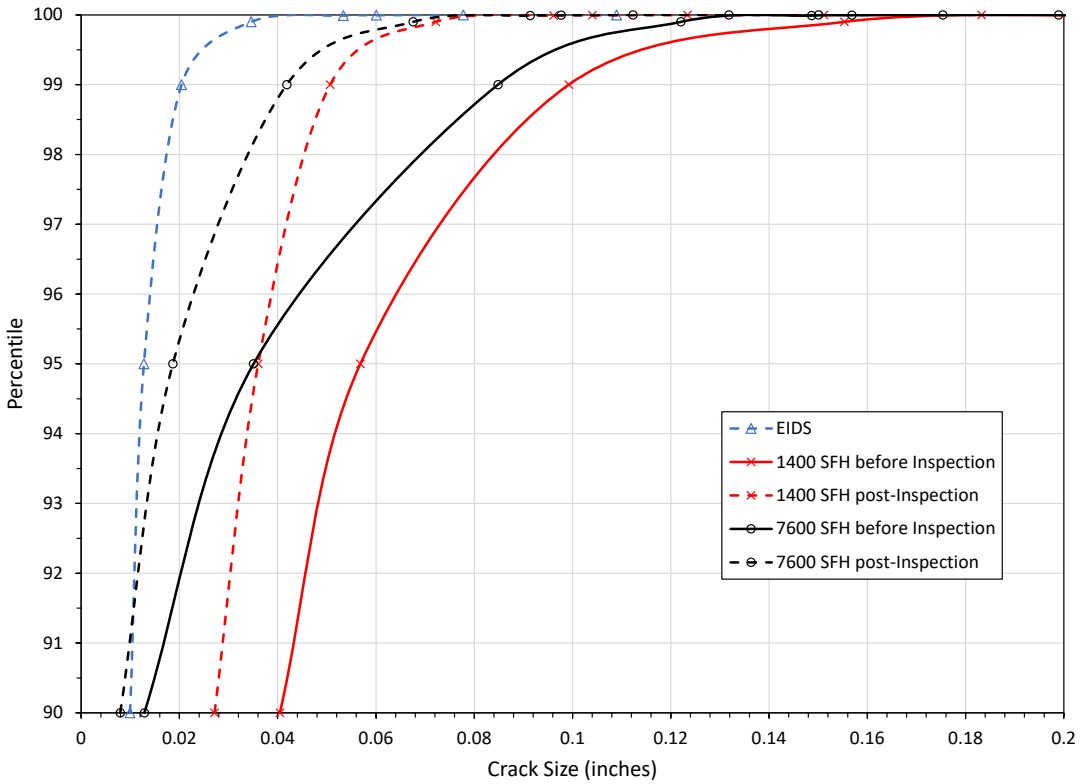

Figure 71. Tail of Crack Size Distribution in PROF at 1,400 and 7,600 SFH

4.4 Summary

P²IAT performed as intended in most cases keeping the maximum SFPOF near 10^{-7}. It was surprising that the frequency of inspections increased compared to CIAT. Risk analyses with PROF for CIAT showed that SFPOF was not significantly less than 10^{-7}, as had been anticipated, for the CPs studied. The more frequent inspections called for by P²IAT was not sufficient to maintain SFPOF below 10^{-7} at every CP. These locations had inspections every 200 SFH, the end of every week of loading. More frequent inspections were not an option in the demonstration

experiment. Allowing inspections as frequently as needed would have enabled P^{2}IAT to keep SFPOF below 10^{-7} at every CP.

The crack sizes in the 90th percentile and higher tail of the crack size distribution were much smaller in P^{2}IAT than in CIAT. The crack sizes in these percentiles also changed more slowly in P^{2}IAT than in CIAT. Despite this difference in the crack size distributions, the peak SFPOF values just before inspections were comparable for eight of the eighteen CPs studied. For the other ten CPs, five had the SFPOF values for P^{2}IAT higher than for CIAT and five had the CIAT values higher than P^{2}IAT. Overall, the different SFPOF calculation methods in P^{2}IAT and CIAT (i.e., PROF) give comparable results.

The Bayesian approach to handling structural inspection results in P^{2}IAT, together with the small crack sizes in the tail of the distribution, results in little change to the crack size distribution. The crack size distribution changes more after an inspection in CIAT even though PROF makes assumptions about cracks being found and repaired, never using inspection results. Thus, SFPOF changes less after an inspection in P^{2}IAT.

5 CONCLUSION

A fatigue damage tracking method for airframe structure, P^{2}IAT, based upon SFPOF was developed and demonstrated. The criterion for scheduling structural inspections for fatigue cracks in P^{2}IAT was SFPOF exceeding 10^{-7}. This is in contrast to the conventional criterion of half the fatigue life from a prescribed crack size. The objective of P^{2}IAT was to reduce the frequency of inspections compared to CIAT.

P^{2}IAT uses a DBN to map explicitly the relationships between all the random variables in the analyses. The mapping changes as needed with each new time increment during the tracking process. Furthermore, the fatigue tracking analysis is updated using information about the state of fatigue cracking obtained from NDI. Probability of failure is calculated using SIR.

The P^{2}IAT software is adaptable to various aircraft and structural configurations. However, the software uses its own fatigue crack growth code. P^{2}IAT cannot use other proven fatigue crack growth codes. Organizations that want to use fatigue crack growth algorithms that they are familiar with will find this a limitation.

Another major drawback of the P^{2}IAT software is that it was written in Python 2.7, which is not supported any more. An effort to translate the P^{2}IAT software into Python 3 was unsuccessful. A substantial rewriting of the software is necessary to bring it up to the latest standards if there is to be further development of P^{2}IAT.

P^{2}IAT was demonstrated by tracking fourteen locations on the outer portion of a fighter aircraft wing. A full-scale fatigue experiment was conducted by loading two wings with different load histories. The experiment was performed to make sure that P^{2}IAT did not miss any catastrophic fatigue cracks in anticipation of P^{2}IAT successfully reducing the frequency of inspections. The frequency of inspections with P^{2}IAT were compared to the frequency with CIAT.

The frequency of inspections with P^{2}IAT was the same or greater than with CIAT. Since there are few safety, or structural integrity, issues with CIAT, structural safety with P^{2}IAT was a mute point. SFPOF values calculated with PROF for CIAT were comparable to the SFPOF values from P^{2}IAT in most cases. Peak SFPOF values in CIAT exceeded 10^{-7} for many of the CPs. So, more inspections would be expected with any fatigue tracking method that seeks to keep SFPOF from exceeding 10^{-7}.

P^{2}IAT included as many random variables as could be identified with the idea that updating the fatigue analysis with NDI results would significantly reduce the uncertainty and SFPOF with it. It does not appear that the reduction in uncertainty after an inspection was that significant. As a result, SFPOF remained high and frequent inspections occurred.

In its present formulation, P^{2}IAT did not demonstrate an advantage over CIAT. If there is any interest in pursuing a probability of failure-based fatigue tracking approach further, a different formulation than P^{2}IAT should be used.

6 RECOMMENDATIONS

P^2IAT did not demonstrate a clear advantage over CIAT. If there is any interest in pursuing a probability of failure-based fatigue tracking approach further, the following recommendations are provided.

1) A Dynamic Bayesian Network should still be the primary structure of the software in order to enable updating of the fatigue tracking analysis from the results of structural inspections. Bayesian Network routines exist in many programming languages, e.g., Python, Matlab. There are even some software packaged developed specifically to construct Bayesian Networks like SPISE® [14] from PredictionProbe.
2) Limit the size of the DBN to the random variables: crack size, loading, material fracture toughness, and NDI probability of detection.
3) Sequential Importance Resampling can be used to calculate the probability of failure. A sufficient sample size should be establish to ensure robust and repeatable SFPOF values. It would be ideal if curve fitting was not needed to determine the probability of failure and SFPOF. Alternative methods such as First Order Reliability Method or Second Order Reliability Method [15] should be investigated since these methods are particularly handling low POF values.
4) Use existing fatigue crack growth codes such as AFGROW or FASTRAN to perform the crack growth calculations. Provide flexibility to utilize company proprietary codes as well. Import material properties from the databases in the fatigue crack growth codes.
5) Use AGILE development to create specific capabilities one at a time in defined sprints ensuring that each capability works as intended before adding more capabilities. Waiting years for software to have all its functionality before exercising it has not historically produced optimal software.
6) The inspection criterion used by P^2IAT should be revisited. The inspection criterion was derived from the Mil-Std-1530D [9] statement: “a probability of catastrophic failure at or below 10^{-7} per flight for the aircraft structure is considered adequate to ensure safety for long-term military operations.” A 400 SFH lead time for scheduling an inspection, equivalent to two weeks of loading, was established in the experiment. P^2IAT rigidly exercised this criterion to the point that if SFPOF was forecast 400 SFH out to be on 9.99 x 10-8, the inspection was put for another week. Other SFPOF values could be considered, as well as completely different criteria such as a first-crossing criterion where the probability of a parameter such as crack size first exceeding a specific value is used.

Finally, P^2IAT attempted to update the mix of missions for the forecasted flights based upon the mix of previous missions. An updated mission mix for future flights should improve the SFPOF forecasts. It was not clear how effectively updating the mission mix worked. Looking at the individual flights flown and using those to update the forecasted flights may be more effective. This will be challenging for actual flights in service, as no two flights are likely ever the same. After other aspects of probability of failure-based fatigue tracking are resolved, it would be worthwhile to explore continuous updating of aircraft usage.

REFERENCES

[1] L. Wang, I. Asher, K. Ryan, G. Khan and D. Ball, "Airframe Digital Twin (ADT) Delivery Order 0001: Scalable, Accurate, Flexible, Efficient, Robust, Prognostic and Probabilistic Individual Aircraft Tracking (SAFER-P2IAT), Volume 1," U.S. Air Force Research Laboratory, Wright-Patterson Air Force Base, OH, 2016.

[2] L. Wang, I. Asher, K. Ryan, G. Khan, R. Longtin, D. Ball, R. Shannon and E. Dakwar, "Airframe Digital Twin Spiral 1 Task Order 0002: Scalable Accurate Flexible Efficient Robust - Prognostic and Probabilistic Individual Aircraft Tracking (SAFER-P2IAT) Full Scale Wing Experiment Plans, Requirements, and Development," U.S. Air Force Research Laboratory, Wright-Patterson Air Force Base, OH, 2017.

[3] L. Wang, S. Atkinson, K. Ryan, G. Khan, R. Longtin, D. Ball, R. Shannon, E. Dakwar and J. Hoffman, "Airframe Digital Twin (ADT) Delivery Order FA8650-17-F-2219: Scalable, Accurate, Flexible, Efficient, Robust, Prognostic and Probabilistic Individual Aircraft Tracking (SAFER-P2IAT) Full-Scale Demonstration Experiment," US Air Force Research Laboratory, Wright-Patterson Air Force Base, OH 45433, 2019.

[4] E. Anagnostou and S. Engel, "Airframe Digital Twin (ADT) - Delivery Order 0002: Demonstration of Prognostic and Probabilistic Individual Aircraft Tracking (P2IAT) vol. 1," Air Force Research Laboratory, Wright-Patterson AFB, OH, 2017.

[5] LexTech, Inc., "AFGROW.NET," LexTech, Inc., [Online]. Available: https://www.afgrow.net/. [Accessed 8 September 2021].

[6] A. H.-S. Ang and W. H. Tang, Probability Concepts in Engineering Planning and Design, Volume I - Basic Principles, New York: John Wiley and Sons, 1975.

[7] A. O'Hagan, "Bayesian analysis of computer code outputs: A tutorial," *Reliability Engineering and System Safety,* vol. 91, pp. 1290-1300, 2006.

[8] M. Ebden, "Gaussian Process: A Quick Introduction," *arXiv.org,* 2015.

[9] U.S. Dept. of Defense, *Department of Defense Standard Practice - Aircraft Structural Integrity Program (ASIP),* U.S. Dept. of Defense, 2016.

[10] E. J. Tuegel, R. P. Bell, A. P. Berens, T. Brussat, J. W. Cardinal, J. P. Gallagher and J. Rudd, "Aircraft Structural Reliability and Risk Analysis Handbook - Volume 1: Basic Analysis Methods," Air Force Research Laboratory, Wright-Patterson AFB, OH, 2018.

[11] *Methodology for Determination of Equivalent Flight Hours and Approaches to Communicate Usage Severity,* Wright-Patterson AFB, OH 45433: U.S. Air Force, 2009.

[12] F. R. Smith, T. R. Boehnlein, P. W. Hovey, P. C. Miedlar and A. P. Berens, "PROF v3.2 PRobability Of Failure - A-10 Fleet Management Analysis Update," University of Dayton Research Institute, Dayton, OH, 2015.

[13] A. P. Berens, P. W. Hovey and D. A. Skinn, "Risk Analysis for Aging Aircraft Fleets, Volume 1 - Analysis," U.S. Air Force Systems Command, Wright-Patterson Air Force Base, OH, 1991.

[14] PredictionProbe, Inc., "Solutions: SPISE," PredictionProbe, Inc., 2020. [Online]. Available: https://predictionprobe.com/solutions/spise/. [Accessed 15 February 2022].

[15] O. Ditlevsen and H. O. Madsen, Structural reliability methods, Chichester: Wiley, 1996.

SYMBOLS, ABBREVIATIONS AND ACRONYMS

a_0	initial crack size distribution (i.e., EIDS)
a	crack size distribution
a_{min}	lower bound crack size for probability of detection curve
a_{50}	crack size with probability of detection of 50%
a_{90}	crack size with probability of detection of 90%
ADT	Airframe Digital Twin
AFGROW	Fatigue crack growth software
c	Variable representing the size of a fatigue crack
CIAT	Conventional Individual Aircraft Tracking
COTS	Commercial Off The Shelf
c_{NDI}	Variable representing the crack size that can be reliably detected with a NDI method
CP	Control Point (fatigue tracking location)
DBN	Dynamic Bayesian Network
EDS	Equivalent Damage Size
EIDS	Equivalent Initial Damage Size, EDS at time zero
EFH	Equivalent Flight Hours
FDR	Flight data recorder
FEM	Finite element model
K	fracture toughness
Kc	critical fracture toughness
LW	Left wing
MERC	Mercer Engineering Research Center
NDI	non-destructive inspection
N_{xcg}	x-direction acceleration at aircraft center of gravity
N_{ycg}	y-direction acceleration at aircraft center of gravity
N_{zcg}	z-direction acceleration at aircraft center of gravity
P^2IAT	Probabilistic and Prognostic Individual Aircraft Tracking
POD	Probability of Detection

POF	cumulative probability of failure
PROF	PRObability of Fracture software
RW	Right wing
SFH	Spectrum flight hour
SFPOF	Single Flight Probability Of Failure
SIF	Stress intensity factor
SIR	Sequential Importance Resampling
USAF	United States Air Force
WBM	Wing bending moment
WT	Wing torque
XW	x-coordinate in the wing reference frame